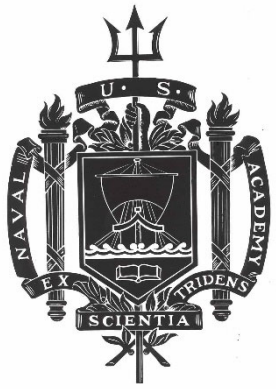
A TRIDENT SCHOLAR PROJECT REPORT

NO. 524

Effects of Gamma Radiation on the Thermal and Mechanical Properties of Additively Manufactured Thermoplastics

by

Midshipman 1/C Logan C. Schoffstall, USN



UNITED STATES NAVAL ACADEMY
ANNAPOLIS, MARYLAND

This document has been approved for public release and sale; its distribution is unlimited.

USNA-1531-2

REPORT DOCUMENTATION PAGE

Form Approved
OMB No. 0704-0188

Public reporting burden for this collection of information is estimated to average 1 hour per response, including the time for reviewing instructions, searching existing data sources, gathering and maintaining the data needed, and completing and reviewing this collection of information. Send comments regarding this burden estimate or any other aspect of this collection of information, including suggestions for reducing this burden to Department of Defense, Washington Headquarters Services, Directorate for Information Operations and Reports (0704-0188), 1215 Jefferson Davis Highway, Suite 1204, Arlington, VA 22202-4302. Respondents should be aware that notwithstanding any other provision of law, no person shall be subject to any penalty for failing to comply with a collection of information if it does not display a currently valid OMB control number. **PLEASE DO NOT RETURN YOUR FORM TO THE ABOVE ADDRESS.**

1. REPORT DATE *(DD-MM-YYYY)*	**2. REPORT TYPE**	**3. DATES COVERED** *(From - To)*
5-16-22		

4. TITLE AND SUBTITLE
Effects of Gamma Radiation on the Thermal and Mechanical Properties of Additively Manufactured Thermoplastics

5a. CONTRACT NUMBER

5b. GRANT NUMBER

5c. PROGRAM ELEMENT NUMBER

6. AUTHOR(S)
Logan C. Schoffstall

5d. PROJECT NUMBER

5e. TASK NUMBER

5f. WORK UNIT NUMBER

7. PERFORMING ORGANIZATION NAME(S) AND ADDRESS(ES)

8. PERFORMING ORGANIZATION REPORT NUMBER

9. SPONSORING / MONITORING AGENCY NAME(S) AND ADDRESS(ES)
U.S. Naval Academy
Annapolis, MD 21402

10. SPONSOR/MONITOR'S ACRONYM(S)

11. SPONSOR/MONITOR'S REPORT NUMBER(S)
Trident Scholar Report no. 524 (2022)

12. DISTRIBUTION / AVAILABILITY STATEMENT

This document has been approved for public release; its distribution is UNLIMITED.

13. SUPPLEMENTARY NOTES

14. ABSTRACT

While the radiation effects on conventionally manufactured polymers has been studied to a limited extent, the effects on additively manufactured components of the same polymers have not been thoroughly documented. The objective of this study is to understand the effect of radiation on the thermal and mechanical properties of additively manufactured polymers. This was accomplished by comparing the tensile strength and thermal stability of these materials under gamma irradiation up to 20 MRad. Two of the most common additive manufacturing techniques are fused deposition modeling (FDM) and selective laser sintering (SLS). Both techniques involve the fusing of successive layers until the desired shape is achieved. The following additively manufactured materials were tested: Nylon-12 (SLS), NylonG – glass fiber filled nylon (FDM), and Nylforce CF – carbon fiber filled nylon (FDM). Nylon-12 was the injection molded material tested. Thermal analysis included thermogravimetric analysis (TGA) and differential scanning calorimetry (DSC) to measure at what temperature polymer degradation occurred and enthalpy heat of fusion, respectively. Tensile testing determined that increased radiation resulted in a decrease in tensile strength. Fractography showed that there was an increase in brittle fracture as the radiation dose increased.

15. SUBJECT TERMS
gamma radiation, thermoplastics, additive manufacturing, Nylon-12, differential scanning calorimetry

16. SECURITY CLASSIFICATION OF:			**17. LIMITATION OF ABSTRACT**	**18. NUMBER OF PAGES**	**19a. NAME OF RESPONSIBLE PERSON**
a. REPORT	**b. ABSTRACT**	**c. THIS PAGE**		76	**19b. TELEPHONE NUMBER** *(include area code)*

U.S.N.A. --- Trident Scholar project report; no. 524 (2022)

EFFECTS OF GAMMA RADIATION ON THE THERMAL AND MECHANICAL PROPERTIES OF ADDITIVELY MANUFACTURED THERMOPLASTICS

by

Midshipman 1/C Logan C. Schoffstall
United States Naval Academy
Annapolis, Maryland

Certification of Advisers Approval

Professor Peter Joyce
Mechanical Engineering Department

Assistant Professor Elizabeth Getto
Mechanical Engineering Department

Commander David P. Durkin, Ph.D., USN
Chemistry Department

Captain Brad Baker, Ph.D., USN
Mechanical Engineering Department

Acceptance for the Trident Scholar Committee

Professor Maria J. Schroeder
Associate Director of Midshipman Research

USNA-1531-2

Abstract

Additive manufacturing represents a highly efficient and cost-effective solution for rapid replacement of aging parts in the defense industry. Such components are often subjected to harsh environments including exposure to radiation. While the radiation effects on conventionally manufactured engineering polymers has been studied to a limited extent, the effects on additively manufactured components of the same polymers have not been thoroughly documented. Therefore, the objective of this study is to understand the effect of radiation on the thermal and mechanical properties of high performance additively manufactured polymers. The objective was accomplished by comparing the tensile strength and thermal stability of these materials under gamma irradiation up to 20 MRad. This work is critical to potential implementation in defense applications such as the Trident missile program. Polymer properties are largely governed by their macrostructure, which includes whether they are amorphous or semicrystalline, and if they exhibit crosslinking between polymer chains. Polymers that do not inherently exhibit crosslinking are known as thermoplastics and these materials are common in additive manufacturing. Two of the most common additive manufacturing techniques are fused deposition modeling (FDM) and powder bed fusion (PBF). Both techniques involve the melting of thermoplastics and fusing successive layers until the desired shape is achieved. Results were compared to the radiation effects on injection-molded samples of the same thermoplastics. The following additively manufactured materials were tested: Nylon-12 (SLS), Ultem 9085 (FDM), NylonG – glass fiber filled nylon (FDM), and Nylforce CF – carbon fiber filled nylon (FDM). Nylon-12 and Ultem 9085 were the injection molded materials tested. Radiation doses from 0.1 up to 20 MRad were tested for each material. Thermal analysis included thermogravimetric analysis (TGA) and differential scanning calorimetry (DSC) to measure at what temperature polymer degradation occurred and enthalpy heat of fusion, respectively. Modulated differential scanning calorimetry (MDSC) was used to minimize the thermal gradients present in data. Tensile testing determined that increased radiation resulted in a decrease in tensile strength. Fractography via scanning electron microscopy (SEM) showed that there was an increase in brittle fracture present in failed specimens as the radiation dose increased. At radiation doses of greater than 10 MRad, the fracture surface exclusively exhibited brittle fracture behavior.
Keywords: gamma radiation, thermoplastics, additive manufacturing, Nylon-12, differential scanning calorimetry.

Acknowledgments

This study was conducted with the help of Dr. Jessica Sargent and Dr. Tyler Churchill of Naval Surface Warfare Center, Crane. Additionally, specimens were fabricated with the help of MakerSpace USNA and SEM was performed at the Center for Materials Characterization at the U.S. Naval Academy. This work was partially funded by the Army Research Office [MIPR# 11720771] and the Defense Threat Reduction Agency. Any opinions, findings, conclusions, or recommendations expressed herein are those of the authors and do not reflect the views of the U.S. Navy or the U.S. Army.

Table of Contents

1. Introduction 3
1.2 Additive Manufacturing Methods 4
1.3 Polymer Chemistry 6
2. Experimentation 7
2.1 Material Preparation 7
2.2 Irradiation 10
2.3 Thermal Properties Testing 11
2.2.1 Thermogravimetric Analysis 11
2.2.2 Differential Scanning Calorimetry 11
2.3 Mechanical Properties Testing 11
2.4 Scanning Electron Microscopy (SEM) 11
3. Results 12
3.1 Thermal Properties 12
3.2 Mechanical Properties 17
3.2.1 SLS Nylon-12 17
3.2.2 FDM NylonG 24
3.2.3 FDM Nylforce CF 28
3.2.4 Ultem 9085 FDM 32
3.2.5 Nylon-12 IM 35
3.2.6 Effects of Fabrication Method 37
3.2.7 Effect of Fiber-Reinforced 3d Printed Composites 38
3.3 Comparison of Thermal and Mechanical Properties Effects 38
4. Conclusions 40
4.1 Thermal Properties 40
4.2 Mechanical Properties 41
5. Future Work 41
5.1 Material Characterization 41
5.2 Additional Analysis 42
6. References 43
7. Appendices 45
7.1 SEM of Nylon-12 SLS 45
7.2 Plots of Tensile Data 60

1. Introduction

1.1 Background

Great advances in additive manufacturing (AM) of polymers in the last ten years provide a pathway for advanced manufacturing practices that may reduce cost and time in manufacturing, repair, and sustainment of components of interest to the U.S. Navy and the Department of Defense [1]. It is estimated that thorough AM implementation in the Navy's maintenance program has the potential to produce cost savings of $1.49 billion annually [2]. However, there are well-documented concerns about defects to the microstructure and macrostructure of AM components especially with variation in process parameters. Furthermore, radiation degradation of polymer AM parts has not been significantly investigated and is a major concern, particularly within the missile community. Radiation effects on AM materials are generally placed into one of two categories based upon the applications for which the materials will be used. The first category is the polymer materials that are irradiated before printing. This is applicable in situations such as AM in space, where the materials will likely be exposed to radiation prior to undergoing the printing process. The second category, and more relevant to the present work, is AM polymer components that undergo radiation damage in service. Studies regarding this category are useful in the application of AM for parts that will be used in an environment in which they may be exposed to radiation. Of particular interest to the U.S. Navy and the Department of Defense are replacement parts on submarine-launched ballistic missiles. Given the radiation emitted by radioactive material within the ballistic missiles, it is a critical concern that replacement parts may fail due to mechanical defects imparted by radiation exposure. We propose to determine the effect of radiation damage on AM parts through a combination of manufacturing, post processing, irradiation, and testing.

National security relies upon the ability to exercise the capabilities of missiles immediately and effectively at any given moment [1]. As such, it is of the utmost importance that these missiles be maintained frequently and are ready for use at the highest rate possible. The Stockpile Stewardship and Management Plan for Fiscal Year 2020 notes that legacy methods for manufacturing may not be effective anymore and AM is the most viable method for maintaining the agility of the nuclear stockpile [1]. For example, radomes, or the structure that protects radars, must be periodically replaced to ensure they fulfill the structural and electrical needs of the system. This differs from other aircraft structures in that they are designed to allow radar frequencies to pass through with maximum transparency while still fulfilling the structural requirements of the component.

Previous nose fairings on Trident missiles have been constructed out of Sitka spruce in conjunction with a fiberglass laminate. Figure 1 illustrates the nose cone of a Trident II D5 ballistic missile, one potential application for additively manufactured replacement parts.



Figure 1. Trident II D5 missile in service [4].

As these parts have aged and replacements are in short supply, maintenance personnel have realized that the production plans for these nose fairings are no longer available and would be unnecessarily complex to produce regardless of availability. In order to maintain the fleet and ensure maximum time of operational capacity, there must be a quick way to manufacture replacement parts that will not need servicing at frequent intervals. AM provides an attractive solution to this problem, with a research team at Oak Ridge National Laboratory currently using Big Area Additive Manufacturing Technology (BAAM) to replicate this exact geometry. However, issues with degradation of materials when irradiated must be studied and addressed to ensure that minimal servicing is required.

1.2 Additive Manufacturing Methods

ASTM52900 defines seven different AM process categories [5]. In polymer AM, the most commonly used method is material extrusion (ME), also referred to as fused deposition modeling (FDM). This method utilizes a polymer filament heated to just below the melting point which is then fed through an extruder nozzle that will heat the filament above the melting point. The nozzle travels over the build plate, extruding material until a single layer of the print is complete. The extruder then moves up as the polymer cools, extrudes another layer, and repeats this process until the component is completed (Figure 2). Typically, parts are not printed with a completely filled structure; rather, an outer wall is printed with a specified percentage filled in the middle in a specified pattern (referred to as infill) that is required.

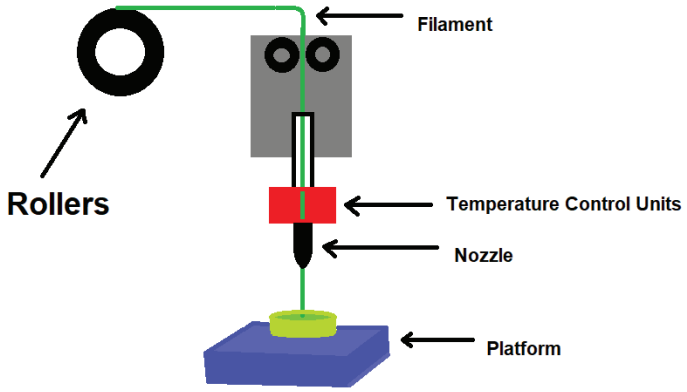


Figure 2. Fused Deposition Modeling diagram.

Powder bed fusion (PBF) is an AM process that utilizes a heat source to fuse powder particles together creating successive layers of the component [6]. Within the category of PBF, there are multiple types of energy sources used to sinter the material. Of note, PBF of polymers is typically performed in a process that uses a laser known as selective laser sintering (SLS). A bed of polymer powder is heated to just below the melting point of the polymer and the laser is used to raise the temperature of selective areas above the melting point of the material. The powder in these locations is sintered together and is then allowed to cool back below the melting temperature of the material. The bed is then moved down and another layer of powder is spread on top using a recoater. Due to the part being completely surrounded by unsintered powder, there is no need for support structures in PBF. This allows for complex geometries to be created with relative ease.

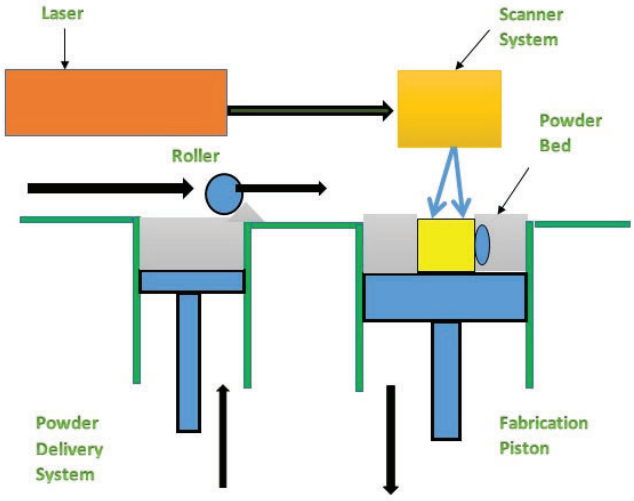


Figure 3. The diagram shows the typical set up and process for selective laser sintering.

1.3 Polymer Chemistry

A polymer is a large molecule made up of repeating units (monomers) that can be linear, branched, or cross-linked. Polymers with a high degree of molecular order are considered crystalline, while polymers with backbones that are not organized in any particular structure are considered amorphous [7]. The chemical composition and structure of the polymer will determine the polymer's properties. There are two common types of polymers used in AM: thermoplastics and thermosets. Thermosets exhibit cross-linking in their structures once they are cured and cannot be melted and reshaped. Thermoplastics are polymers that do not naturally exhibit cross-linking and therefore are able to be heated to their melting point and consolidated repeatedly. Polymer structure is largely driven by temperature.

One driving factor of the physical properties of a polymer is the percent crystallinity. Crystallinity refers to the degree of structural order that exists in the polymer. A material with high percent crystallinity would be stronger and stiffer than a sample of the same material with a lower degree of crystallization. The percent crystallinity can be determined by comparing the thermal properties of a sample to that of a 100% crystalline sample of the same material [10]. Percent crystallinity is a property that can be measured and compared across samples to evaluate whether the structure of the polymer has changed after undergoing irradiation. Nylon-12 is a largely amorphous polymer that may have smaller regions of crystalline structure throughout.

Nylon-12 exhibits similar mechanical properties to other forms of nylon, such as Nylon-6,6 and Nylon-6 with some notable differences. Specifically, Nylon-12 is an amorphous polymer that exhibits little order in the polymer structure. As a result, it has a low melting temperature and is therefore more easily processed. These material properties, however, can change as a result of radiation damage.

Gamma radiation is a particle of electromagnetic energy that is emitted from the nucleus of radioactive atoms. The photons, or high energy particles, are very penetrative and are capable of entering a material and exciting the chemical bonds within that material. As a result, macromolecules of a polymer can be broken apart to form radicals that are then able to form new bonds in a cross-linking process [11]. It is also possible for the radicals to remain separated in a chain-scissioning process. The chain-scission process, opposite to cross-linking, typically results in a weaker and less brittle material.

The objective of this research is to investigate the radiation damage mechanism of additively manufactured thermoplastics. The method of investigation will be the testing of thermal and mechanical properties, as well as imaging of the observed structure of thermoplastics before and after irradiation at an array of gamma radiation doses. Additionally, the effects of conventionally manufactured thermoplastics will be studied to compare the effects of fabrication on the radiation damage mechanism.

2. Experimentation

2.1 Material Preparation

The materials of interest in this study include both amorphous and semi-crystalline engineering thermoplastics. They are fabricated through the use of FDM, SLS, and injection molding to allow for the comparison of various types of AM to injection molded samples. Injection molding is the style of fabrication that will be considered as the conventional method for processing polymers as it is very common within industry. It involves the melting and injection of melted plastic into a mold. It is then left to cool and removed from the mold. The complete test matrix is shown in Table 1.

Table 1. Test matrix including fabrication method and radiation dose.

Material	Processing Method	Radiation Dose (MRad)	Number of Specimens (per dose)
Nylon-12	Injection Molding (IM)	0, 0.1, 0.5, 1, 5, 10, 15, 20	5
	Selective Laser Sintering (AM)	0, 0.1, 0.5, 1, 5, 10, 15, 20	5
NylonG	Fused Deposition Modeling (AM)	0, 1, 5, 10, 15, 20	5
Nylforce CF	Fused Deposition Modeling (AM)	0, 1, 5, 10, 15, 20	5
Ultem 9085	Injection Molding (IM)	0, 0.1, 0.5, 1, 5, 10, 15, 20	5
	Fused Deposition Modeling (AM)	0, 0.1, 0.5, 1, 5, 10, 15, 20	5

Three nylon-based materials were chosen in this test matrix for their availability and relative ease in additive manufacturing. Nylon-12 is an amorphous polymer that, as mentioned in Section 1, may exhibit strengthening as a result of crosslinking or weakening as a result of chain scission of the polymer backbone chains. Nylon-12 was printed using the FormLabs Fuse 1 Nylon-12 sold through the same vendor as the printer. It is a pure version of Nylon-12 precipitated into a fine powder form. All powder used in printing these samples was brand new virgin powder. NylonG is a glass fiber-filled nylon-based polymer composite filament. It has an unknown density and type of glass fiber filler since that information is proprietary. Similarly, Nylforce CF is a carbon fiber-filled nylon-based polymer composite filament. The type and density of its carbon fiber filler is also proprietary. Ultem 9085 is a polyetherimide polymer filament that is semicrystalline.

To maintain consistency and relevance of the data, the same geometry of samples were used whenever possible. Tensile testing specimens (i.e., dogbones) were fabricated according to the ASTM D638 Type I specimen model at 50% scale. It was important to manufacture specimens in the same build batch as much as possible to minimize the number of changing variables when comparing across varying levels of radiation exposure. However, this necessity introduced the

limiting factor of the physical size of the build plates and the number of specimens that needed to be printed. It was for this reason that the tensile test samples were printed at 50% scale.

The specimens used in thermal properties analysis were also manufactured according to specific geometries to maximize consistency across the test matrix. Through an iterative process, an optimal geometry of 3 mm width and 0.44 mm thickness was used to minimize the thickness while maximizing the surface area in contact with the sample pan (Figure 4). Increased thickness of samples would result in large thermal gradients that would make it difficult to recognize changes in the samples' thermal properties. The final design of the disc was 30% of the thickness of the original iteration and had a greater surface area in contact with the pan, which is desirable. These discs were then also used in the thermogravimetric analysis because they are consistent with the size of the apparatus that holds the specimen in the instrument.

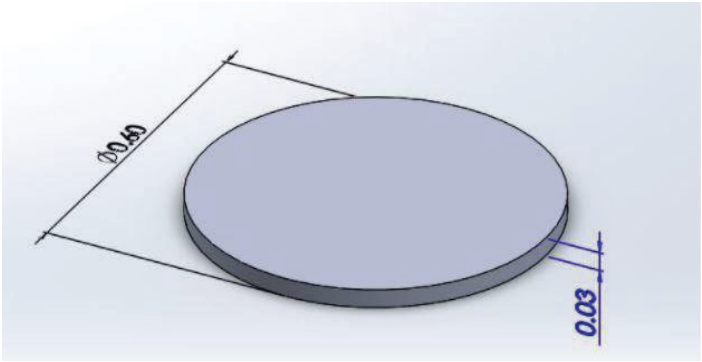


Figure 4. Discs used for DSC and TGA testing (all dimensions in in.).

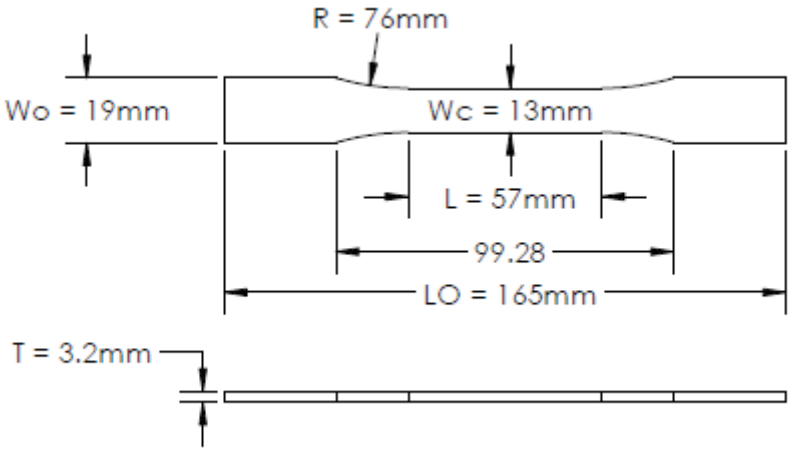


Figure 5. ASTM D638 Type 1 full scale specimen dimensions [12].

2.1.1 Material Extrusion

Two material extrusion printers were used to fabricate specimens in this study. The Ultimaker S5 was used in the fabrication of NylonG and Nylforce CF specimens. When printing with an engineering quality material such as NylonG or Nylforce CF, the equipment and settings must be

modified to account for the special qualities of the materials. The glass and carbon fibers found in fiber filled polymer composites are abrasive and will typically cause printing errors, so a hardened steel nozzle must be used to prevent damage to the nozzle and any print errors associated with that damage. Additionally, Nylon typically has trouble adhering to the standard print bed surfaces, so a Garolite bed is necessary to ensure adhesion to the build plate that will result in an accurate component. The build plate was organized as shown in Figure 6.

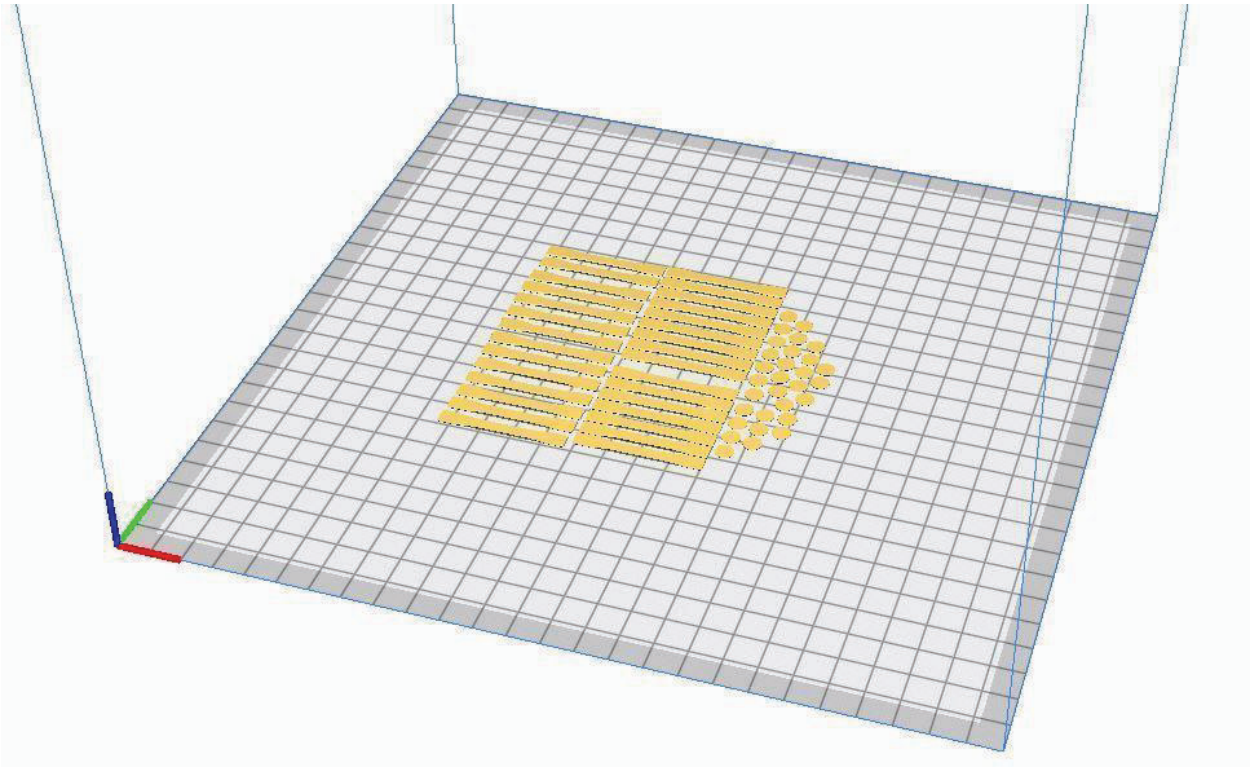


Figure 6. Ultimaker build plate layout.

2.1.2 Selective Laser Sintering

In this study, Nylon-12 powder purchased from FormLabs [8] was used in a selective laser sintering (SLS) process using a FormLabs Fuse1 printer. Each build plate included tensile specimens and discs for thermal analysis as well as notched Izod impact specimens (However, Izod impact testing did not fall within the scope of this study). Figure 7 shows the build plate organization with the axes labeled appropriately.

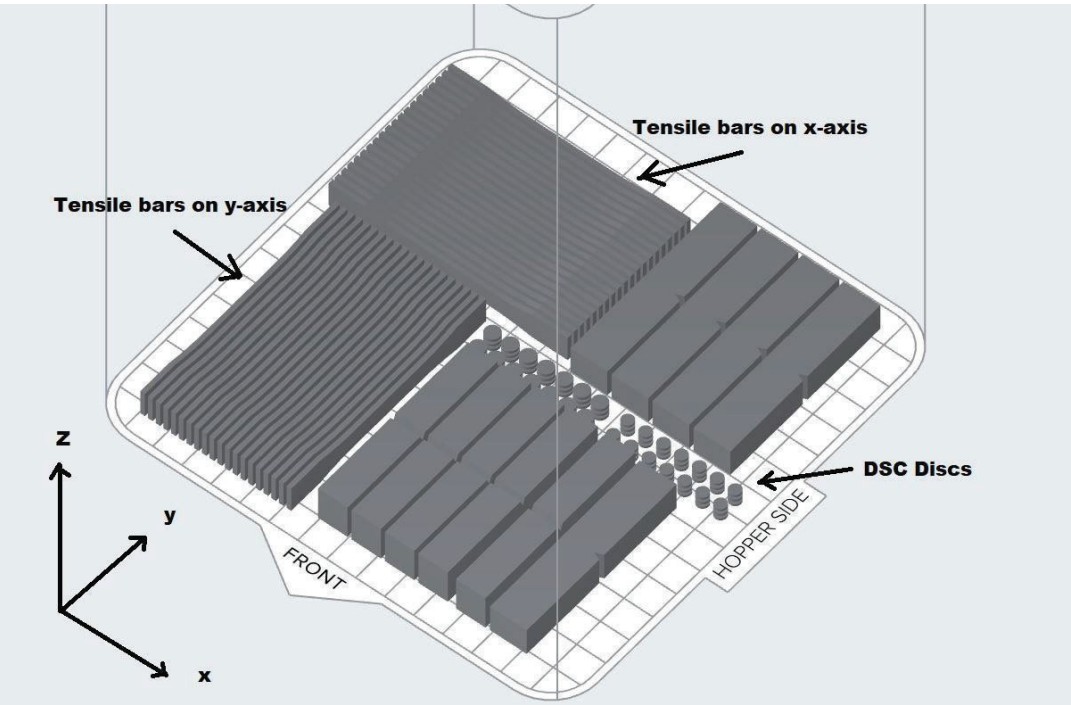


Figure 7. Build plate layout showing tensile bars and discs for Fuse1.

The tensile specimens were printed on their sides with a number of samples lying with their longitudinal axes parallel with the *y*-axis and a number lying with their longitudinal axes parallel to the *x*-axis. The specimens were organized in the build plate using the "array" function that is available in FormLabs' PreForm software with a default spacing between each specimen of 1 mm. For reference, the *x*-axis is parallel to the front of the build plate facing the door of the printer. The *y*-axis is perpendicular to the front face of the printer. After an initial print, it was determined that there was no difference in the UTS of samples printed parallel to the x and y-axes. Subsequent builds to fabricate specimens to be irradiated were printed with the longitudinal axis parallel to the *x*-axis.

2.2 Irradiation

After fabrication, the specimens were sent to NSWC-Crane to undergo irradiation. They were irradiated in an isotropic ^{60}Co irradiator. The samples were placed into custom-made trays that would allow for specimens to be removed at each dose to be studied. Irradiation was completed in two batches ranging from 0 to 10 MRad in the first batch and 0 to 20 MRad in the second batch. The second batch took approximately 4 days to complete. This irradiation regime allowed for the testing of unirradiated samples as well as those at doses irradiated to about 6 orders of magnitude higher than would be expected in missile sustainment applications.

2.3 Thermal Properties Testing

2.3.1 Thermogravimetric Analysis

Thermogravimetric analysis (TGA) (TA Instruments Q500) was used to evaluate the thermal decomposition profile for each sample. TGA was conducted on 3 mg (±0.5mg) samples in N_2 at a heating rate of 10 °C min^{-1}.

2.3.2 Differential Scanning Calorimetry

Modulated Differential Scanning Calorimetry (MDSC) (TA Instruments, Q20) was used to evaluate the enthalpy of melting during repetitive heating/cooling cycles under N_2. Material in a standard geometry (see Figure 4, ca. 6-8mg) was sealed in a standard DSC pan. Modulated DSC parameters were optimized in accordance with TA Note TN45 [10]. From the melting endotherm for the first and third MDSC cycles (2 °C min^{-1} rate of heating/cooling, modulation ± 0.5 °C every 90 sec), the reversible and non-reversible heat flows were extracted and analyzed.

2.4 Mechanical Properties Testing

The ultimate tensile strength of each sample was measured according to ASTM D638, primarily using an ADMET MtestQuattro tensile tester. Prior to testing, the width and thickness of each specimen was recorded to calculate the cross-sectional area. The specimens were loaded into the tensile testing grips and tightened firmly in place. The specimen alignment was measured with a square to ensure the specimens were parallel to the load train then they were pulled at a rate of 50 mm/min. Figure 8 shows the tensile testing setup.

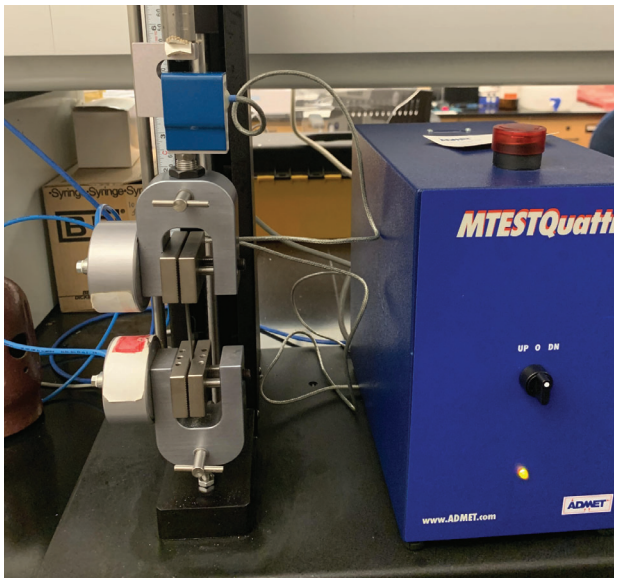


Figure 8. Tensile testing setup

2.5 Scanning Electron Microscopy (SEM)

Scanning electron microscopy (SEM) using a TESCAN MIRA3 located at USNA in the Center for Materials Characterization was used to evaluate the surface morphology of fractured samples

before and after irradiation. Samples were sputtered with a thin (<5nm) coating of gold prior to analysis. All SEM images were collected at energies from 2-5 kV and in scattered electron mode.

3. Results

3.1 Thermal Properties

3.1.1 SLS Nylon-12

The thermogravimetric analysis (TGA) shows decomposition of the material upon heating under N_2. Figure 9 shows TGA results for all nylon variants. The samples originally tested with TGA were the unirradiated specimen to get a baseline temperature to which DSC could be cycled to.

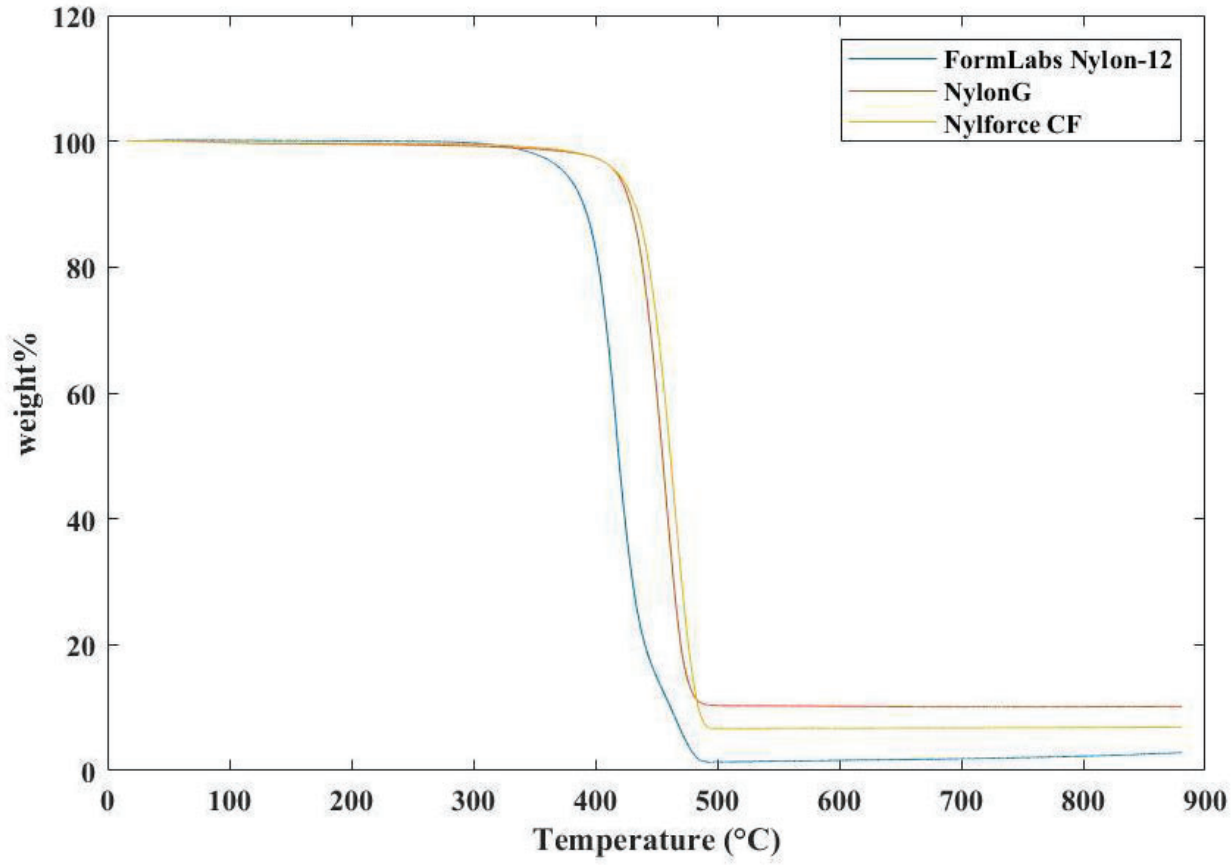


Figure 9. Thermogravimetric analysis of Nylon-12 in nitrogen.

The TGA indicates that the AM nylon-12 samples tested were thermally stable up to ca. 300°C. Therefore, the maximum temperature in each MDSC heating cycle was 275°C.

A standard DSC test with a heating rate of 10 °C/min did not yield distinguishable endothermic events that would signify a glass transition. Modulated DSC (MDSC) was used to further increase the possibility of measuring endothermic events and reversible heat flow. MDSC testing differs from standard DSC in that the modulation component of the heat flow allows for the

thermodynamic and kinetic components of the heat flow to be separated. In MDSC, the total heat flow is separated into reversible and non-reversible components, based on sample response to the modulating heat signal. The reversing heat flow is related to the heat capacity of the material and can be used to identify thermodynamic events. Conversely, the non-reversible heat flow is related to kinetic components such as cold crystallization and perfect crystallinity [13].

Optimizing MDSC parameters required an isothermal experiment where the reversible heat capacity was measured as a function of modulating frequency. Based on the results of this experiment, shown in Figure 10, the optimal period is the first one where the reversible heat capacity value plateaus (ca. 90s, as identified by the arrow in Figure 10).

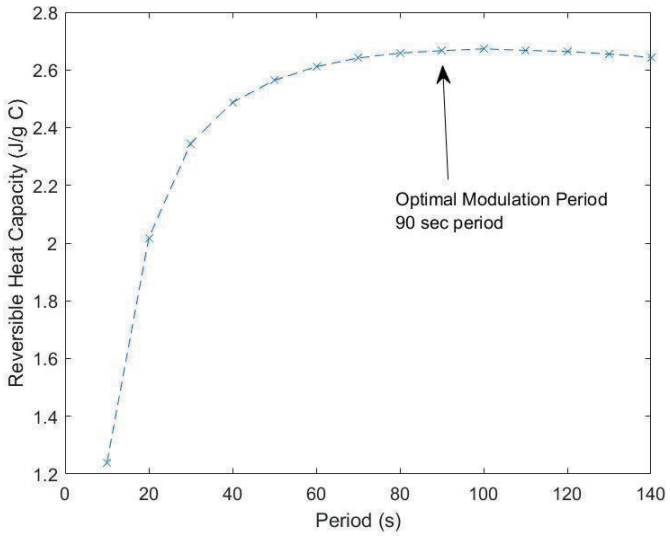


Figure 10. Isothermal MDSC test of Nylon-12 showing the reversible heat capacity as a function of period.

Further standard DSC experiments determined that a heating rate of 2℃ would be necessary based on the full width at half height, number of cycles, and period of modulation [13]. Representative data collected from an MDSC experiment are shown in Figure 11.

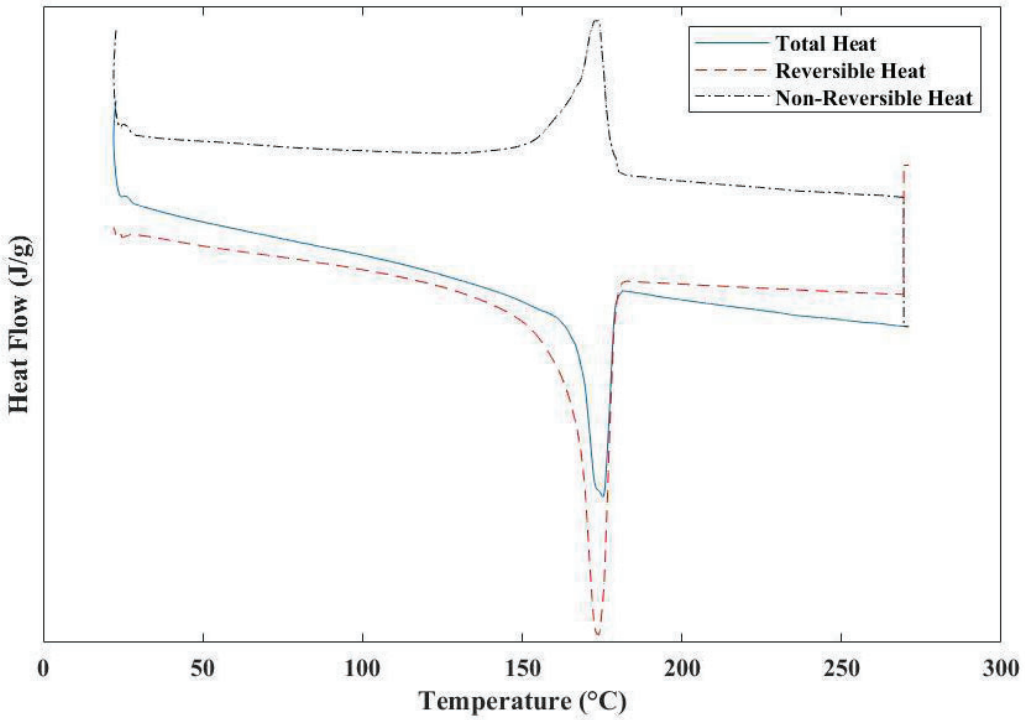


Figure 11. MDSC test of Nylon-12 sample.

By integrating the area under the curve of these transitions, microstructural changes of each heat component can be evaluated. The MDSC data from the first heating cycle were used to determine the percent crystallinity of the sample by comparing the enthalpy of fusion of each sample evaluated to that of a 100% crystalline Nylon-12. In calculating the percent crystallinity, the *reversible heat flow* was used, as that is the portion of the heat flow responsible for the thermodynamic transition. The relationship between the heats of fusion and the percent crystallinity of the sample is expressed as:

$$x^c = \frac{H}{H_0}\frac{\rho_a}{\rho_c}\left[1 - \left(1 - \frac{\rho_a}{\rho_c}\right)\right] \quad (1)$$

where $\rho_a = 0.990\ g/cm^3$ and $\rho_c = 1.085\ g/cm^3$ are the densities of the amorphous and crystalline states, respectively [16, 17]. For example, the Nylon-12 SLS unirradiated sample has a reversible heat flow value of $H \approx 99.95\ J/g$. The value of a completely crystalline Nylon-12 sample is shown to be $H_0 \approx 245\ J/g$, resulting in a percent crystallinity of ~34% [15]. This approach for calculating percent crystallinity is only valid for the Nylon-12 SLS because the density values are not accurate for NylonG or Nylforce CF.

Table 2. Reversible heat flow as measured in MDSC tests of each AM material at varying radiation doses measured in J/g. Percent crystallinity is calculated for Nylon-12. Data for 0 MRad represents tests done in triplicate with stdev in parentheses; data for 1-20 MRad doses were obtained from a single set of samples.

Dose (MRad)	Nylon-12		NylonG	Nylforce CF
	Rev Heat (J/g)	X_c (%)	Rev Heat (J/g)	Rev Heat (J/g)
0	99.95 (0.98)	34.0	108.9 (0.74)	120.9 (0.86)
1	81.94	27.8	96.33	118
5	78.8	26.8	112.4	111.9
10	96	32.6	116.4	110
15	89.6	30.4	118	99.3
20	79.86	27.1	101	104.2

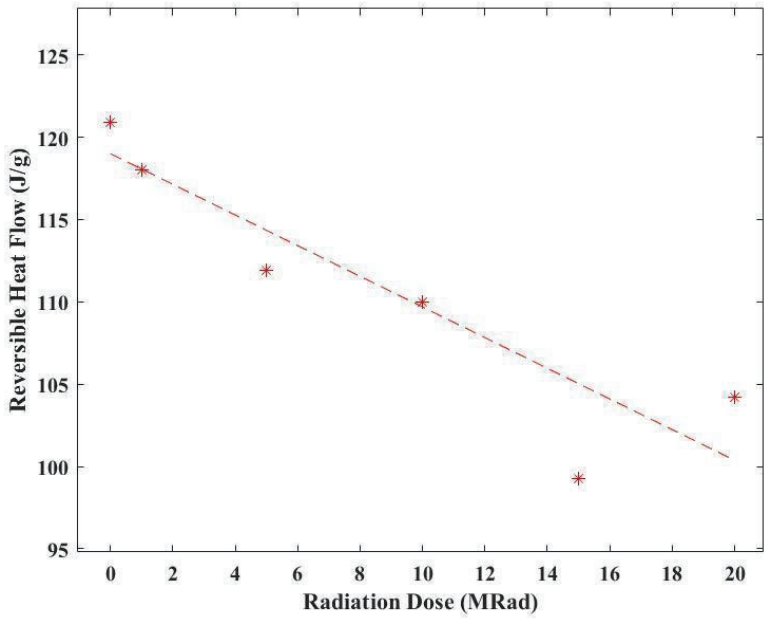


Figure 12. Plot of reversible heat flow as a function of radiation dose with linear regression line for Nylforce CF

Based on the data shown in Table 2 and the plot in Figure 12, only Nylforce CF exhibits a linear correlation between the increasing irradiation and reversible heat flow (R^2 = 0.83 when the plotted data are evaluated by linear regression). On the other hand, no trend was observed in the

reversible heat flow of any NylonG sample. It is postulated that differences in response between NylonG and Nylforce CF is due to the nature of the short fiber-filler used. NylonG is filled with insulating glass microfibers, while the Nylforce CF are filled with conductive carbon microfibers, which may directly impact their fate during irradiation and/or subsequent thermal analysis in the DSC. The conductive carbon fiber filler will more likely provide a path for heat and/or energy (i.e., gamma radiation) to dissipate through the sample uniformly, impacting the interfacial adhesion of the composite. This may be disrupted to some extent by the presence of the insulating glass fiber filler. Without knowledge of the nature, type and amount of each filler, no further conclusions can be made from these data. While Nylon-12 does not exhibit a linear correlation (i.e., systematic drop in % crystallinity as irradiation dose increases), each of the irradiated samples do exhibit lower reversible heat flow (and therefore % crystallinity) than unirradiated samples, with a maximum 21.2% decrease at 20 MRad. Further TGA for specimens at all radiation conditions showed that the thermal stability decreased with radiation, confirming that the polymer structures were damaged. As was discussed in Section 1, it can be predicted that the mechanical properties of the material will suffer as a result of the structural changes induced by radiation exposure.

TGA data showed that the T_5 for each of the materials continued to decrease, meaning that the polymer required less and less heat for 5wt% of the material to pyrolyze. This is indicative of the polymer's bonds being severed and a less thermally stable material being left. Table 3 contains the data that shows these trends and the varying degrees of change can be seen in Figure 13. The most drastic change was found in the Nylforce CF which is consistent with the linear trend in decreasing reversible heat shown in MDSC results. Additionally, it can be concluded from the char yield data that the carbon filler is 4.5wt% and glass fiber filler is 7.5wt%.

Table 3. ΔT_5 and char yield data for various irradiation conditions of all nylon-based materials

Dose (MRad)	Nylon-12		NylonG	Nylforce CF
	Rev Heat (J/g)	X_c (%)	Rev Heat (J/g)	Rev Heat (J/g)
0	99.9	34.0	108.9	120.9
1	81.9	27.8	96.3	118.0
5	78.8	26.8	112.4	111.9
10	96.0	32.6	116.4	110.0
15	89.6	30.4	118.0	99.3
20	79.8	27.1	101.0	104.2

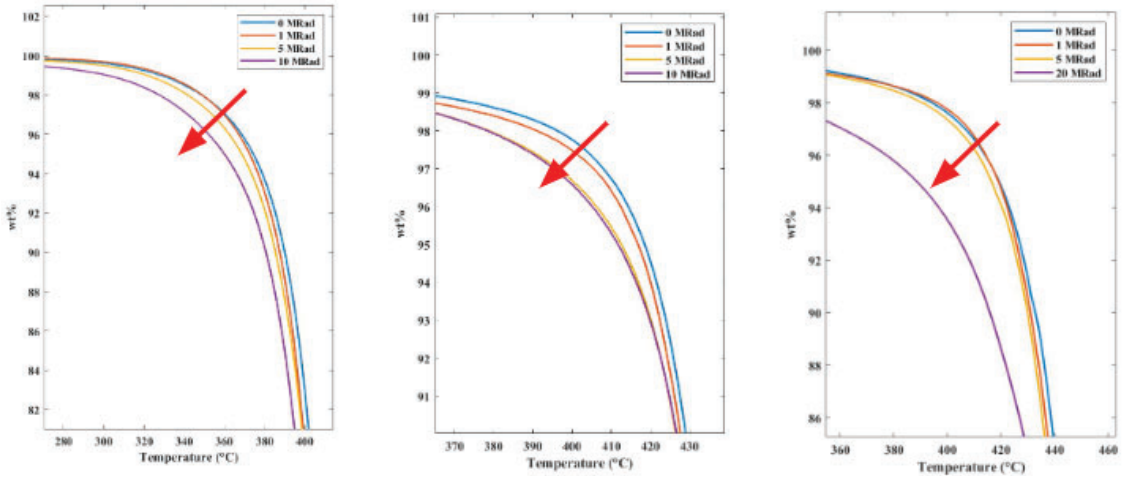


Figure 13. TGA results for all nylon-based materials at various radiation conditions

3.2 Mechanical Properties

3.2.1 SLS Nylon-12

The ultimate tensile strength of Nylon-12 manufactured via SLS using the Fuse1 printer was assessed using standard tensile test. Figure 14 shows the sample after failure and the location of failure is clearly within the gage section for each, indicating that failure was not due to stress concentration at the fillet of the specimen.

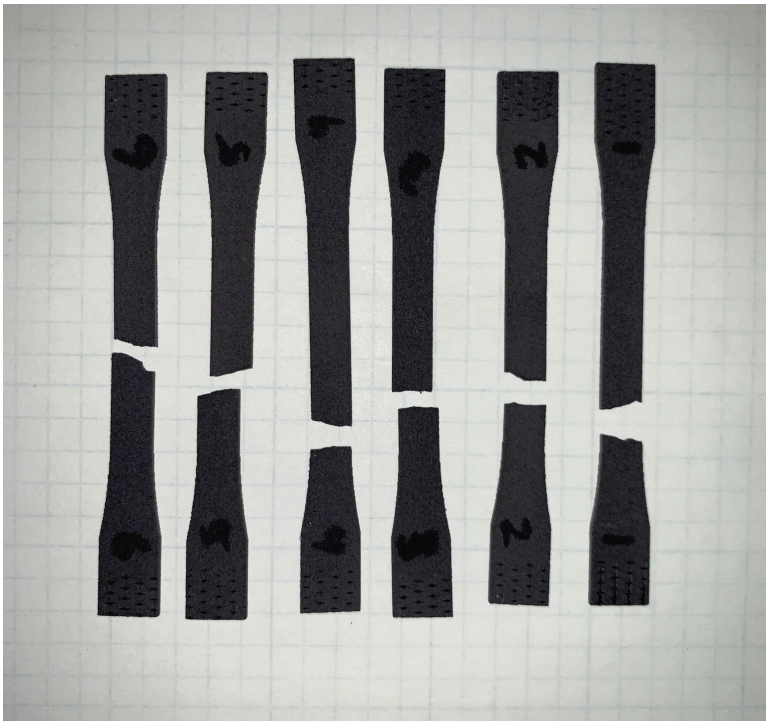


Figure 14. SLS tensile test specimens after reaching failure.

Initial tensile testing was conducted with samples of the SLS Nylon-12 that had been irradiated at 0.1, 0.5, 1, 5, and 10 MRad in what will be referred to as "batch 1" of irradiation. The specimens were then conditioned by leaving them in a dry box with desiccant for a period of 72 hours to avoid moisture uptake between irradiation and testing. Once conditioned, three specimens at each radiation level were tested. The results showed that at lower radiation levels (below 5 MRad), the ultimate tensile strength was largely unaffected. This behavior changed at a radiation level of 10 MRad, where the ultimate tensile strength dropped markedly. Figure 15 shows a box and whisker plot of the UTS measured for each specimen. For instance, from 1 to 10 MRad the tensile strength dropped from 4.36 to 3.33 ksi. Additionally, the specimens began shattering at failure. The gage sections of all specimens were broken in more than one place and sent ejected fragments of Nylon-12 in multiple directions. This behavior was not seen in the fracture of specimens at any other radiation level, which suggests radiation caused brittle fracture.

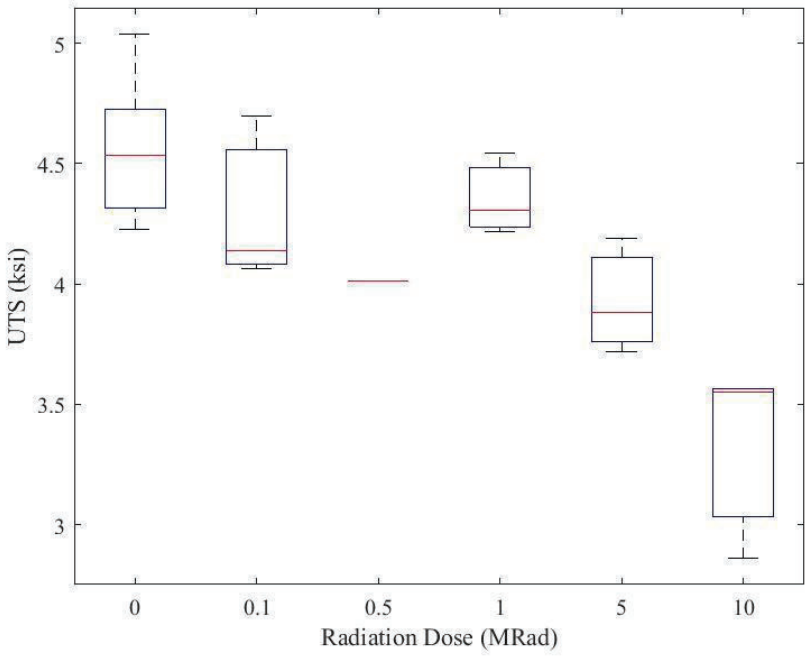


Figure 15. Box and whisker plot for batch 1 of Nylon-12 SLS

After initially testing batch 1, another round of testing was conducted on batch 2, which consisted of samples irradiated at 1, 5, 10, 15, and 20 MRad so 1) a reproducibility study could be performed and 2) higher doses could be tested. Batch 2, however, was not conditioned in a similar manner to batch 1 because TGA testing showed that the samples did not absorb moisture between the time of fabrication and testing. The same pattern of shattered sample behavior was observed in samples irradiated at 10 MRad and above suggesting brittle fracture, which was consistent with the specimen behavior from batch 1.

Similar to batch 1, batch 2 showed little variation among the measured UTS values for samples irradiated to the same dose as illustrated by the stress strain curves plotted in Figure 16 as an example data set.

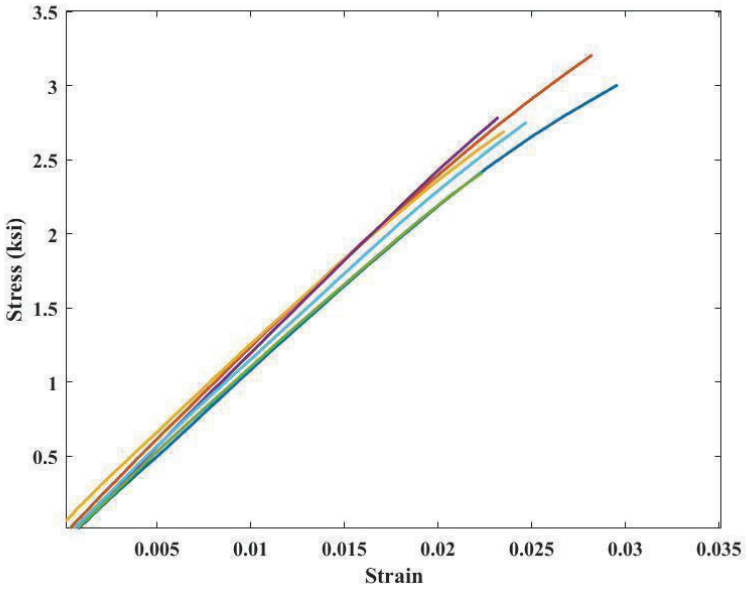


Figure 16. Stress-strain curves of all specimens from the 20 MRad sample set

The same pattern of shattered sample behavior was observed in samples irradiated at 10 MRad and above suggesting brittle fracture, which was consistent with the specimen behavior from batch 1.

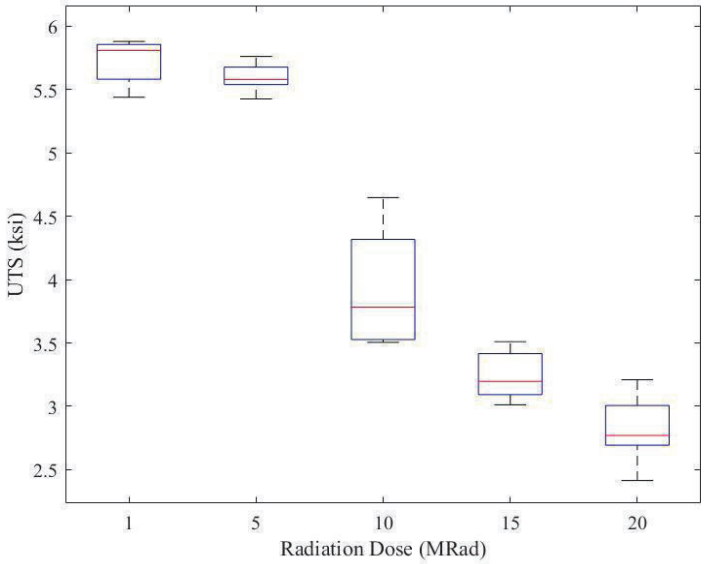


Figure 17. Average UTS of Nylon-12 SLS batch 2 with error bars based on standard deviation of six specimens for each sample

Representative stress strain curves of tensile testing of Nylon-12 SLS in batch 2 of irradiation showed that as the radiation dose increased, the UTS of the specimen decreased and the ductility, as measured by strain at failure, decreased as a function of increasing dose. Batch 2 doses were 1, 5, 10, 15, and 20 MRad shown in Figure 18. A box and whisker plot summarizing the average behavior for multiple specimen conditions and the overall trend is shown in Figure 19 and summarized in Table 4. Similar to batch 1, the UTS stayed approximately constant from 1 to 5 MRad (5.73 to 5.59 ksi, respectively) then dropped off at 10 MRad (3.93 ksi).

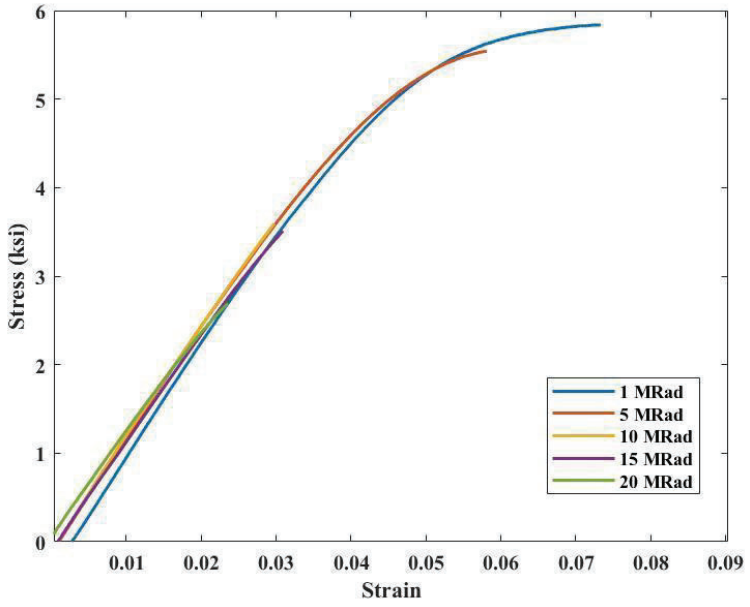


Figure 18. Representative stress strain curves for each irradiation dose in Nylon-12 SLS

Average UTS is plotted in Figure 19. There was a clear decrease in the UTS as a function of increased radiation dose regardless of batch. However, the measured UTS of batch 1 was approximately 20% lower at the same measured dose. For instance at 10 MRad, the batch 1 sample had a UTS of 4.33 ksi and the batch 2 sample had a UTS of 3.93 ksi. This difference is attributed to the manufacturing process, because samples were fabricated in different builds between batches. TGA data showing that the polymer degradation was the same for materials tested immediately after printing and three months after printing occurred at the same temperatures (Figure 9) confirms that this change was not due to moisture absorption. Thus, it is concluded that batch to batch variation explains the difference. The reproducibility of the quality and mechanical properties for additive manufacturing is a critical issue and will need to be further investigated in the future.

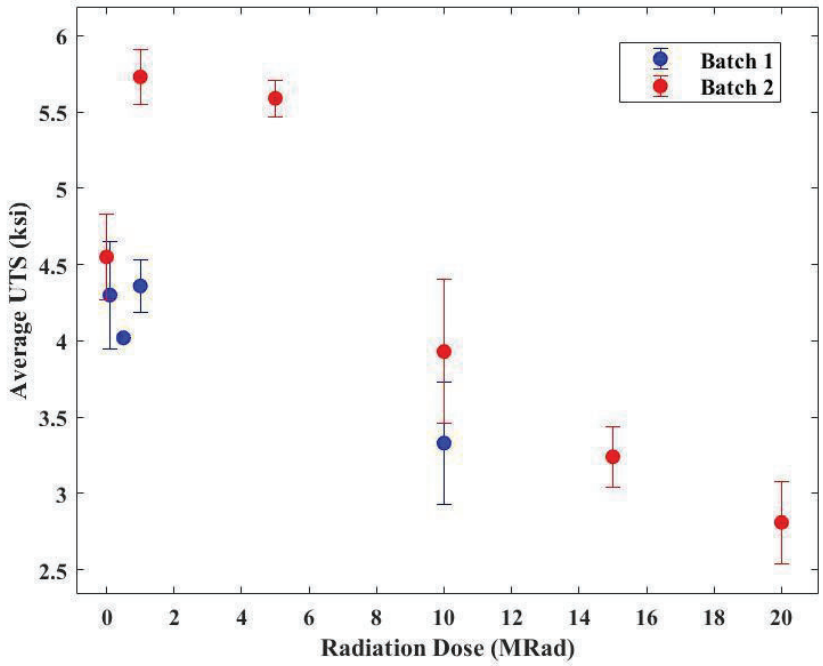


Figure 19. Comparison of Average UTS across batches.

Table 4. Summary of Nylon-12 SLS ultimate tensile stress

	Batch #	Dose (MRad)	Average Ultimate Strength (ksi)	Standard Deviation (ksi)
Nylon-12-SLS	Batch 1	0	4.55	0.28
		0.1	4.30	0.35
		*0.5	4.02	-
		1	4.36	0.17
		10	3.33	0.40
	Batch 2	1	5.73	0.18
		5	5.59	0.12
		10	3.93	0.47
		15	3.24	0.20
		20	2.81	0.27

* Of the samples tested at the 0.5 MRad condition, only one sample failed within the gage section.

The UTS in both Batch 1 and Batch 2 exhibited the same behavior; the strength is retained below 5 Mrad then decreases up to high dose (Figure 19). Furthermore, there was a decrease in ductility, as measured by percent elongation at the sample fracture (Figure 17). To determine the mechanism behind this observed softening, thermal analysis and fractography using a scanning electron microscope (SEM) were performed.

Scanning electron microscopy was used to image the fracture surface of one of the SLS, unirradiated samples after gold sputter coating to ensure a conductive surface. Images were taken with secondary electrons operating at 5 kV and are shown in Figure 20 with the entire surface shown in Figure 20a. From the fracture surface, there were localized areas with both ductile behavior as evidenced by the formation of microvoids and spider webbing (Figure 20c) and brittle behavior as evidenced by more faceted areas (Figure 20b).

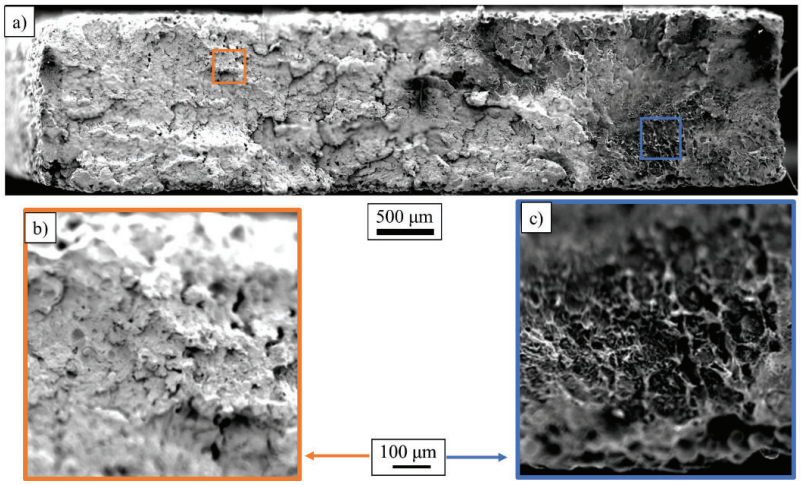


Figure 20. SEM micrographs of fracture surface of SLS, x-axis orientation (Batch 1- sample 3).

The SEM images taken of the fractured irradiated (10 MRad) specimen showed evidence consistent with the observations of a more brittle fracture, which was observed during the tensile tests where samples started to shatter at fracture. There are some localized areas of ductile behavior, but overall faceted surfaces indicating brittle fracture increased in areal density (Figure 21), which is consistent with the decrease in ductility observed in Figure 18.

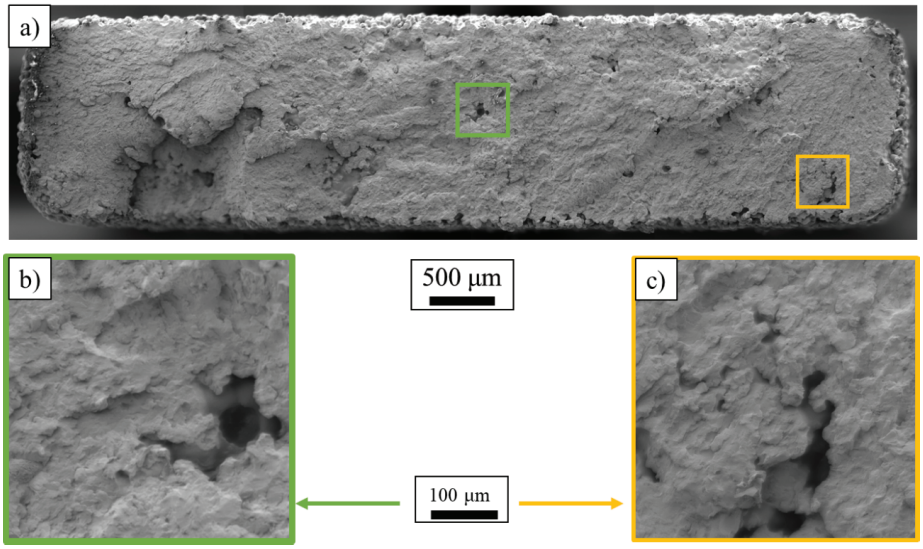


Figure 21. SEM images of the fracture surface of a 10 MRad SLS Nylon-12 specimen (Batch 1).

The trend toward increasingly brittle fracture continued up to 20 MRad, shown in Figure 22. Due to the increased brittle fracture, there was vertical and regular arrangement of facets, likely an effect of the laser path. This vertical arrangement of facets is spaced at an interval of approximately 100 µm which would indicate that it is a result of the layering process in SLS. As each successive layer is fused together, the layer thickness is nominally 110 µm according to FormLabs' documentation [18]. As the material becomes more brittle with irradiation, it has a tendency to create faceting along the layer interface upon fracture.

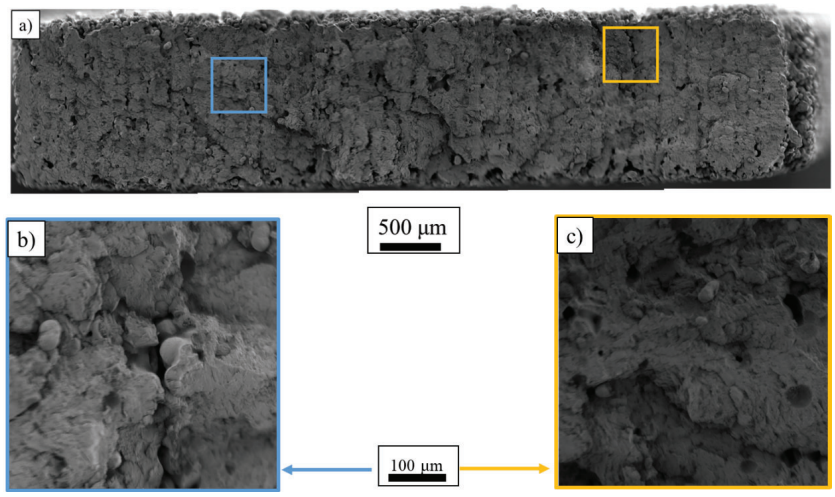


Figure 22. SEM images of the fracture surface of a 20 MRad SLS Nylon-12 specimen.

A feature that has been identified as pre-existing pores are tracked in the top row of Figure 23. At 0 MRad, spider webbing exists within the pore indicating ductility. As dose increases this spider webbing- which indicates ductile failure starts to disappear. It was especially apparent at 0 MRad and by 10 MRad has disappeared. The bottom row of Figure 23 shows other representative areas with more faceted behavior, especially as radiation dose increases.

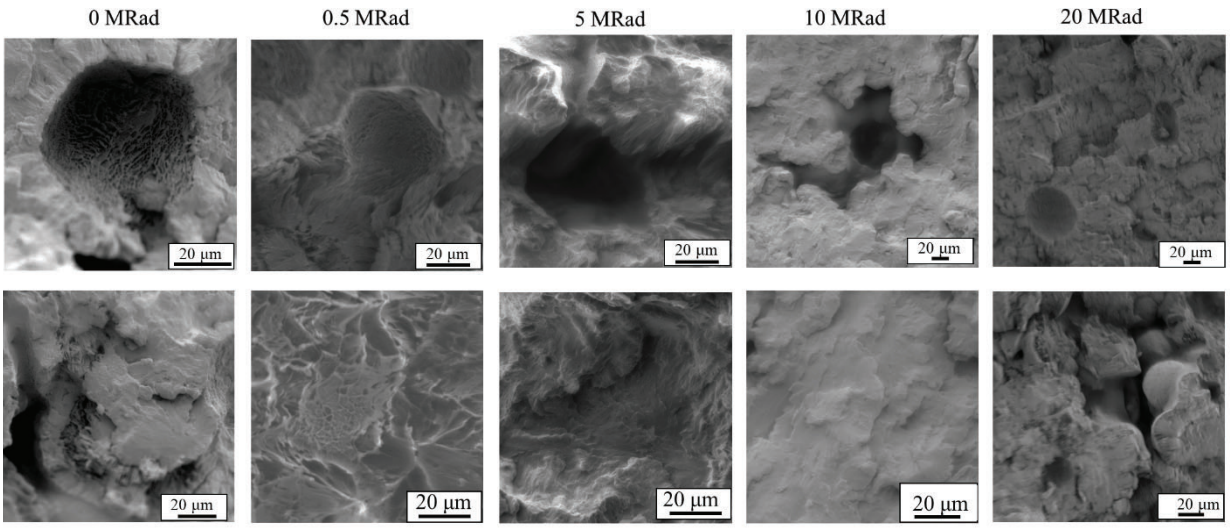


Figure 23. Representative areas of the fracture surface with increased radiation dose.

3.2.2 FDM NylonG

Tensile testing was also used to measure the ultimate tensile strength of NylonG samples fabricated using FDM. Figure 24 shows a representative sample for each radiation dose after irradiation and before tensile testing. The samples did not exhibit any discoloration or other physical deformation after irradiation.

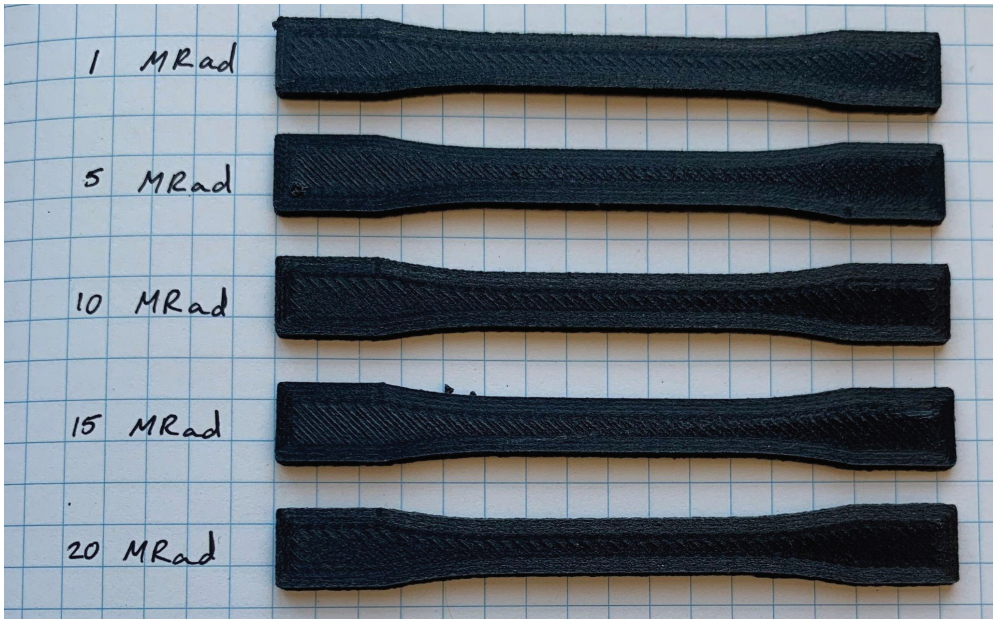


Figure 24. NylonG specimens after undergoing radiation, before tensile testing.

The specimens were tested under the tensile testing procedure outlined previously and an example dataset at 20 MRad is plotted in Figure 25. These results showed that the UTS of NylonG specimens was far less consistent than that of the Nylon-12 SLS samples. The UTS at

20 MRad ranged from 2.4-3.3 ksi; there was an average standard deviation of about 1.26 ksi across all radiation levels relative to the standard deviation in Nylon-12 SLS which was 0.27 ksi.

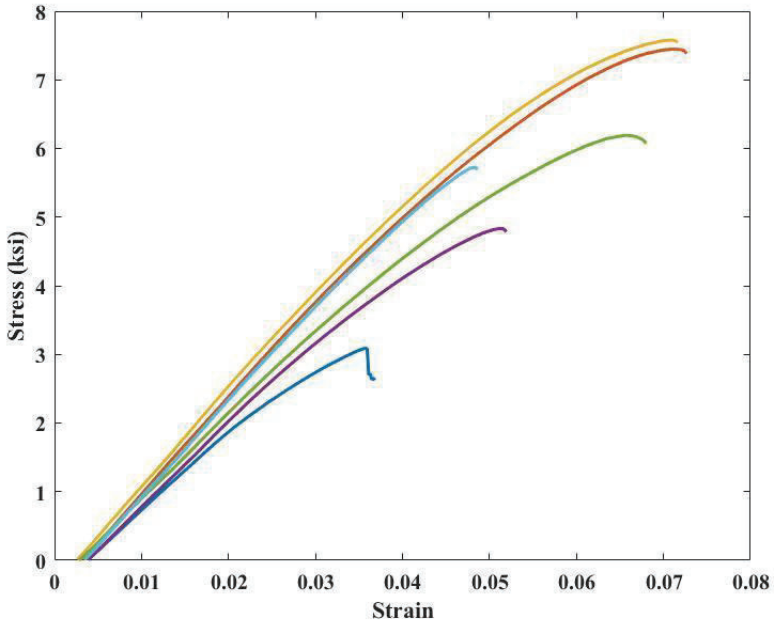


Figure 25. Stress-strain curves illustrating the variability within a sample set.

The variability among specimens in a sample set is likely a result of the inhomogeneity of internal structure of short fiber-filled materials. Due to the manufacturing process, which deposits filament with randomly oriented fibers, the internal structure of these materials can vary greatly. Nevertheless, despite the increased variability, the average UTS still decreased as a function of dose, which is shown in Figure 26 within a box and whisker plot that represents the confidence interval and error bars from a sample of 6 specimens. A summary of average values is also provided in Table 5. It is also worth noting that the average UTS is higher than that of Nylon-12 for all conditions, which is to be expected of a short fiber-filled polymer [19].

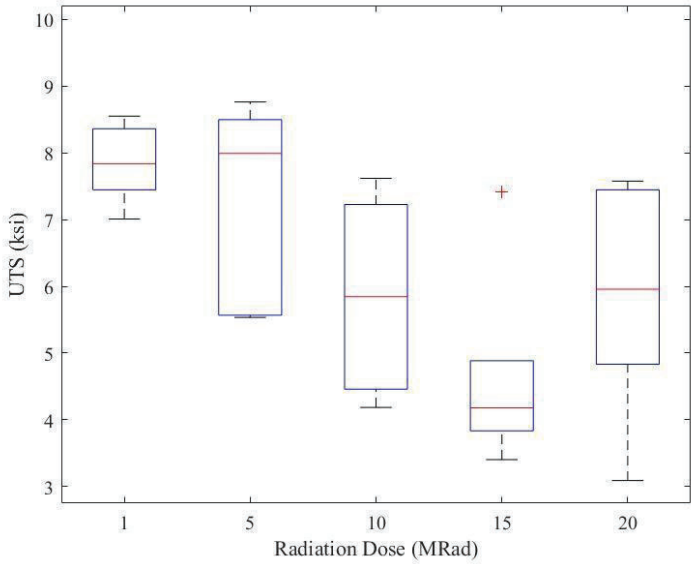


Figure 26. Average UTS with standard deviation error bars plotted as a function of radiation dose.

Table 5. Summary of NylonG data up to 20 MRad.

	Dose (MRad)	Average Ultimate Tensile Strength (ksi)	Standard Deviation (ksi)
Nylon G	0	6.88	0.98
	1	7.84	0.57
	5	7.39	1.46
	10	5.86	1.41
	15	4.65	1.46
	20	5.81	1.69

This evident decrease in average UTS is not reflected in the thermal properties data. Though there was no evidence that the percent crystallinity of the sample had decreased as a result of irradiation, it does appear that some structural changes had taken place that were not necessarily evident in the thermal testing (Figure 26). This may be due to the insulating nature of glass fibers and thus a less effective measurement by MDSC.

SEM imaging (Figure 27) of the fracture surfaces of NylonG FDM 0 MRad showed various regions of brittle and ductile fracture as observed in Nylon-12. The most obvious difference is the presence of the short fiber-fillers in the microstructure. There was also no apparent pattern or preferred orientation of these fibers as was postulated previously. The fibers are about 10 micrometers in diameter with varying lengths that are approximately an order of magnitude larger (Figure 27, 28).

The fracture surfaces of two different specimens irradiated to the same dose varied greatly (Figure 29). This is consistent with the tensile testing data, with all of the samples exhibiting a much larger standard deviation and confidence interval than that of non fiber-filled materials.

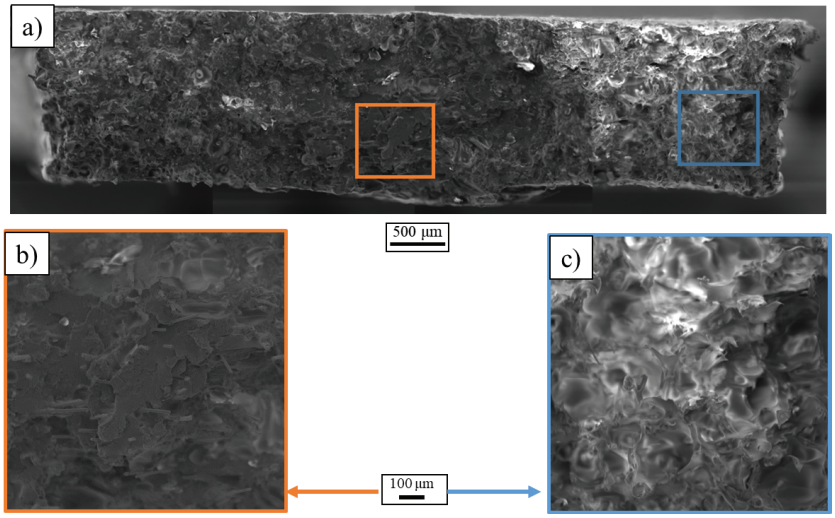


Figure 27. Representative fractography for NylonG 0 MRad.

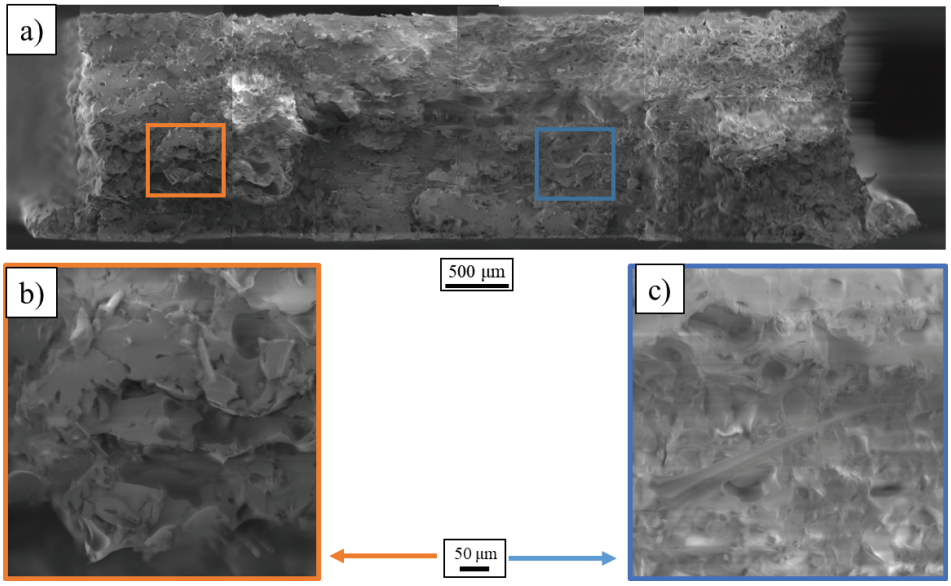


Figure 28. Representative fractography for NylonG 20 MRad (F26).

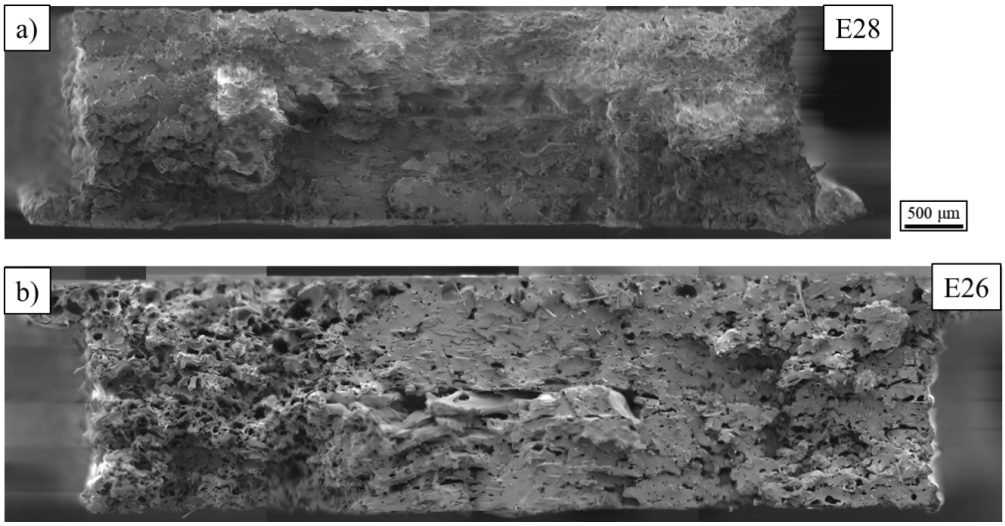


Figure 29. Fracture surfaces of Nylon G sample E28 and sample E26.

3.2.3 FDM Nylforce CF

The ultimate tensile strength is measured via tensile testing of the NylforceCF samples fabricated using FDM. Figure 30 shows a representative sample from each radiation dose after irradiation, but before tensile testing. The samples did not exhibit any discoloration or obvious changes as a result of irradiation.

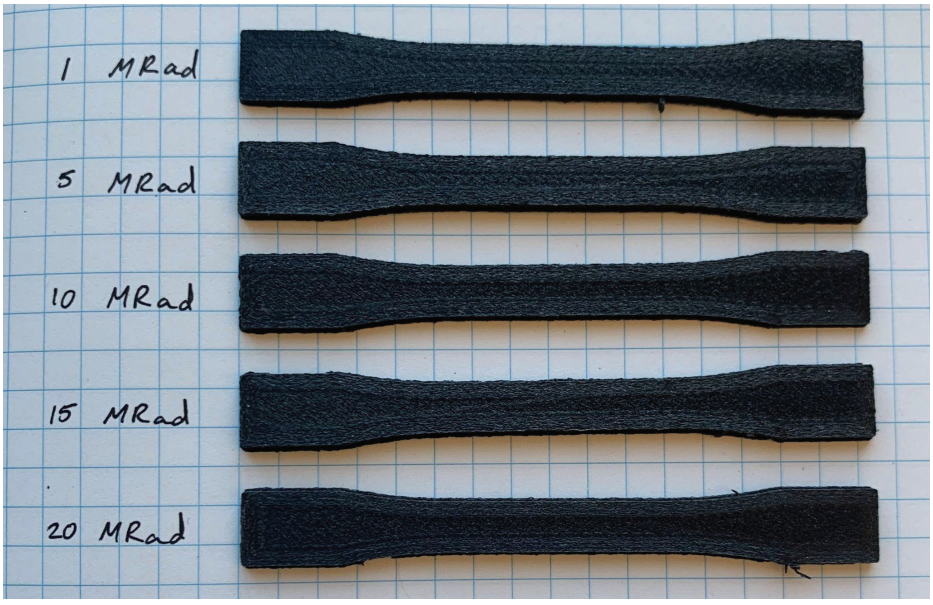


Figure 30. Nylforce CF samples after undergoing irradiation, but before tensile testing

Figure 31 shows the stress strain curve for 20 MRad. It is evident that there are significant inconsistencies in the UTS of the Nylforce CF specimens within each radiation dose; the only other material that exhibits this trend is NylonG. This inconsistency is due to the inherent

anisotropic nature of fiber-filled polymer composites [19]. The orientation of fibers is random within the polymer matrix and as a result, there is a high likelihood that the UTS of components manufactured using this method will have a high degree of variation. Despite the variation, the Nylforce CF samples exhibit an overall trend of decreasing average UTS with increased radiation dosage similar to all other nylon-based samples shown in Figure 32 and Table 6. This trend was muted relative to the decrease in strength observed in Nylon-12 but stronger than that observed in NylonG (Figure 26).

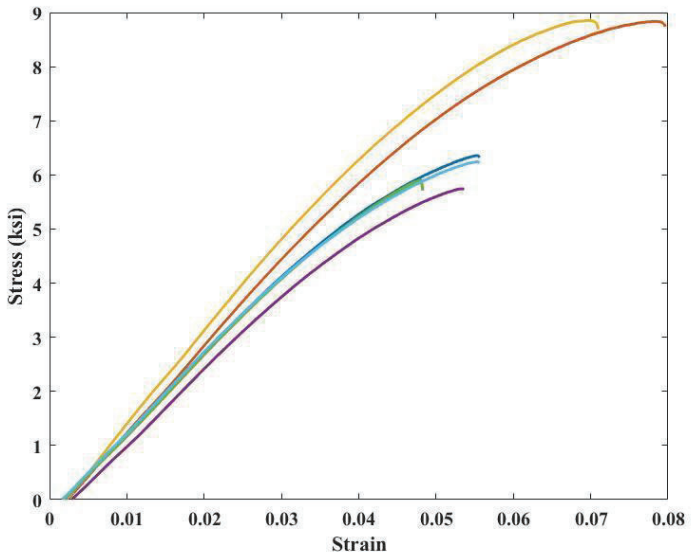


Figure 31. Stress-strain curve for Nylforce CF FDM 20 MRad sample set

Table 6. Summary of ultimate tensile stress in NylforceCF

	Dose (MRad)	Average Ultimate Strength (ksi)	Standard Deviation (ksi)
NylforceCF	0	8.95	0.26
	1	8.06	0.57
	5	8.85	1.03
	10	7.49	1.33
	15	7.04	1.14
	20	6.99	1.46

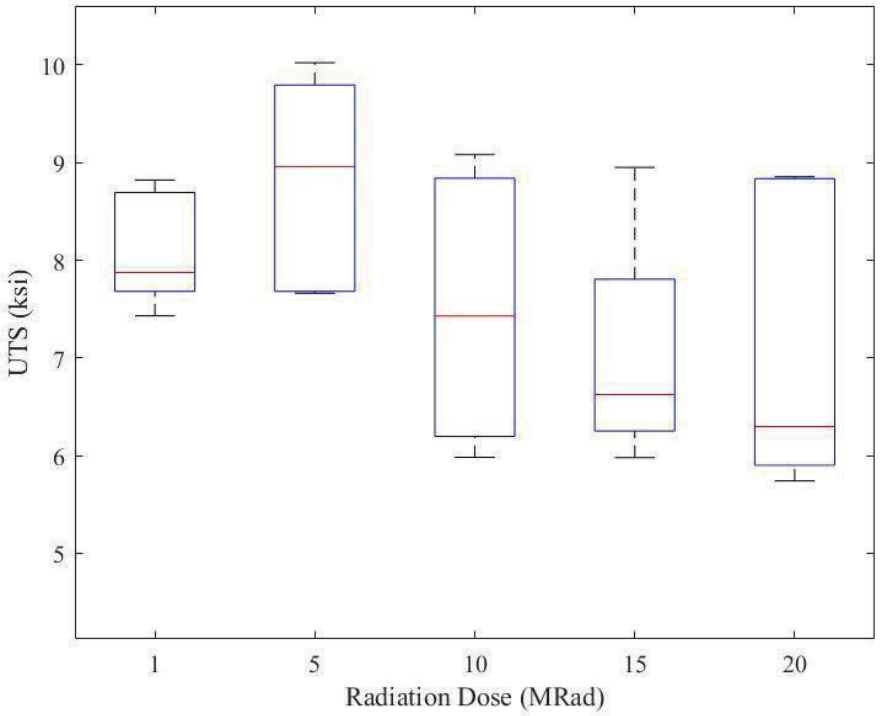


Figure 32. Average UTS with standard deviation error bars plotted as a function of radiation dose.

Nylforce CF 0 MRad exhibited the expected ductile behavior mixed with areas of brittle fracture with the carbon fibers oriented in random directions throughout the matrix. An example of each area on a fracture surface is shown in Figure 33. This is a likely cause of the variability that was present in the tensile data for this material. The 20 MRad condition also exhibited a similar mixture of ductility and brittleness on the fracture surface as shown in Figure 34. Figure 35 compares two different specimens in the same radiation dose sample, illustrating that the fracture surfaces can look vastly different resulting in largely different recorded UTS. Figure 35a exhibits a mixture of regions with both ductile and brittle fracture while Figure 35b exhibits a larger areal density of brittle fracture.

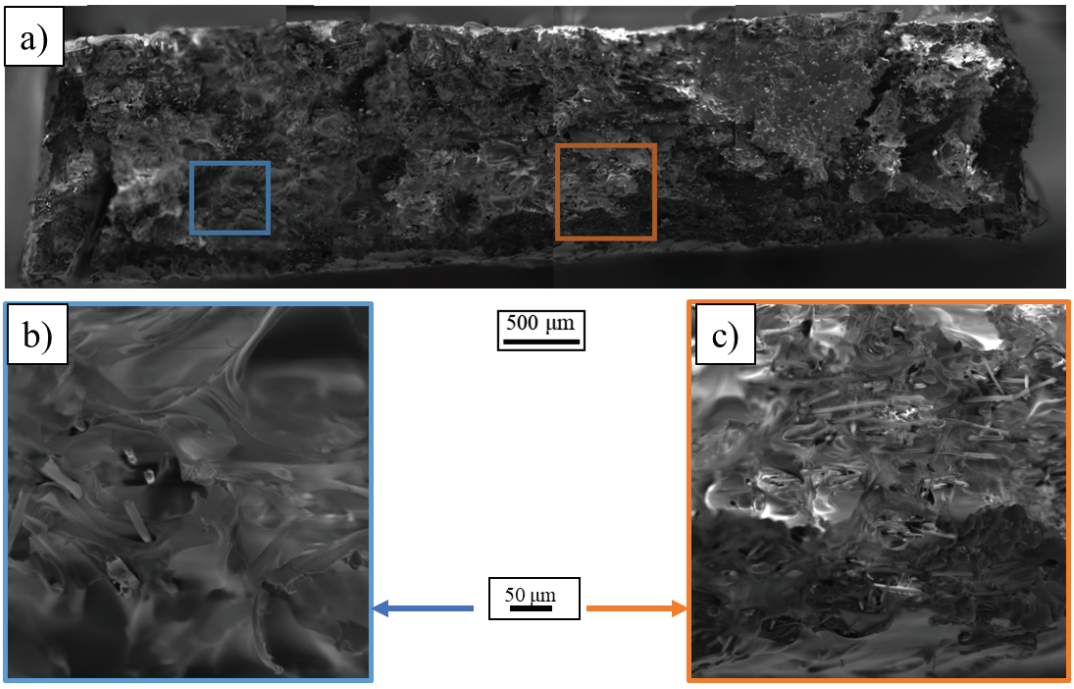


Figure 33. Fractography of Nylforce CF sample (0 MRad)

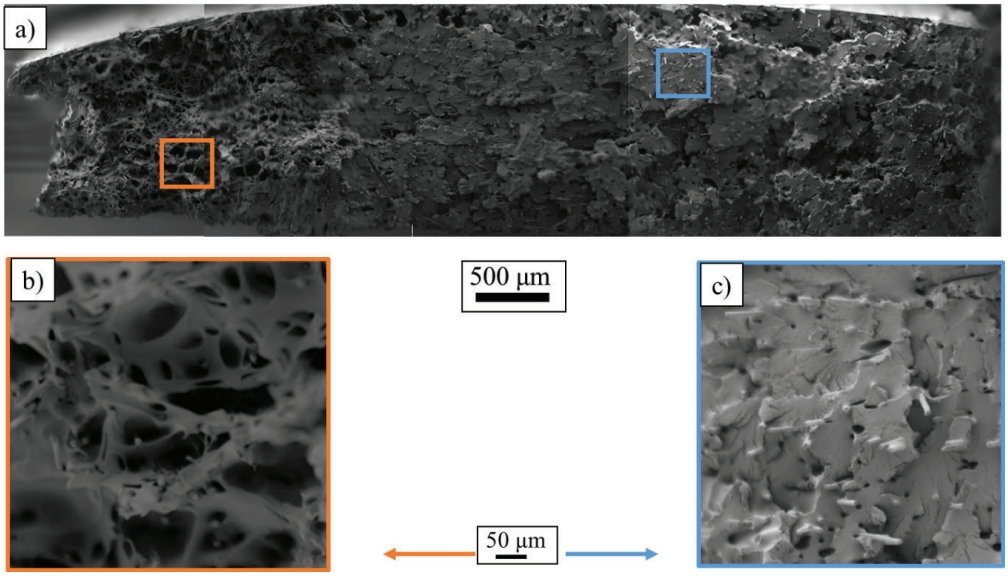


Figure 34. Fractography of Nylforce CF sample (20 MRad)

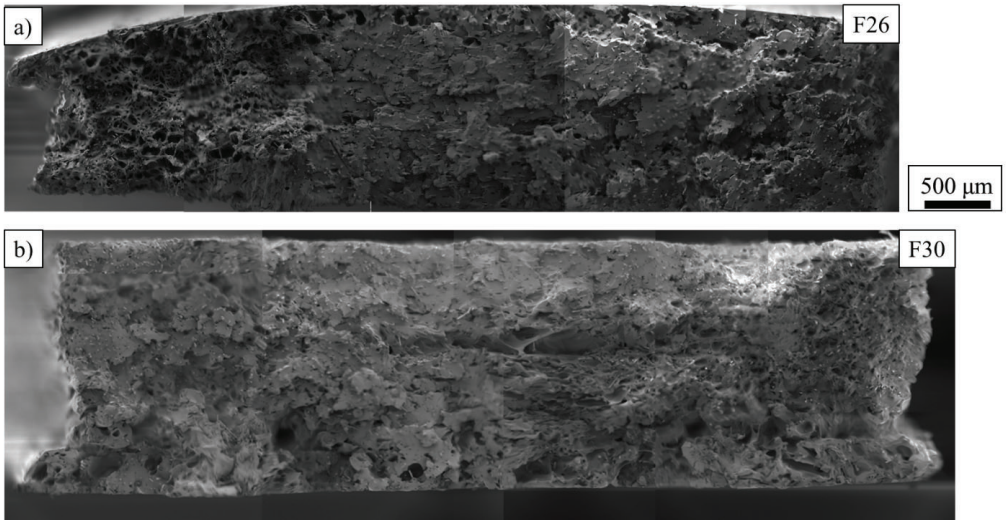


Figure 35. Comparison of fracture surface for sample F26 and F30.

3.2.4 Ultem 9085 FDM

Tensile tests measured the ultimate tensile strength of Ultem 9085 samples fabricated using FDM. The samples did not exhibit any discoloration or obvious changes after undergoing irradiation. Figure 36 shows a representative sample for each radiation dose after irradiation and before tensile testing.

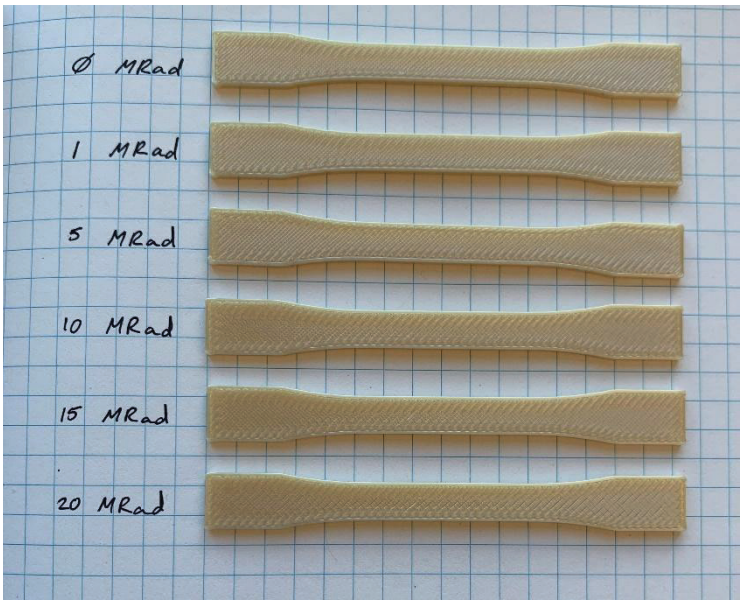


Figure 36. Ultem 9085 FDM specimens from each sample set after irradiation, but before tensile testing

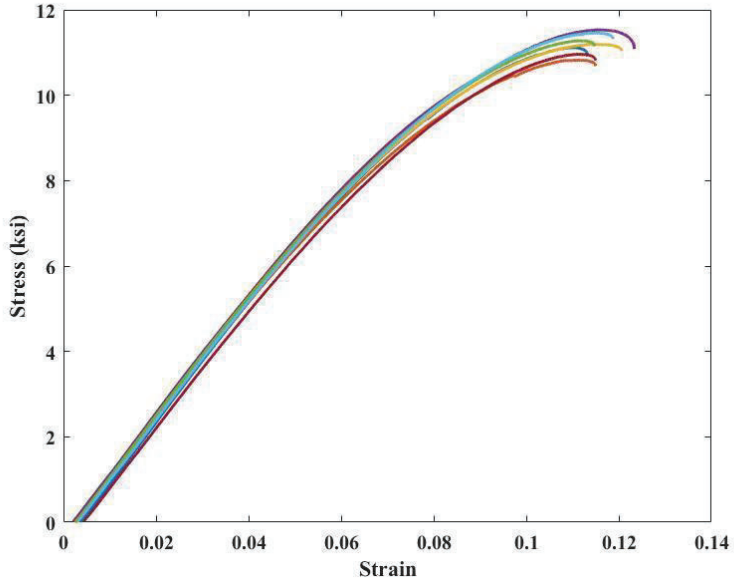


Figure 37. Stress-strain curves for all samples within the 20 MRad condition

Ultem 9085 FDM was also tested with two batches that were fabricated and irradiated separately. The samples from batch 1 showed very little variation with an average standard deviation of 0.182 ksi. Figure 37 shows the 20 MRad sample set as an example of the variation within one sample. This is consistent with the idea that there was a more consistent microstructure within homogeneous polymers without any fiber fillers. The average UTS of the samples was essentially unaffected by increased radiation dose, indicating that there was no effect caused by radiation. As shown in Figure 38 and summarized in Table 7, the average UTS does not change appreciably as a function of increased radiation dose.

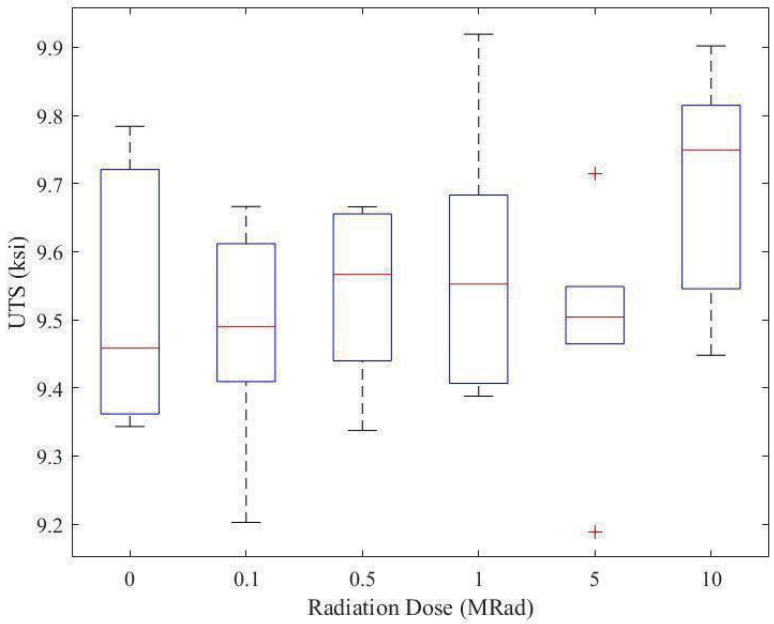


Figure 38. Ultimate tensile strength as a function of dose for FDM Ultem 9085 (batch 1).

Table 7. Summary for FDM Ultem-9085 ultimate tensile strength.

	Batch #	Dose (MRad)	Average Ultimate Stress (ksi)	Standard Deviation (ksi)
FDM Ultem 9085	Batch 1	0	9.53	0.20
		0.1	9.48	0.20
		0.5	9.54	0.13
		1	9.58	0.20
		10	9.70	0.18
	Batch 2	1	11.24	0.36
		5	11.21	0.34
		10	11.25	0.14
		15	11.25	0.14
		20	11.17	0.27

This data set does not provide a very complete picture of the radiation effects due to the fact that there were not any doses between 1 and 10 MRad that data was collected upon. A second batch of Ultem 9085 FDM was a more complete data set with more doses. Figure 38 shows the average UTS of samples tested in Batch 2.

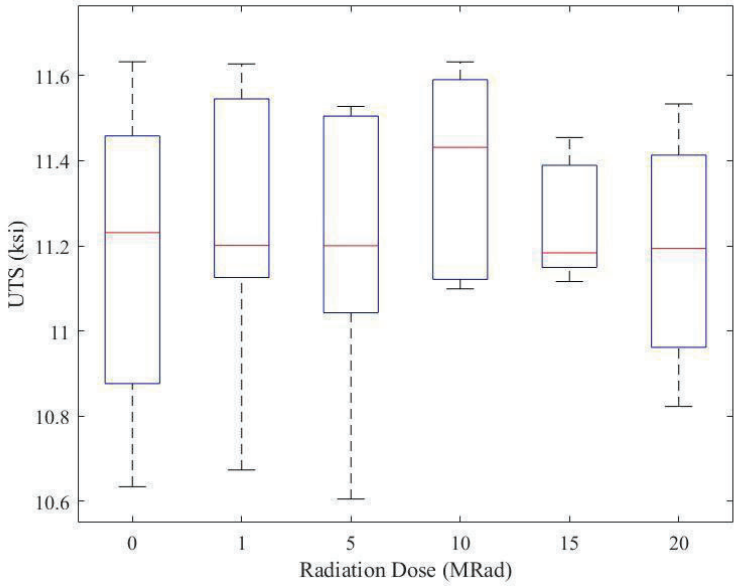


Figure 39. Ultimate tensile strength as a function of dose for FDM Ultem 9085 (batch 2).

It is evident from the plot in Figures 38 and 39 that there is indeed no effect on UTS as a result of increased radiation dose. This differs from the softening observed in all of the nylon-based materials discussed thus far. Unfortunately, the scope of this study does not include injection-molded variants of Ultem 9085 that would allow for the comparison between additively manufactured and conventionally manufactured samples. This initial data does suggest, however, that there was no damage done to the microstructure that caused changes in the mechanical properties.

3.2.5 Nylon-12 IM

Injection molded Nylon-12 served as a comparison point to determine if radiation effects on AM polymers differ from conventionally manufactured variants. The ultimate tensile strength of Nylon-12 samples fabricated using injection molding was assessed using tensile testing. The specimens were imaged prior to tensile testing (Figure 40) and exhibited a very stark, noticeable discoloration as a result of increased radiation exposure. The usually white, translucent polymer exhibited an increasingly yellow hue as the radiation dose increased.

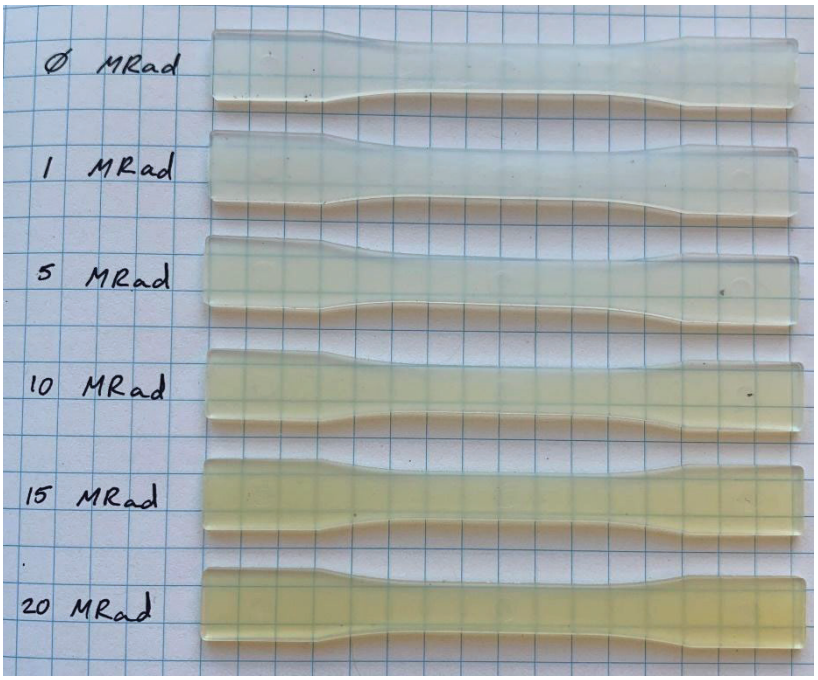


Figure 40. Irradiated Nylon-12 specimens before undergoing tensile testing

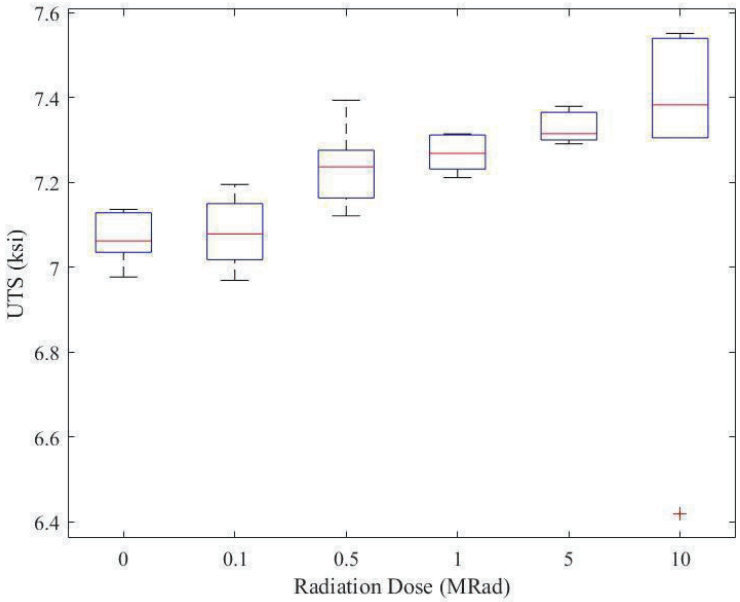


Figure 41. UTS of Nylon-12 IM batch 1.

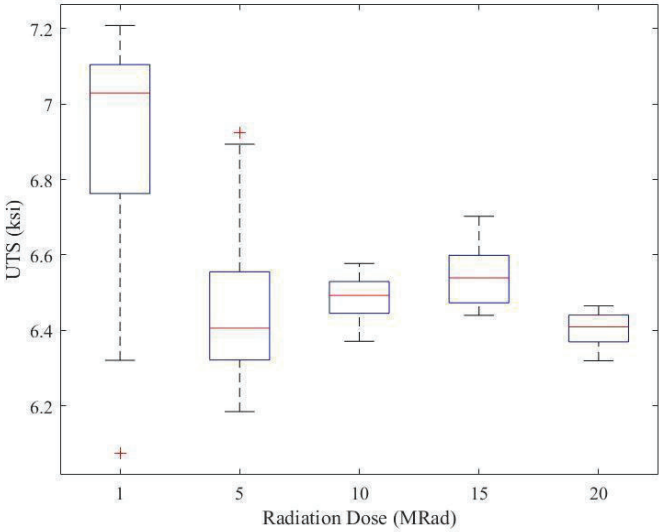


Figure 42. UTS of Nylon-12 IM batch 2.

The results indicated that there was not a decrease in UTS as a function of radiation dose in batch 1 (Figure 41) or batch 2 (Figure 42). Of note, after a dose of 1 MRad, all of the following doses showed a lower UTS though not in a consistent relationship. This differs from the damage observed in Nylon-12 SLS, which exhibited decreased UTS with irradiation. However, this result is consistent with studies that have suggested that discoloration of polymers due to radiation exposure are not correlated with any changes to mechanical properties [20]. Interestingly, there was batch to batch variation between the two sets of injection molded samples with Batch 2 samples approximately 10% lower at a given dose.

Table 7. Summary of IM Nylon-12 ultimate tensile strength.

	Batch #	Dose (MRad)	Average Ultimate Tensile Stress (ksi)	Standard Deviation (ksi)
Nylon-12-IM	Batch 1	0	7.071	0.064
		0.1	7.082	0.064
		0.5	7.238	0.096
		1	7.268	0.042
		10	7.264	0.425
	Batch 2	1	6.865	0.396
		5	6.472	0.263
		10	6.481	0.071
		15	6.543	0.084
		20	6.402	0.049

3.2.6 Effects of Fabrication Method

A central goal of this research was to determine whether the damage mechanisms present in standard thermoplastics are different from those present in additively manufactured thermoplastics. The best two materials to assess this comparison are Nylon-12 IM and Nylon-12 SLS. They are both the same variety of nylon, with only fabrication methods differing between the two. Additionally, the nominal tensile strengths are comparable due to specimens of each having an essentially 100% density infill. Thermal properties data was not run for the IM version of Nylon-12, so those properties cannot be compared. However, the measured tensile strength properties for each material were different.

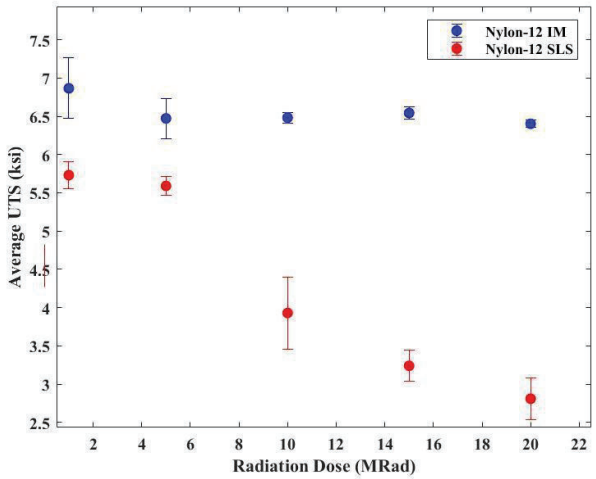


Figure 43. Comparison of UTS between Nylon-12 fabricated using IM and SLS.

Figure 43 plots both materials to illustrate the difference that fabrication method causes in radiation response. As noted in section 3.2.1, the average UTS of Nylon-12 SLS was decreased consistently as a function of radiation dose with the 20 MRad sample decreasing by as much as 38%. This was not the case with the Nylon-12 IM. The injection molded variant did not exhibit a trend of consistently decreasing average UTS values, however it did show that all irradiated conditions had a lower average UTS value than the unirradiated condition. The greatest percent difference was for the 20 MRad condition with a decrease of ~9%. Further investigation of thermal properties and the microstructure are needed to determine why the damage in Nylon-12 SLS is more significant than in Nylon-12 IM.

3.2.7 Effect of Fiber-Reinforced Additively Manufactured Composites

The presence of fiber fillers in the material impacted the effect of radiation on Nylon-12. It was also determined that the type of fiber filler caused different effects on the properties of the material. Figure 44 shows the Average UTS as a function of radiation dose with all three AM materials plotted. The NylonG and Nylforce CF have less reduction in tensile strength with increased radiation than the Nylon-12 did. However, all fiber-filled materials exhibited higher average UTS for any given radiation dose.

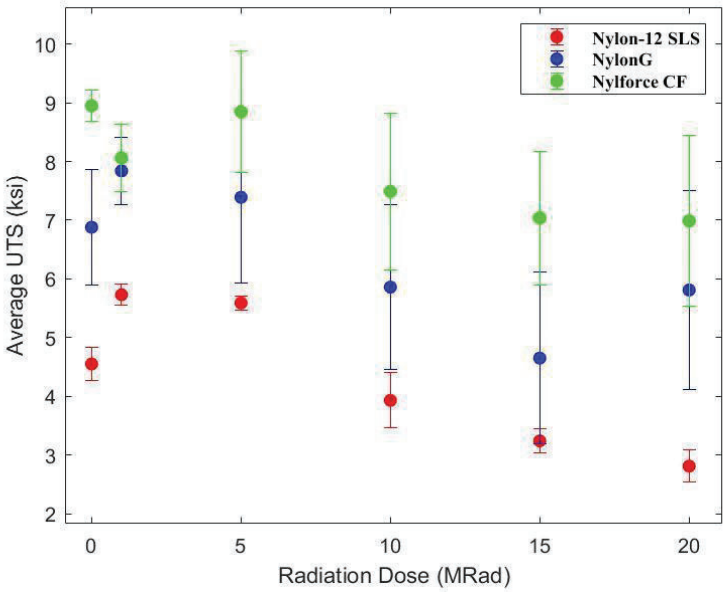


Figure 44. Comparison of Nylon-12 to Nylon G and Nylforce CF as a function of dose. Error bars were given as the standard deviation.

3.3 Comparison of Thermal and Mechanical Properties Effects

In some cases, the changes in thermal properties indicated structural changes that were verified in the mechanical properties. Specifically, Nylforce CF showed a decrease in the reversible heat flow as a result of increased radiation dose. This is verified in the mechanical data because as shown in Figure 45, the average UTS of the material decreases at a similar rate with the radiation dose. It is postulated that these effects are due to gamma radiation imparting enough energy to

sever polymer macromolecules in a chain scissioning process, reducing the crystallinity of the Nylon-12 within the composite.

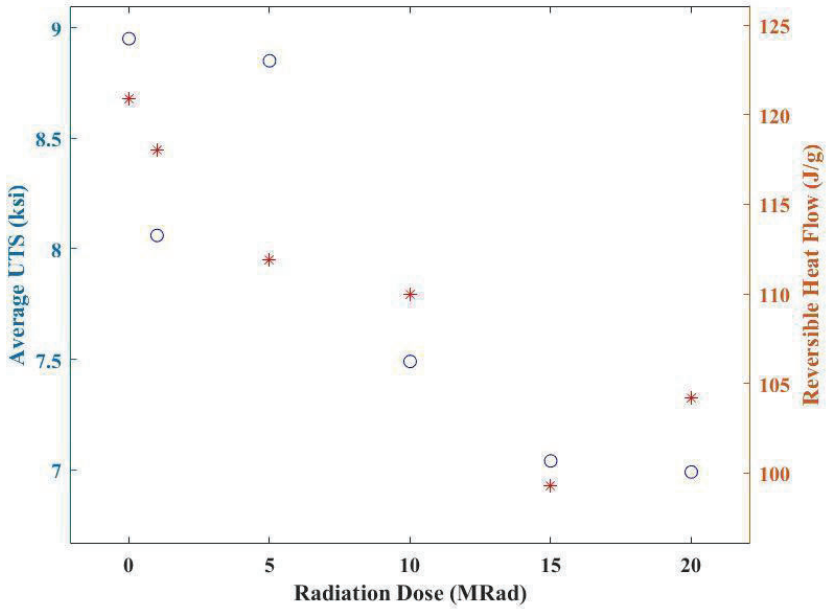


Figure 45. Comparison of the thermal and mechanical properties of Nylforce CF

This result is interesting because the same pattern of matching trends is not quite the same in the other two nylon-based polymers. The thermal and mechanical properties comparison of NylonG are shown in Figure 46.

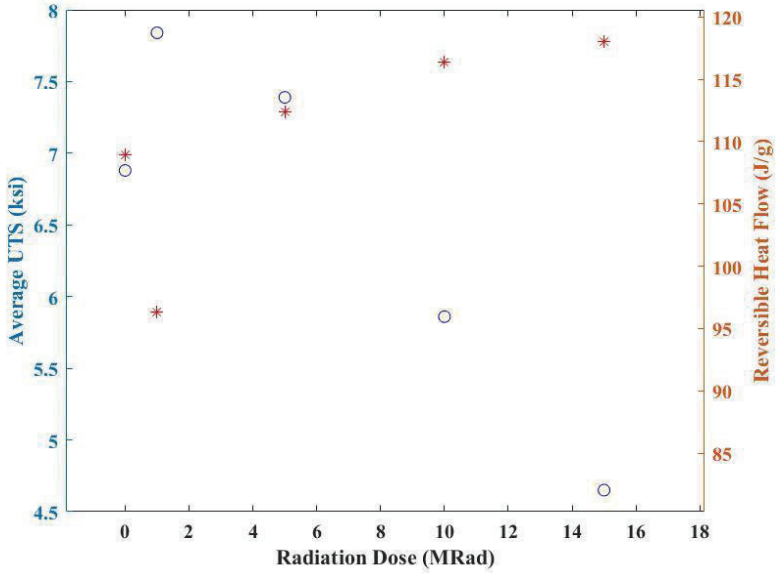


Figure 46. Comparison of the thermal and mechanical properties of NylonG

NylonG does show a similar decrease in the average UTS that Nylforce CF does, but there is no such correlation in the reversible heat flow. This difference is attributed to the nature of the insulating glass fibers in the polymer matrix and how they differ from short carbon fiber filler. Though the polymer matrix loses some of its strength upon irradiation, as both fibers likely present similar interfacial adhesion to the polymer, which would deliver similar mechanical impacts. However, the insulating nature of the glass fibers could disrupt energy flow (from heat during the MDSC experiment and/or from gamma radiation) through the fiber filled composite. Further systematic analysis of carbon and glass filled Nylon-12 fiber composites of known composition would be required in order to understand these effects more fully. Figure 47 shows the comparison between the thermal and mechanical properties of Nylon-12 SLS.

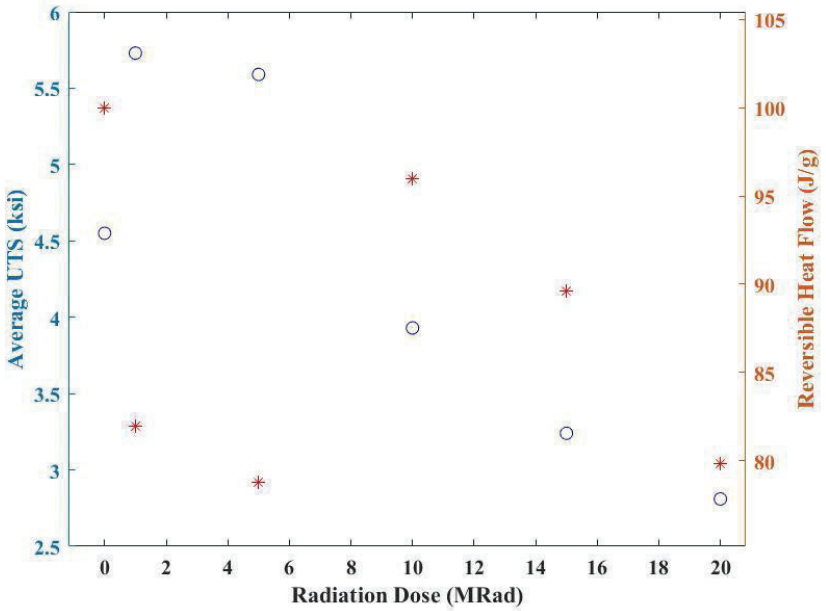


Figure 47. Comparison of thermal and mechanical properties for Nylon-12 SLS

Nylon-12 SLS has a similar trend to NylonG in that the average UTS decreases with radiation dose while the reversible heat flow remains without a clear, consistent trend. It is interesting, however, that the reversible heat flow is consistently lower for all irradiated cases than the unirradiated condition. In the absence of any fiber-filler, Nylon-12 is clearly impacted (thermally and mechanically) with radiation doses 1MRad or higher. Further investigation is necessary to determine the precise microstructural changes occurring that cause a consistently decreasing average UTS, but do not affect the reversible heat flow in the same manner.

4. Conclusions

4.1 Thermal Properties

The following conclusions can be drawn from the collected results:

- The temperature at which Nylon-12, Nylforce CF, and NylonG began to degrade during pyrolysis in N_2 is ~300°C, suggesting that all materials were Nylon-12 based.

- Nylforce CF is susceptible to radiation damage (more so than pure Nylon-12 or NylonG) as evidenced by the reversible heat flow and percent crystallinity of Nylforce CF decreasing ~20% as a result of increased radiation dose.
- NylonG showed no significant changes in reversible heat flow and percent crystallinity as a result of increased radiation dose.
- The reversible heat flow and percent crystallinity of Nylon-12 were reduced at radiation doses as low as 1MRad, with a maximum decrease of 4.1% observed at 10 MRad. All nylon-based samples had enthalpies of fusion within 6.8% percent of each other. This is still consistent with the conjecture that they are all made of a Nylon-12 base because the difference is most likely due to the fiber filler in the composite samples.

4.2 Mechanical Properties

The following conclusions can be drawn from the collected results:

- The difference between the ultimate tensile stresses of the samples printed in line with the *x*-axis and *y*-axis are not appreciable.
- The ultimate tensile stress of additively manufactured specimens decreased with increased radiation exposure, suggesting that radiation exposure has a weakening effect on the materials.
- Nylon-12 manufactured with the SLS process is more susceptible to radiation damage than the same material manufactured through injection molding. The average UTS of Nylon-12 SLS decreased by a greater margin than the Nylon-12 IM with each decreasing by 38% and 9% respectively.
- SEM imaging confirmed that the fracture behavior is more brittle for greater doses of radiation.
- It can also be concluded that radiation exposure of greater than 10 MRad in Nylon-12 will result in brittle fracture behavior. This is evidenced by the fact that specimens above this radiation threshold deformed less and showed brittle fracture surfaces in fractography. This behavior is not present in unirradiated Nylon-12 or samples exposed to less than 10 MRad.

5. Future Work

5.1 Material Characterization

Additional thermal studies will be conducted including MDSC tests for IM materials. It will also be necessary to conduct TGA testing of irradiated conditions for all materials. These data will be useful in determining whether the thermal stability of the material has degraded. Additionally, it would be beneficial to conduct more tensile testing on the NylonG and Nylforce CF to ensure that any variability is, in fact, due to the random nature of the fiber orientation. SEM imaging of more conditions across the test matrix would allow for a comprehensive comparison of the observed microstructures within the polymer matrix and determine whether there are structural changes not being detected by MDSC.

5.2 Additional Analysis

Expanding on this work, further investigation should be done on the effects that fiber fillers play in the radiation damage mechanisms of materials. It is also important to look at whether there is a possibility of using radiation at lower levels to induce crosslinking across layers that would help promote better layer adhesion, solving a pervasive problem in the additive manufacturing world.

6. References

[1] Gordon-Hagerty, L., et al. (2019). *Fiscal Year 2020 Stockpile Stewardship and Management Plan*. National Nuclear Security Agency.

[2] Kenney, M.E. (2013). *Cost Reduction Through the Use of Additive Manufacturing and Collaborative Product Life Cycle Management Technologies to Enhance the Navy's Maintenance Programs* [Master's thesis, Naval Postgraduate School]. Calhoun: The NPA Institutional Archive DSpace Repository. https://calhoun.nps.edu/bitstream/handle/10945/37648/13Sep_Kenney_Michael.pdf?sequence=1&isAllowed=y

[3] Meyer, G., et al. *Dielectric Materials for Use in Radomes and Other Applications*. General Plastics Manufacturing Company.

[4] *Trident II D-5 Ballistic Missile*. Global Security.org. https://www.globalsecurity.org/wmd/systems/d-5-pics.htm

[5] ISO / ASTM52900-15, Standard Terminology for Additive Manufacturing – General Principles – Terminology, ASTM International, West Conshohocken, PA, 2015, www.astm.org

[6] Singh, G., Gupta, A., Tripathi, O., et al. Powder Bed Fusion Process in Additive Manufacturing: An Overview. *Materials Today: Proceedings*. (2020). 26. 3058-3070. 10.1016/j.matpr.2020.02.635.

[7] Linear, Branched, and Cross-Linked Structures in Polymers. Mechanical Base. https://mechanicalbase.com/molecular-weight-and-degree-of-polymerization-terms/

[8] Balani, K., Verma, V., Agarwal, A., Narayan, R. Biosurfaces: A Materials Science and Engineering Perspective. John Wiley and Sons Inc.(2019).

[9] Hendrixson, S. Ultem, PEEK or PEKK? Choosing Between High-Temperature Plastics. Additive Manufacturing.(2019) https://www.additivemanufacturing.media/articles/ultem-peek-or-pekk-choosing-between-high-temperature-plastics

[10] Blaine, R. Determination of Polymer Crystallinity by DSC. TA Instruments.

[11] Otaguro, Harumi & Lima, L.F.C.P. & Parra, Duclerc & Lugao, Ademar & Chinelatto, Marcelo & Canevarolo, Sebastião. (2010). High-energy radiation forming chain scission and branching in polypropylene. Radiation Physics and Chemistry - RADIAT PHYS

CHEM. 79. 318-324. 10.1016/j.radphyschem.2009.11.003.

[12] ASTM, ASTM D638-14: Standard Test Method for Tensile Properties of Plastics, ASTM Stand., 2014, 08(01), p 1-15

[13] Choosing Conditions in Modulated DSC. TA Instruments: TN45.

[14] Wunderlich, Bernhard. Thermal Analysis. Boston: Academic Press, 1990. Print.

[15] Blaine, R. Polymer Heats of Fusion. TA Instruments. <http://www.tainstruments.com/pdf/literature/TN048.pdf>

[16] Minogianni, Chrysa & Gatos, Konstantinos & Galiotis, Costas. (2005). Estimation of Crystallinity in Isotropic Isotactic Polypropylene with Raman Spectroscopy. Applied spectroscopy. 59. 1141-7. 10.1366/0003702055012681.

[17] Li, Liangbin & Koch, Michel & Jeu, Wim. (2003). Crystalline Structure and Morphology in Nylon-12: A Small- and Wide-Angle X-ray Scattering Study. Macromolecules. 36. 1626-1632. 10.1021/ma025732l.

[18] FormLabs. Fuse 1 Technical Specifications.

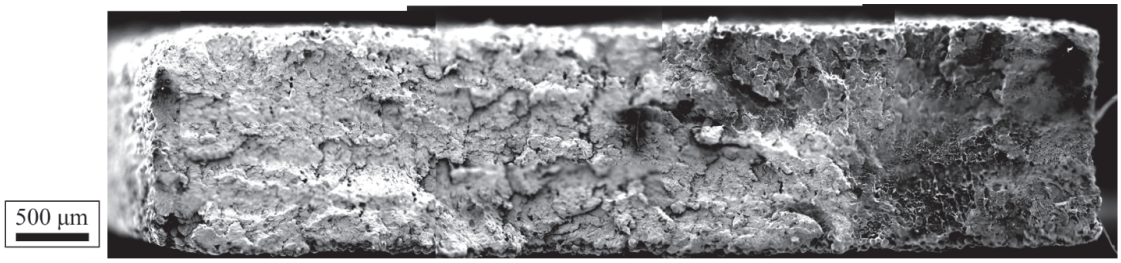
[19] Hemanth, Rajashekaraiah & Sekar, M. & Bheemappa, Suresha. (2014). Effects of fibers and fillers on mechanical properties of thermoplastic composites. Indian J Adv Chem Sci. 2. 28-35.

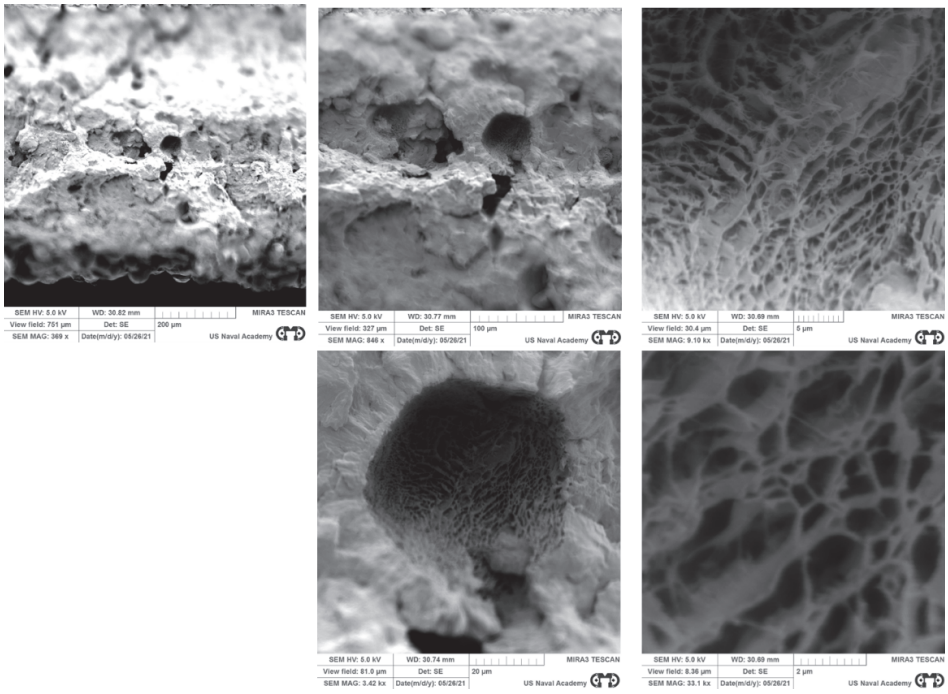
7. [20] Clough, R. L., Gillen, K. T., Malone, G. M., and Wallace, J. S., “Color formation in irradiated polymers”, *Radiation Physics and Chemistry*. (1996). 48. 583–594. 10.1016/0969-806X(96)00075-8.

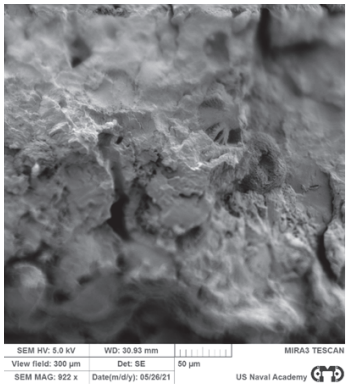
8. APPENDICES

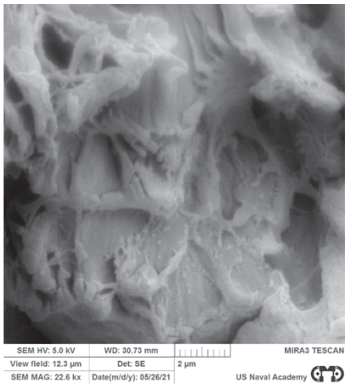
8.1 SEM of Nylon-12 SLS

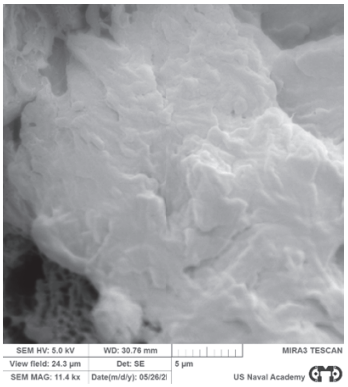
SLS Nylon 12- Batch 1 Sample 3

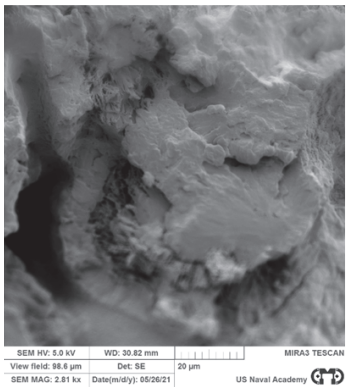


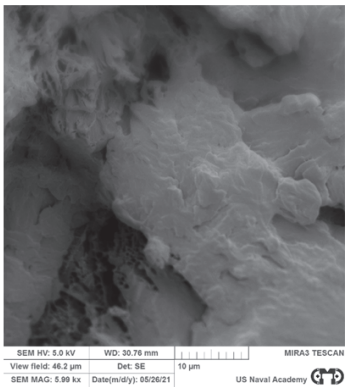


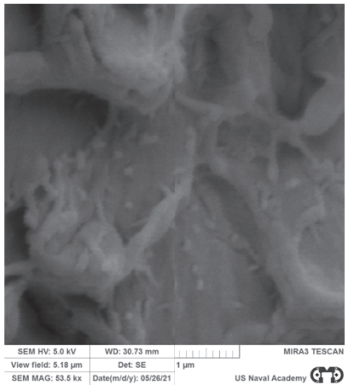

SEM HV: 5.0 kV
WD: 30.93 mm
MIRA3 TESCAN
View field: 300 µm
Det: SE
50 µm
SEM MAG: 922 x
Date(m/d/y): 05/26/21
US Naval Academy


SEM HV: 5.0 kV
WD: 30.73 mm
MIRA3 TESCAN
View field: 12.3 µm
Det: SE
2 µm
SEM MAG: 22.6 kx
Date(m/d/y): 05/26/21
US Naval Academy

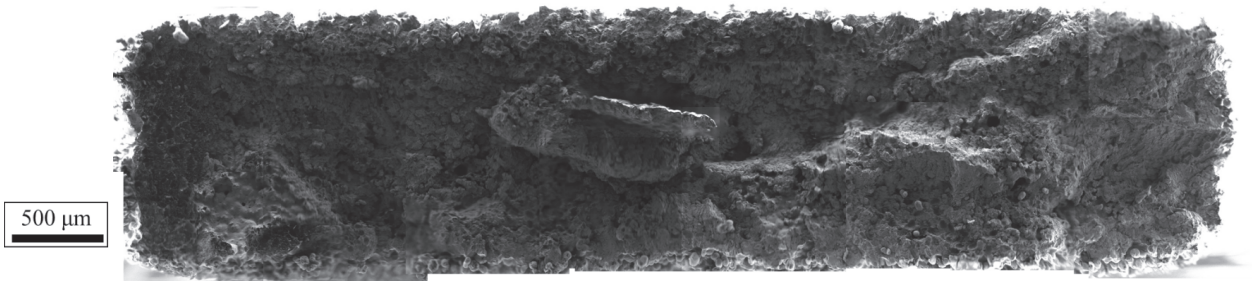

SEM HV: 5.0 kV
WD: 30.76 mm
MIRA3 TESCAN
View field: 24.3 µm
Det: SE
5 µm
SEM MAG: 11.4 kx
Date(m/d/y): 05/26/2
US Naval Academy

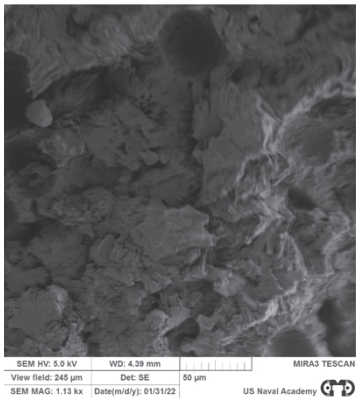

SEM HV: 5.0 kV
WD: 30.82 mm
MIRA3 TESCAN
View field: 98.6 µm
Det: SE
20 µm
SEM MAG: 2.81 kx
Date(m/d/y): 05/26/21
US Naval Academy

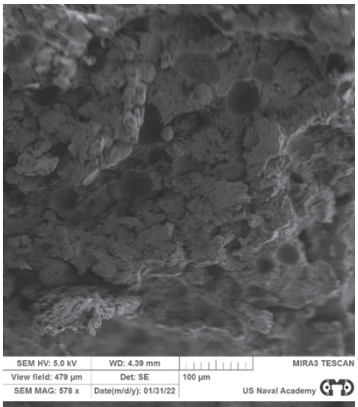

SEM HV: 5.0 kV
WD: 30.76 mm
MIRA3 TESCAN
View field: 46.2 µm
Det: SE
10 µm
SEM MAG: 5.99 kx
Date(m/d/y): 05/26/21
US Naval Academy

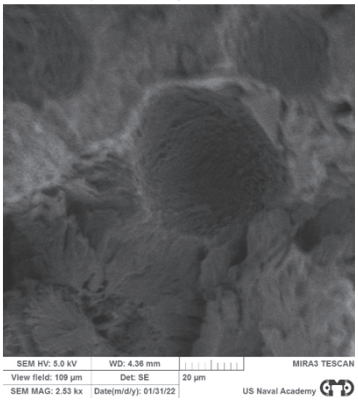

SEM HV: 5.0 kV
WD: 30.73 mm
MIRA3 TESCAN
View field: 5.18 µm
Det: SE
1 µm
SEM MAG: 53.5 kx
Date(m/d/y): 05/26/21
US Naval Academy

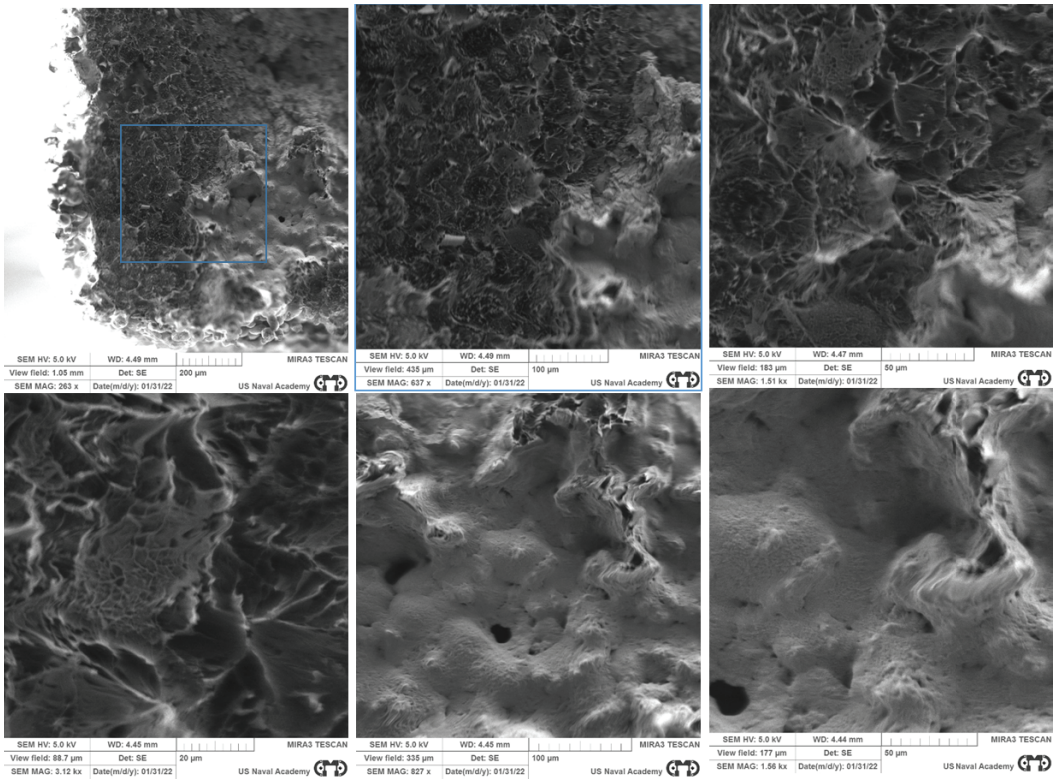
SLS Nylon 12- Batch 1- 0.5 MRad



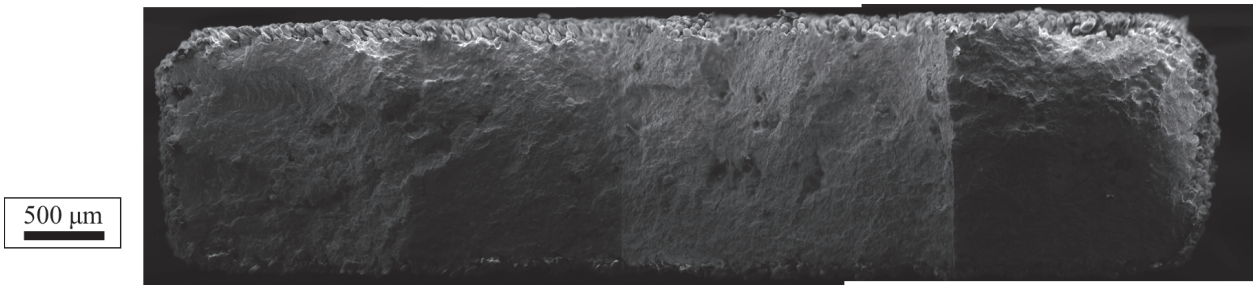


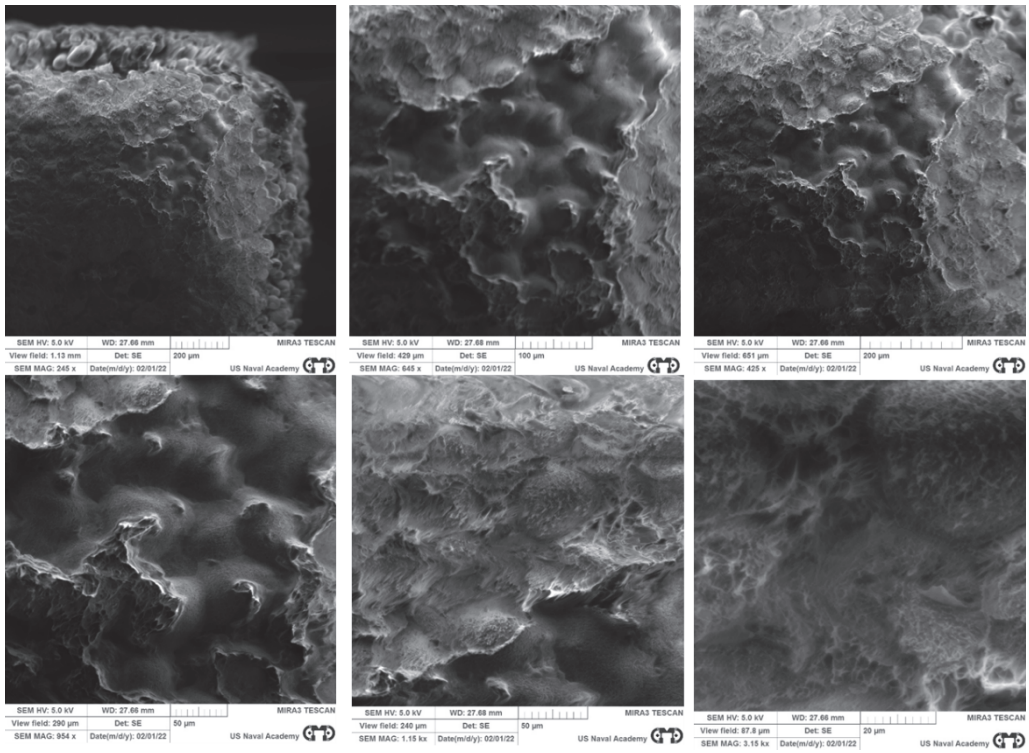


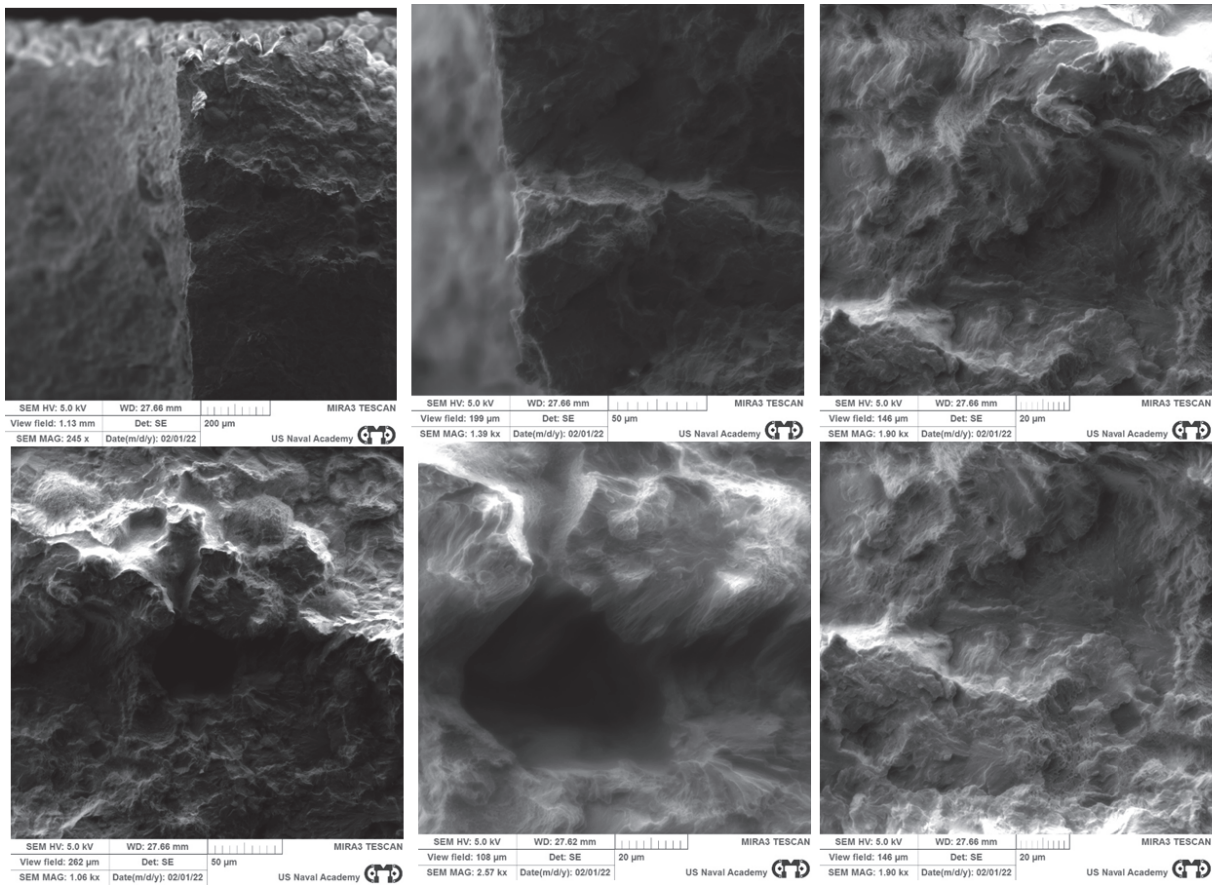



SEM HV: 5.0 kV
WD: 4.49 mm
MIRA3 TESCAN
View field: 1.05 mm
Det: SE
200 µm
SEM MAG: 263 x
Date(m/d/y): 01/31/22
US Naval Academy
SEM HV: 5.0 kV
WD: 4.49 mm
MIRA3 TESCAN
View field: 435 µm
Det: SE
100 µm
SEM MAG: 637 x
Date(m/d/y): 01/31/22
US Naval Academy
SEM HV: 5.0 kV
WD: 4.47 mm
MIRA3 TESCAN
View field: 183 µm
Det: SE
50 µm
SEM MAG: 1.51 kx
Date(m/d/y): 01/31/22
US Naval Academy
SEM HV: 5.0 kV
WD: 4.45 mm
MIRA3 TESCAN
View field: 88.7 µm
Det: SE
20 µm
SEM MAG: 3.12 kx
Date(m/d/y): 01/31/22
US Naval Academy
SEM HV: 5.0 kV
WD: 4.45 mm
MIRA3 TESCAN
View field: 335 µm
Det: SE
100 µm
SEM MAG: 827 x
Date(m/d/y): 01/31/22
US Naval Academy
SEM HV: 5.0 kV
WD: 4.44 mm
MIRA3 TESCAN
View field: 177 µm
Det: SE
50 µm
SEM MAG: 1.56 kx
Date(m/d/y): 01/31/22
US Naval Academy

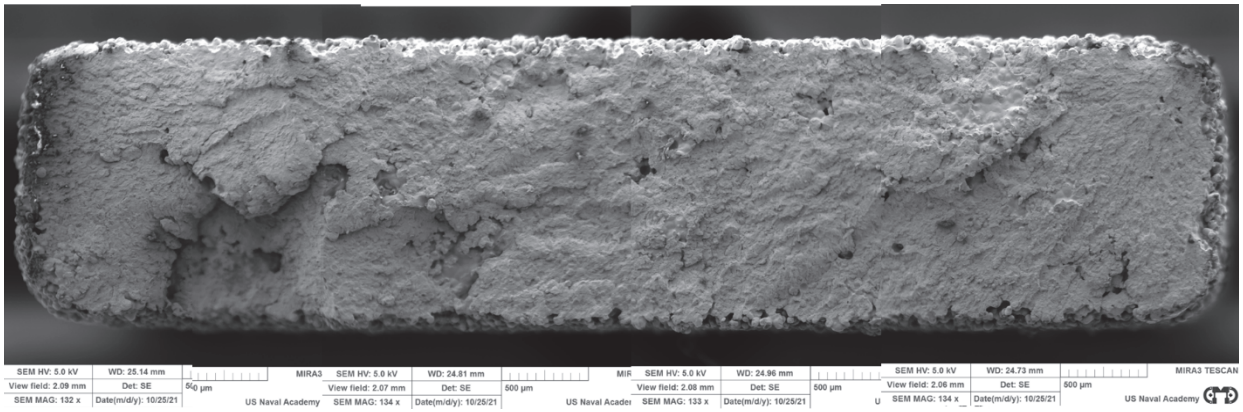
SLS Nylon 12- Batch 1- 5 MRad

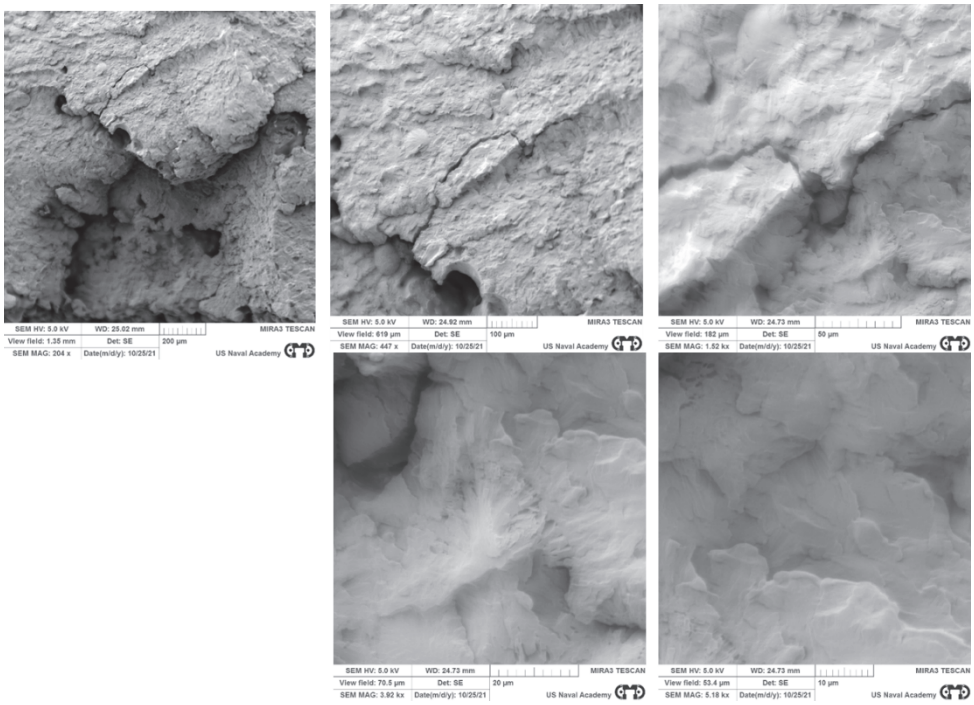


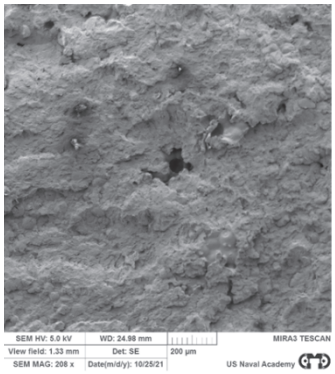


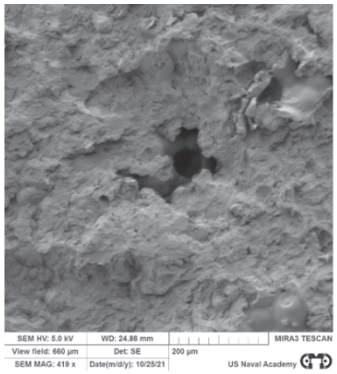

SEM HV: 5.0 kV
WD: 27.66 mm
MIRA3 TESCAN
View field: 1.13 mm
Det: SE
200 µm
SEM MAG: 245 x
Date(m/d/y): 02/01/22
US Naval Academy
SEM HV: 5.0 kV
WD: 27.66 mm
MIRA3 TESCAN
View field: 199 µm
Det: SE
50 µm
SEM MAG: 1.39 kx
Date(m/d/y): 02/01/22
US Naval Academy
SEM HV: 5.0 kV
WD: 27.66 mm
MIRA3 TESCAN
View field: 146 µm
Det: SE
20 µm
SEM MAG: 1.90 kx
Date(m/d/y): 02/01/22
US Naval Academy
SEM HV: 5.0 kV
WD: 27.66 mm
MIRA3 TESCAN
View field: 262 µm
Det: SE
50 µm
SEM MAG: 1.06 kx
Date(m/d/y): 02/01/22
US Naval Academy
SEM HV: 5.0 kV
WD: 27.62 mm
MIRA3 TESCAN
View field: 108 µm
Det: SE
20 µm
SEM MAG: 2.57 kx
Date(m/d/y): 02/01/22
US Naval Academy
SEM HV: 5.0 kV
WD: 27.66 mm
MIRA3 TESCAN
View field: 146 µm
Det: SE
20 µm
SEM MAG: 1.90 kx
Date(m/d/y): 02/01/22
US Naval Academy

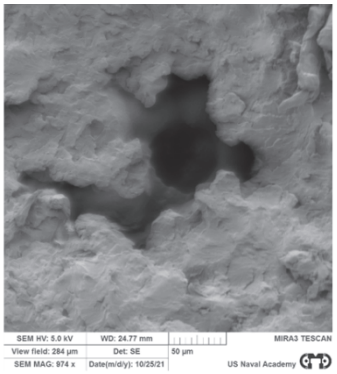
Nylon-12- Batch 1 10 MRad

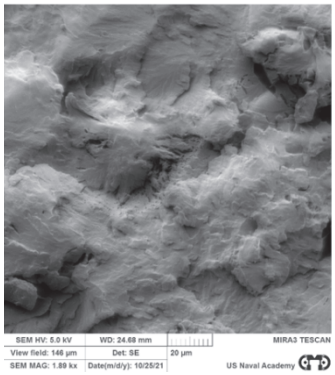


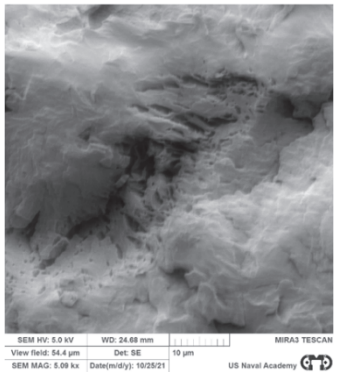


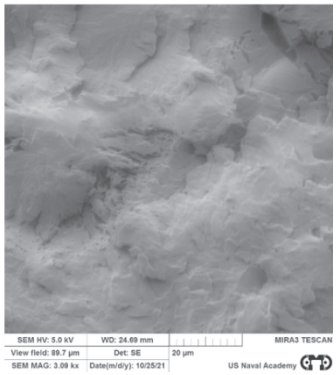

SEM HV: 5.0 kV
WD: 24.98 mm
MIRA3 TESCAN
View field: 1.33 mm
Det: SE
200 µm
SEM MAG: 208 x
Date(m/d/y): 10/25/21
US Naval Academy


SEM HV: 5.0 kV
WD: 24.86 mm
MIRA3 TESCAN
View field: 660 µm
Det: SE
200 µm
SEM MAG: 419 x
Date(m/d/y): 10/25/21
US Naval Academy

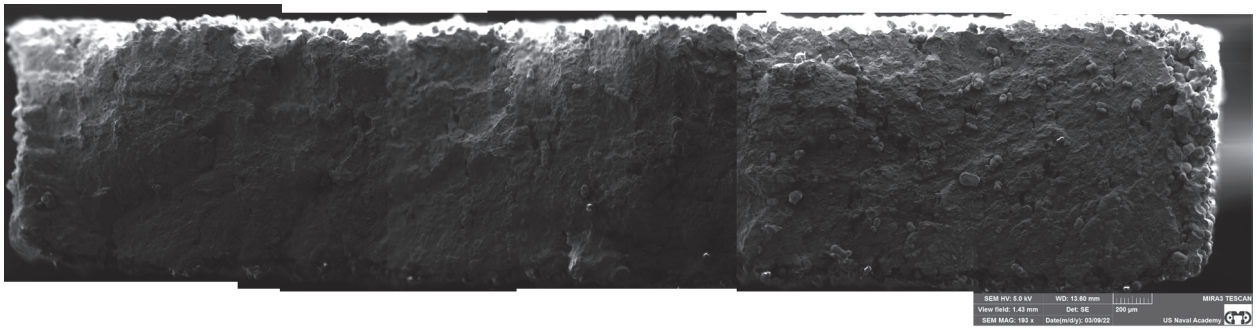

SEM HV: 5.0 kV
WD: 24.77 mm
MIRA3 TESCAN
View field: 284 µm
Det: SE
50 µm
SEM MAG: 874 x
Date(m/d/y): 10/25/21
US Naval Academy

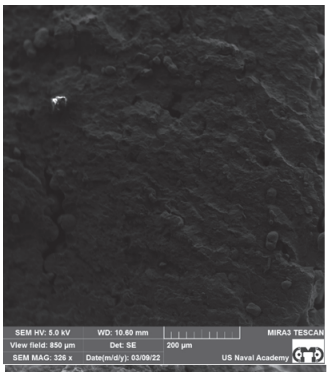

SEM HV: 5.0 kV
WD: 24.68 mm
MIRA3 TESCAN
View field: 146 µm
Det: SE
20 µm
SEM MAG: 1.89 kx
Date(m/d/y): 10/25/21
US Naval Academy

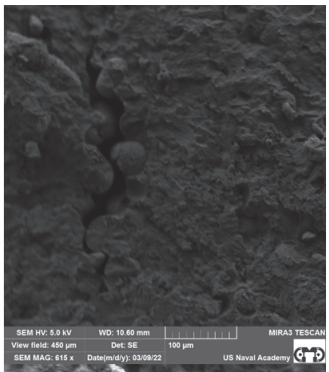

SEM HV: 5.0 kV
WD: 24.68 mm
MIRA3 TESCAN
View field: 54.4 µm
Det: SE
10 µm
SEM MAG: 5.09 kx
Date(m/d/y): 10/25/21
US Naval Academy

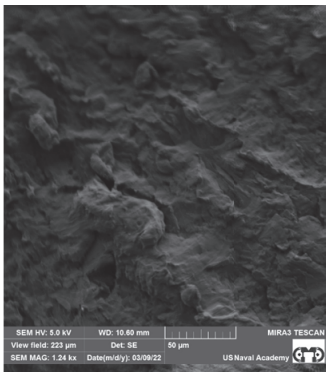

SEM HV: 5.0 kV
WD: 24.69 mm
MIRA3 TESCAN
View field: 89.7 µm
Det: SE
20 µm
SEM MAG: 3.09 kx
Date(m/d/y): 10/25/21
US Naval Academy

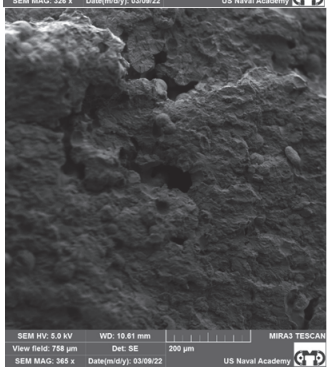
Nylon-12- Batch 2- 10 MRad

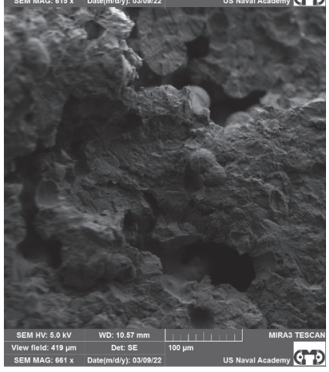


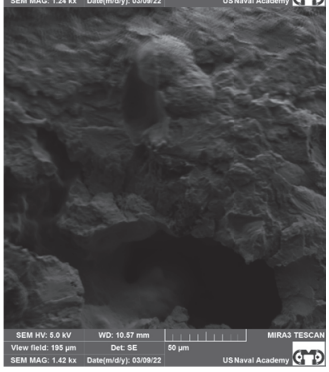


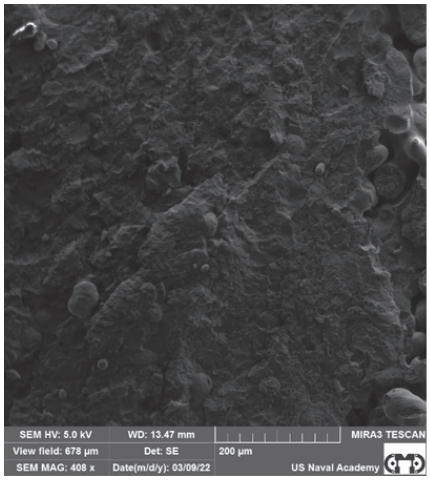


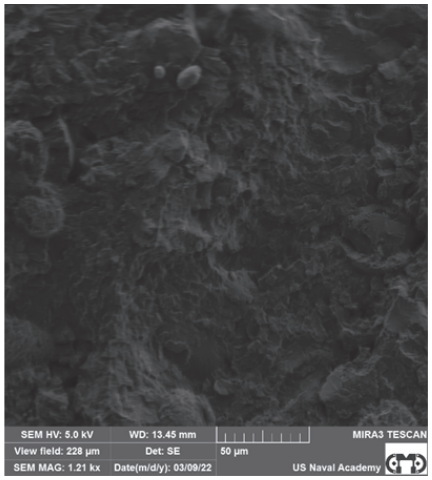


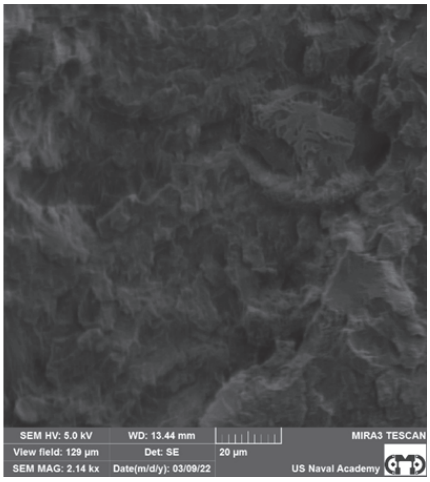




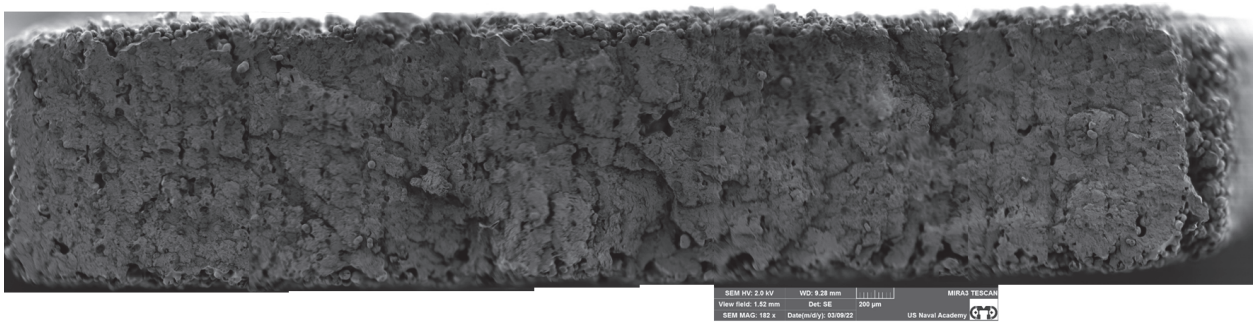


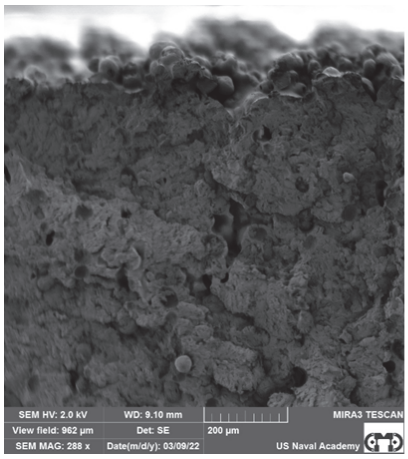

SEM HV: 5.0 kV
WD: 13.47 mm
MIRA3 TESCAN
View field: 678 µm
Det: SE
200 µm
SEM MAG: 408 x
Date(m/d/y): 03/09/22
US Naval Academy

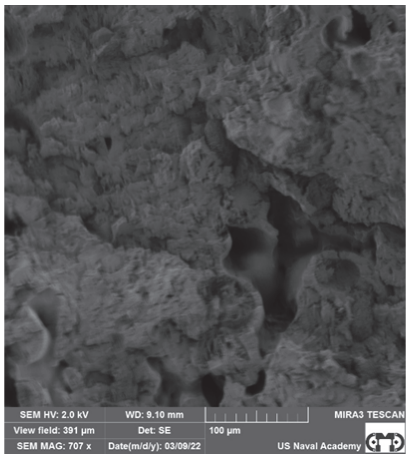

SEM HV: 5.0 kV
WD: 13.45 mm
MIRA3 TESCAN
View field: 228 µm
Det: SE
50 µm
SEM MAG: 1.21 kx
Date(m/d/y): 03/09/22
US Naval Academy

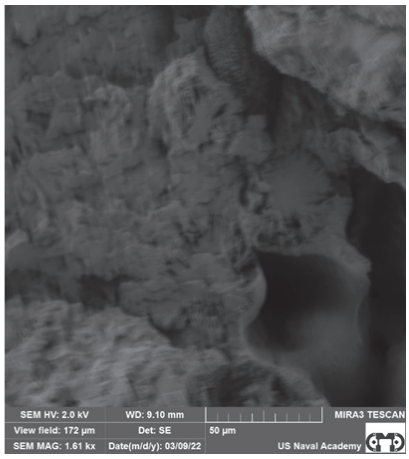

SEM HV: 5.0 kV
WD: 13.44 mm
MIRA3 TESCAN
View field: 129 µm
Det: SE
20 µm
SEM MAG: 2.14 kx
Date(m/d/y): 03/09/22
US Naval Academy

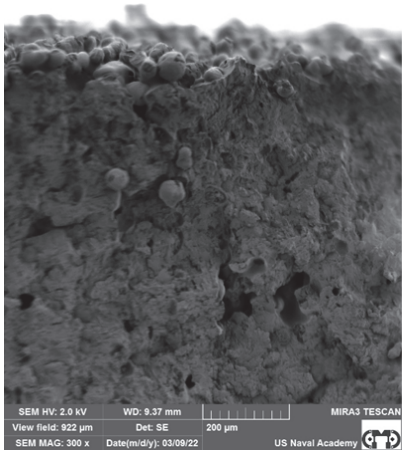
Nylon-12- Batch 2- 20 MRad

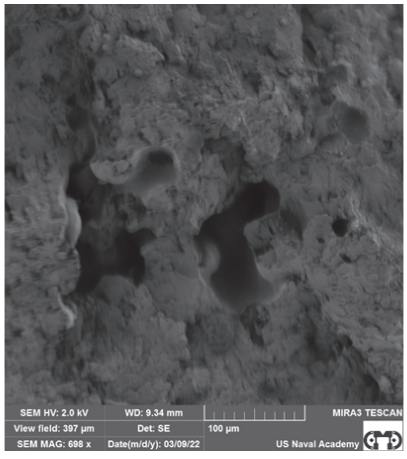


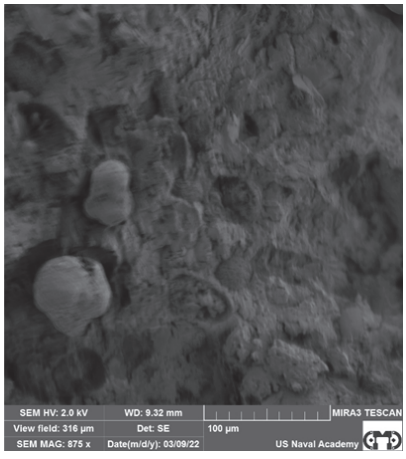






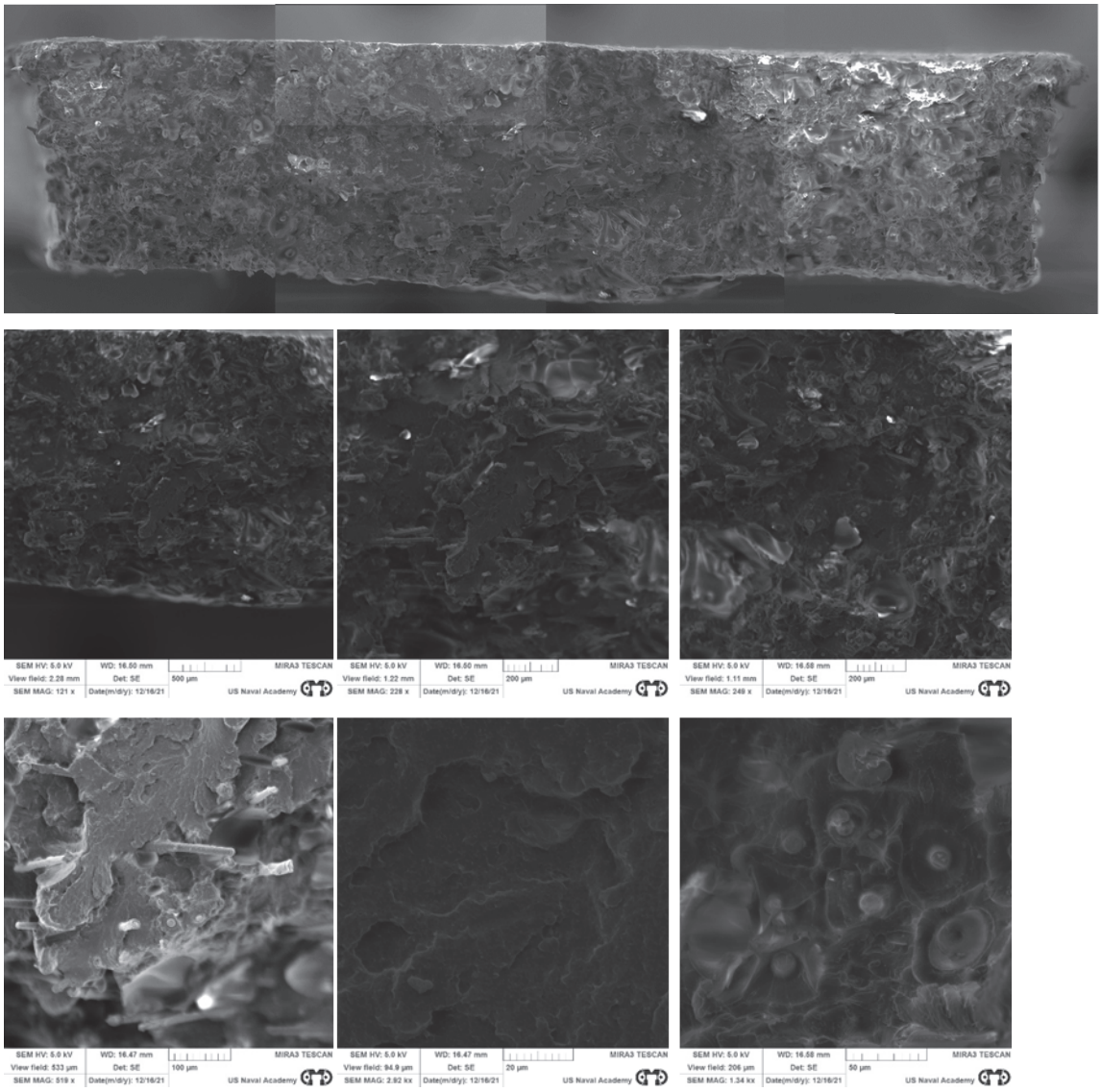


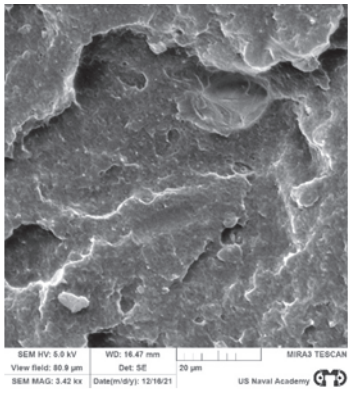


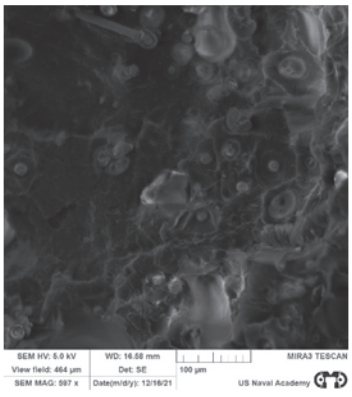


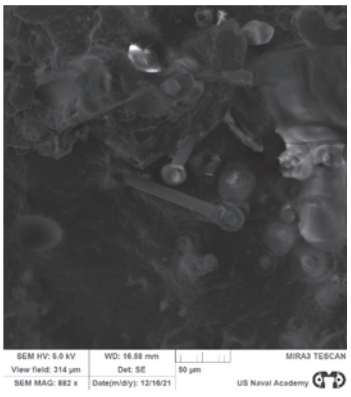
8.2 SEM of NylonG

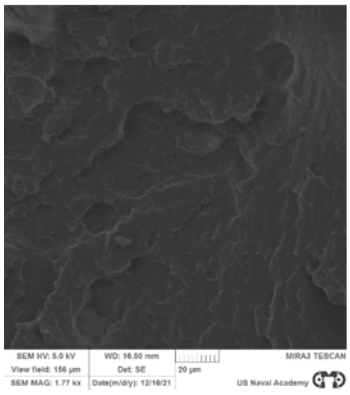
NylonG As printed

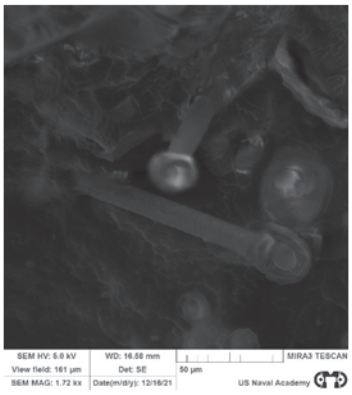


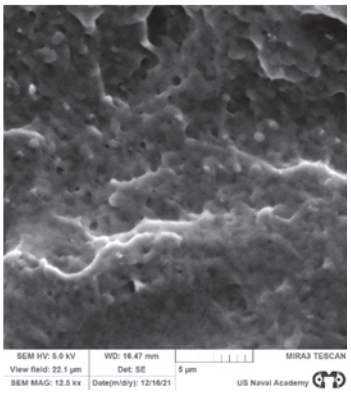

SEM HV: 5.0 kV
WD: 16.47 mm
MIRA3 TESCAN
View field: 80.9 µm
Det: SE
20 µm
SEM MAG: 3.42 kx
Date(m/d/y): 12/16/21
US Naval Academy


SEM HV: 5.0 kV
WD: 16.58 mm
MIRA3 TESCAN
View field: 464 µm
Det: SE
100 µm
SEM MAG: 597 x
Date(m/d/y): 12/16/21
US Naval Academy

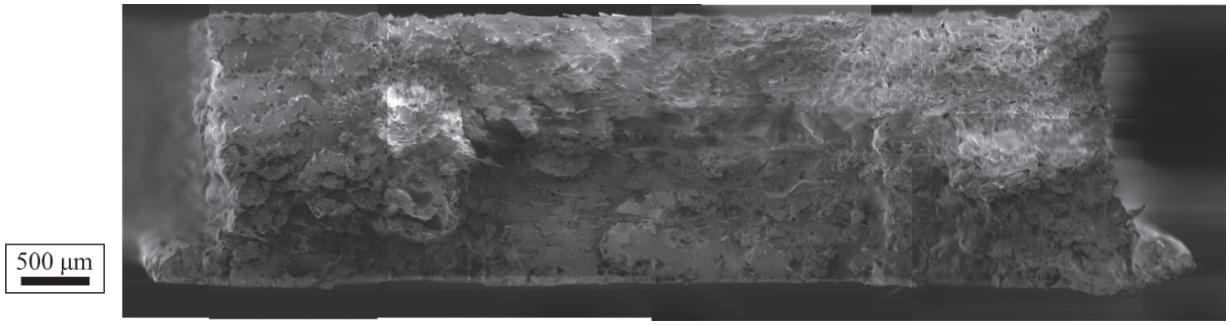

SEM HV: 5.0 kV
WD: 16.58 mm
MIRA3 TESCAN
View field: 314 µm
Det: SE
50 µm
SEM MAG: 882 x
Date(m/d/y): 12/16/21
US Naval Academy

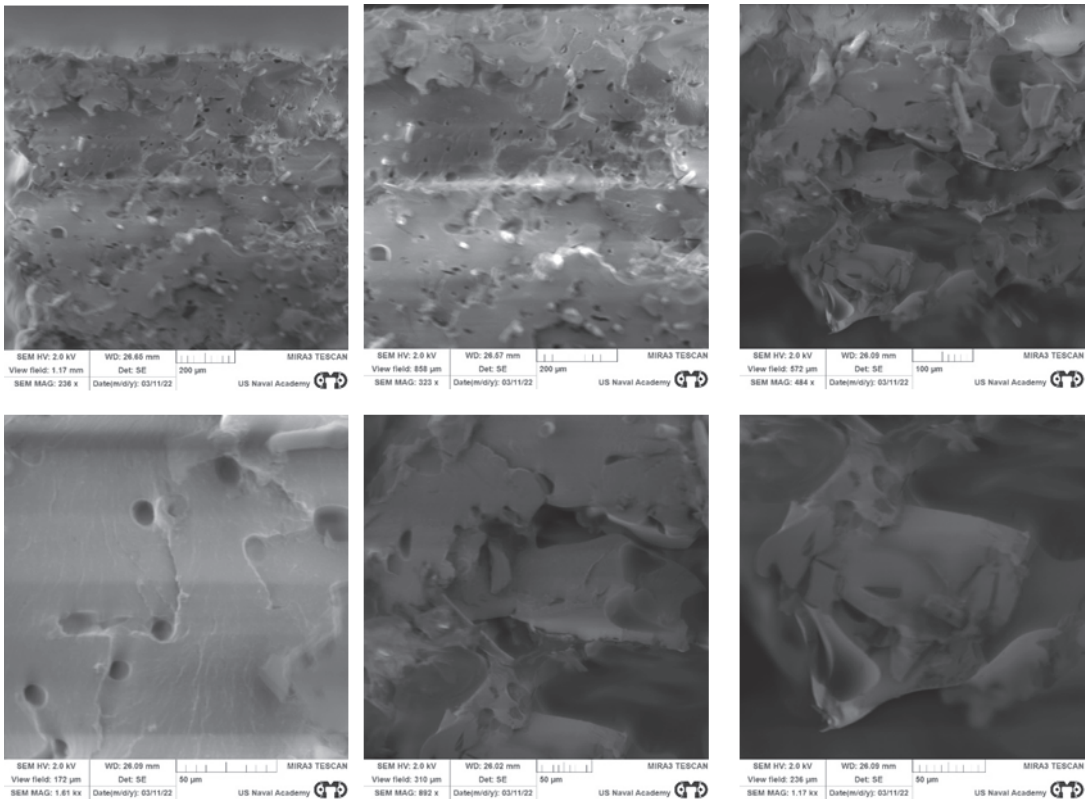

SEM HV: 5.0 kV
WD: 16.60 mm
MIRA3 TESCAN
View field: 156 µm
Det: SE
20 µm
SEM MAG: 1.77 kx
Date(m/d/y): 12/16/21
US Naval Academy

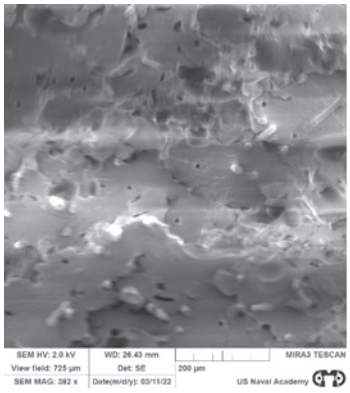

SEM HV: 5.0 kV
WD: 16.58 mm
MIRA3 TESCAN
View field: 161 µm
Det: SE
50 µm
SEM MAG: 1.72 kx
Date(m/d/y): 12/16/21
US Naval Academy

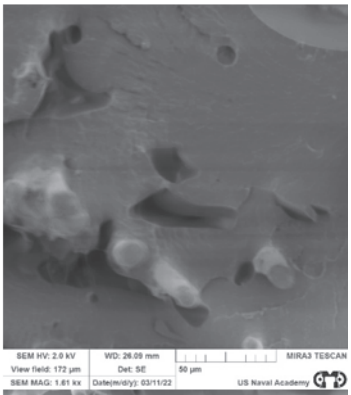

SEM HV: 5.0 kV
WD: 16.47 mm
MIRA3 TESCAN
View field: 22.1 µm
Det: SE
5 µm
SEM MAG: 12.5 kx
Date(m/d/y): 12/16/21
US Naval Academy

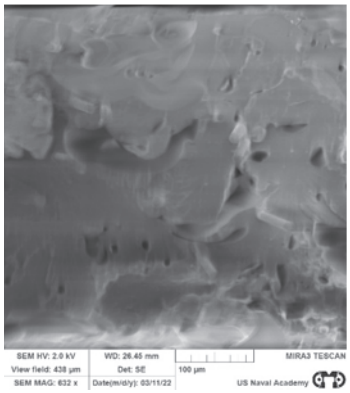
NylonG 20 Mrad (E26)

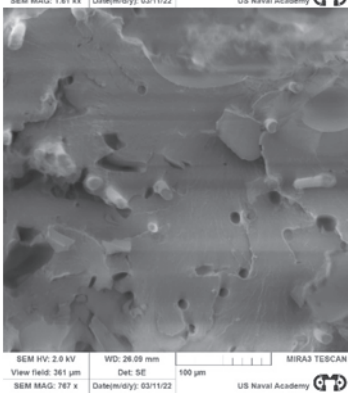





SEM HV: 2.0 kV
WD: 26.43 mm
MIRA3 TESCAN
View field: 725 µm
Det: SE
200 µm
SEM MAG: 382 x
Date(m/d/y): 03/11/22
US Naval Academy


SEM HV: 2.0 kV
WD: 26.09 mm
MIRA3 TESCAN
View field: 172 µm
Det: SE
50 µm
SEM MAG: 1.61 kx
Date(m/d/y): 03/11/22
US Naval Academy

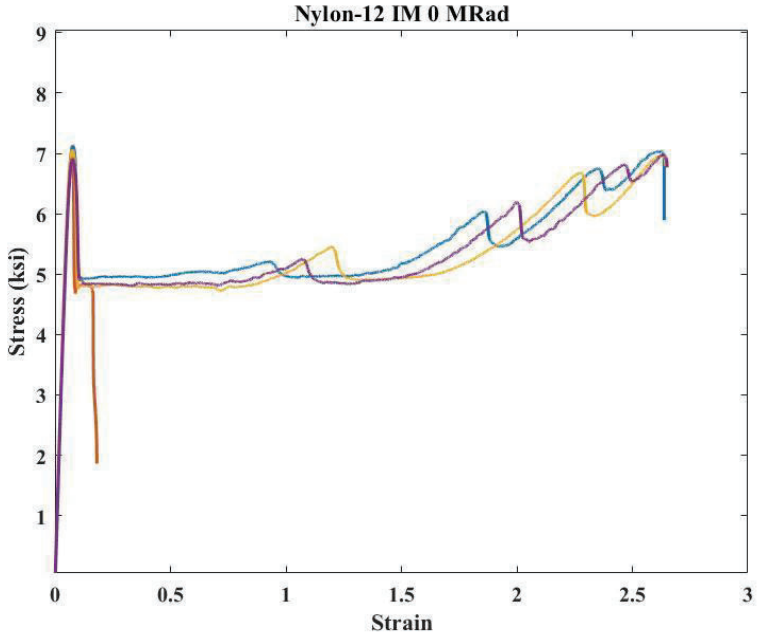

SEM HV: 2.0 kV
WD: 26.46 mm
MIRA3 TESCAN
View field: 438 µm
Det: SE
100 µm
SEM MAG: 632 x
Date(m/d/y): 03/11/22
US Naval Academy

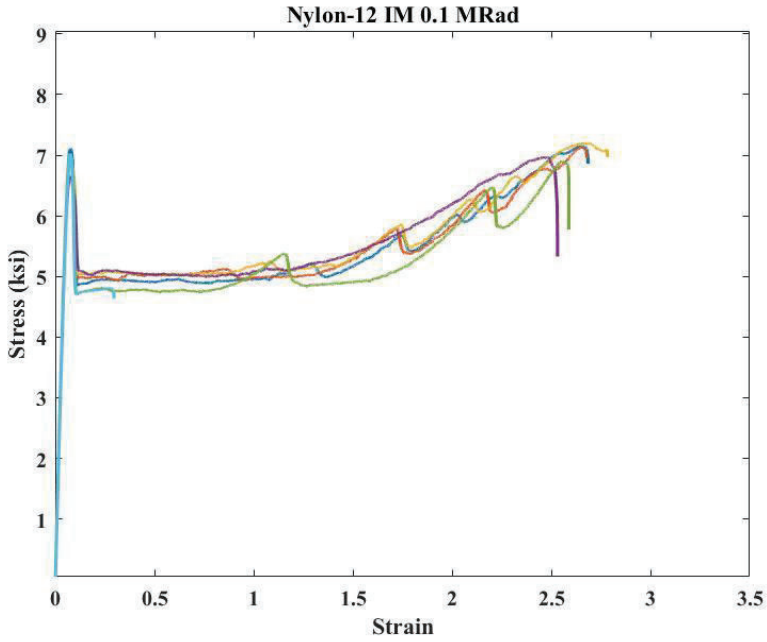

SEM HV: 2.0 kV
WD: 26.09 mm
MIRA3 TESCAN
View field: 261 µm
Det: SE
100 µm
SEM MAG: 767 x
Date(m/d/y): 03/11/22
US Naval Academy

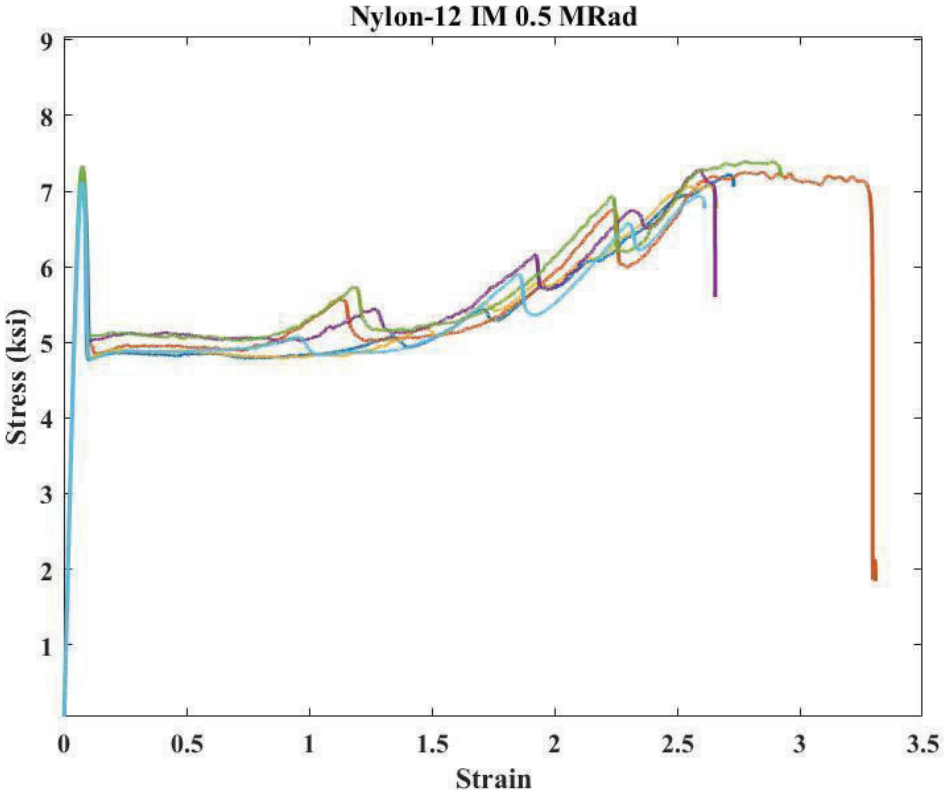
8.3 Plots of Tensile Data

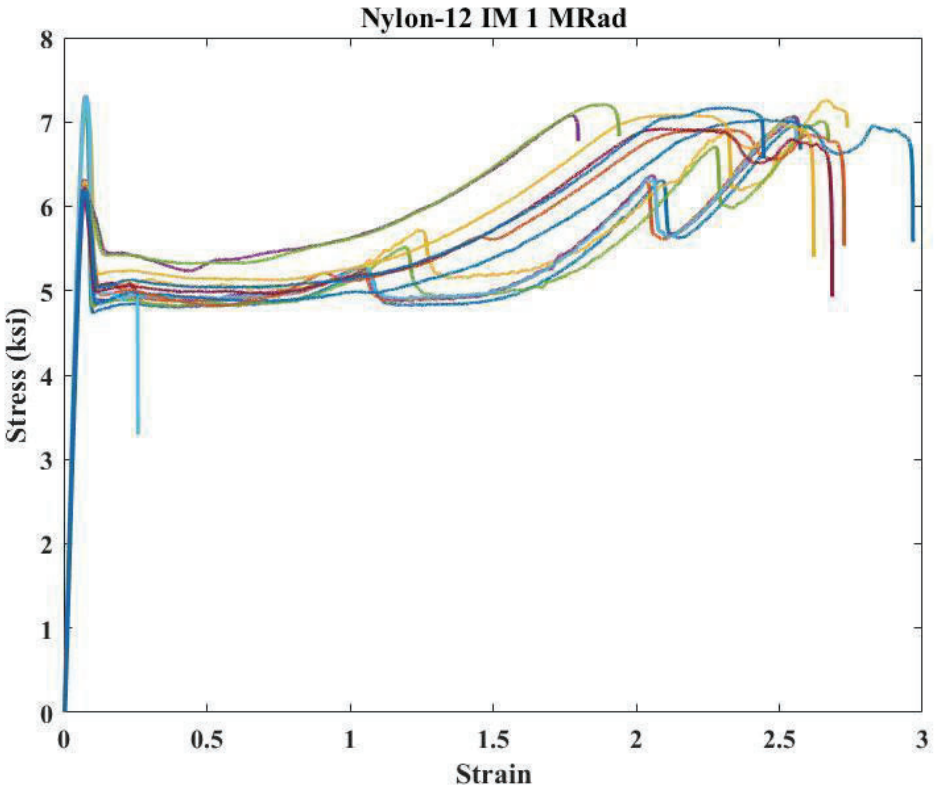
The following plots show the stress-strain curves of all of the specimens tested. They are organized within each material by radiation dose.

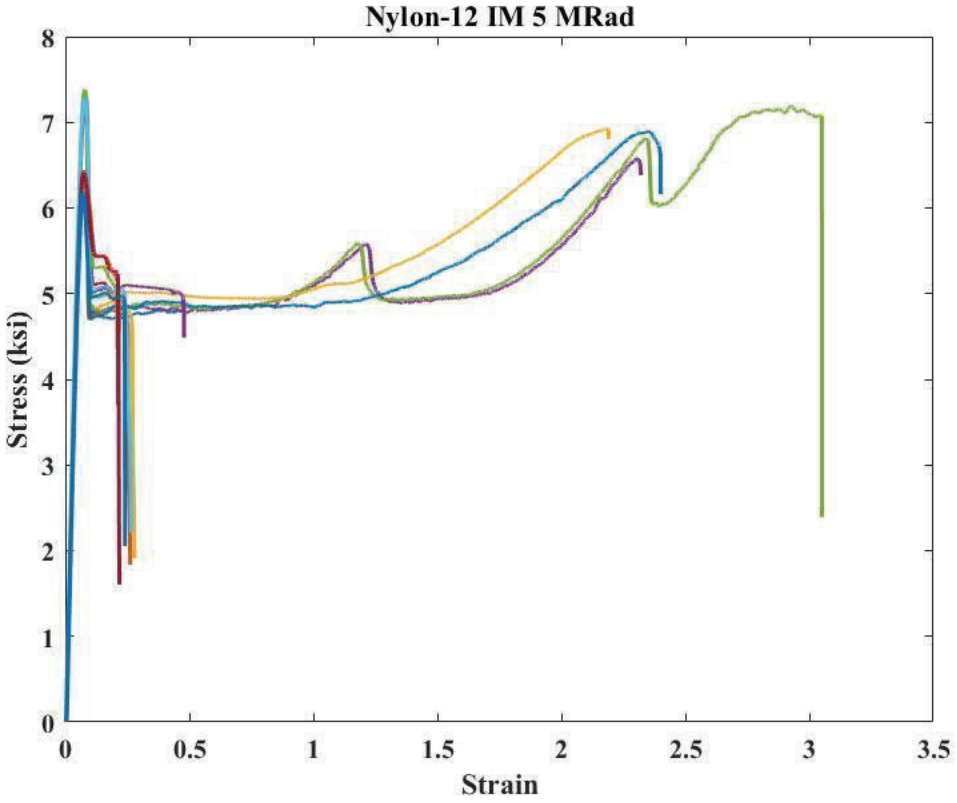
Nylon-12 Injection Molded

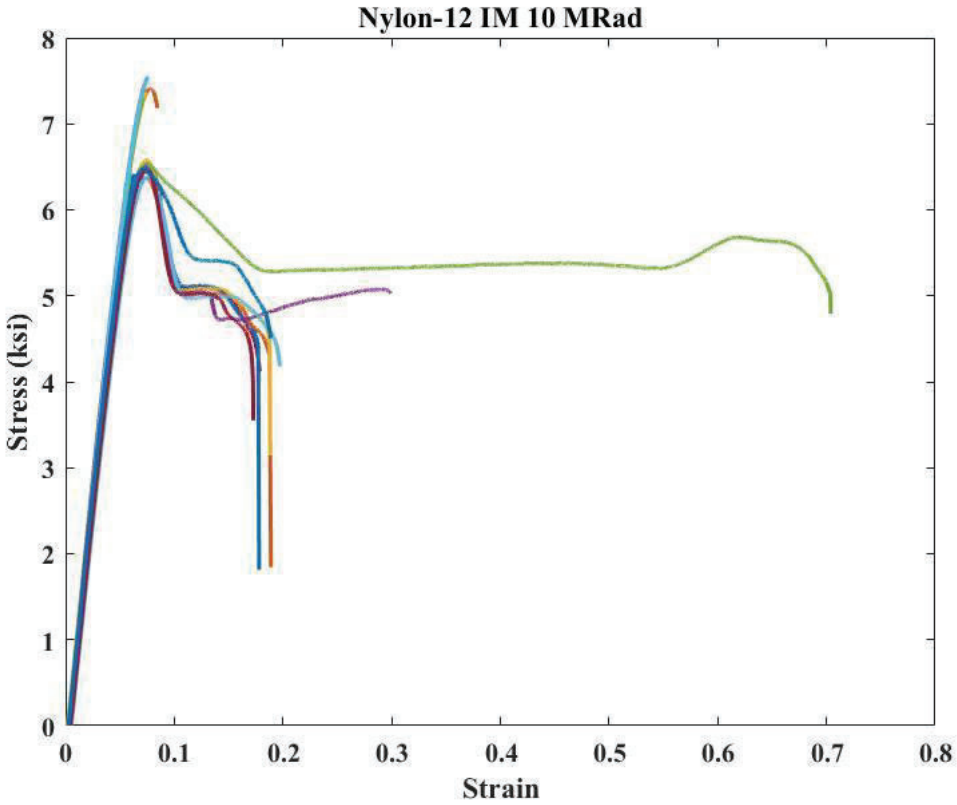


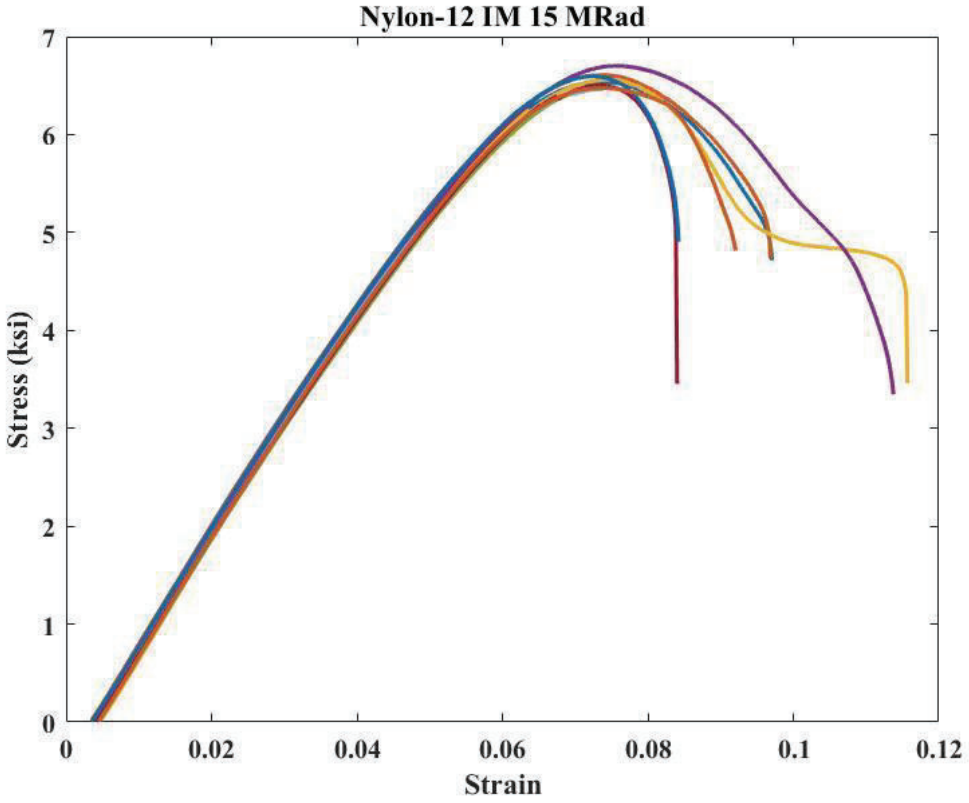


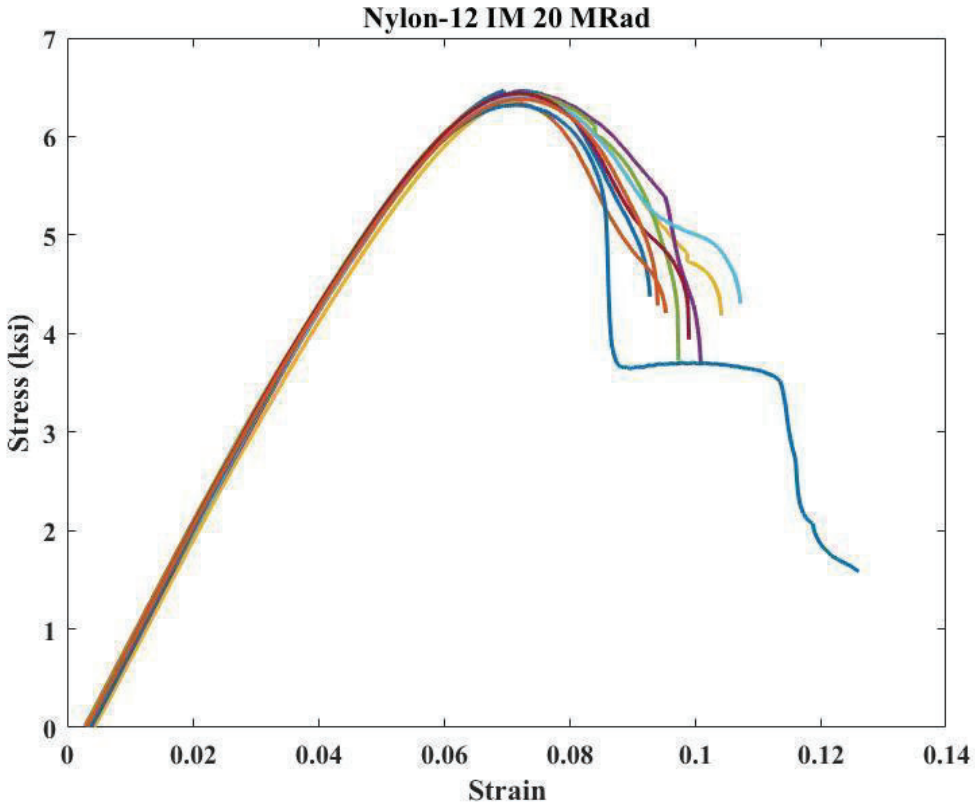

Nylon-12 IM 0.5 MRad
Stress (ksi)
Strain
0
0.5
1
1.5
2
2.5
3
3.5
1
2
3
4
5
6
7
8
9


Nylon-12 IM 1 MRad
Stress (ksi)
Strain
0
0.5
1
1.5
2
2.5
3
0
1
2
3
4
5
6
7
8

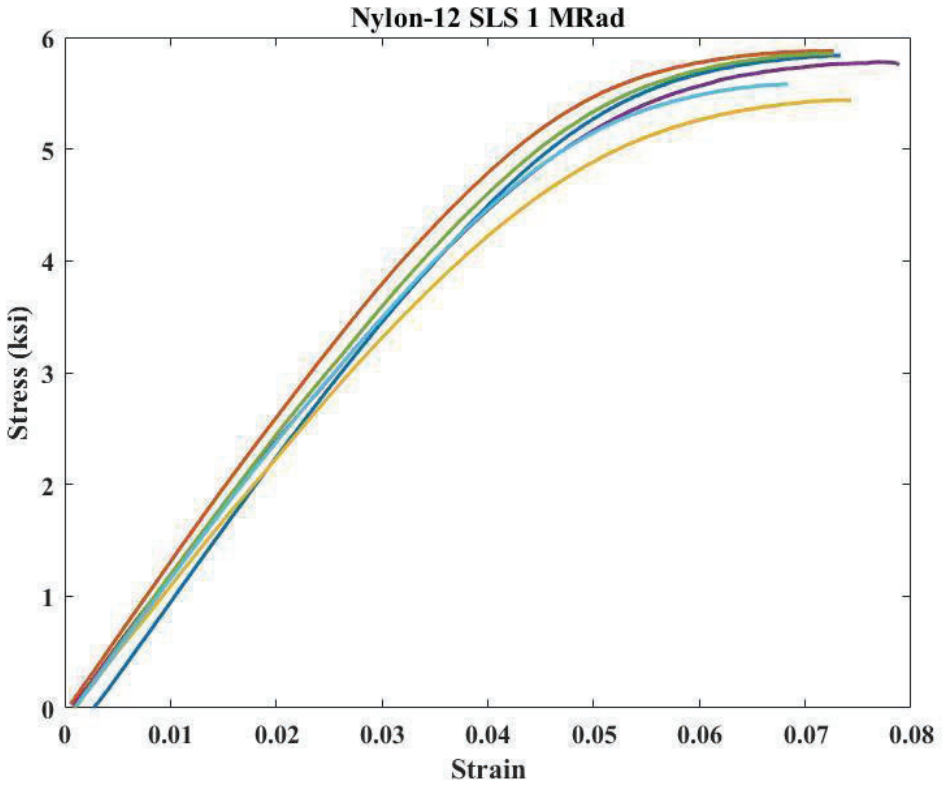

Nylon-12 IM 5 MRad
Stress (ksi)
Strain
0
1
2
3
4
5
6
7
8
0
0.5
1
1.5
2
2.5
3
3.5

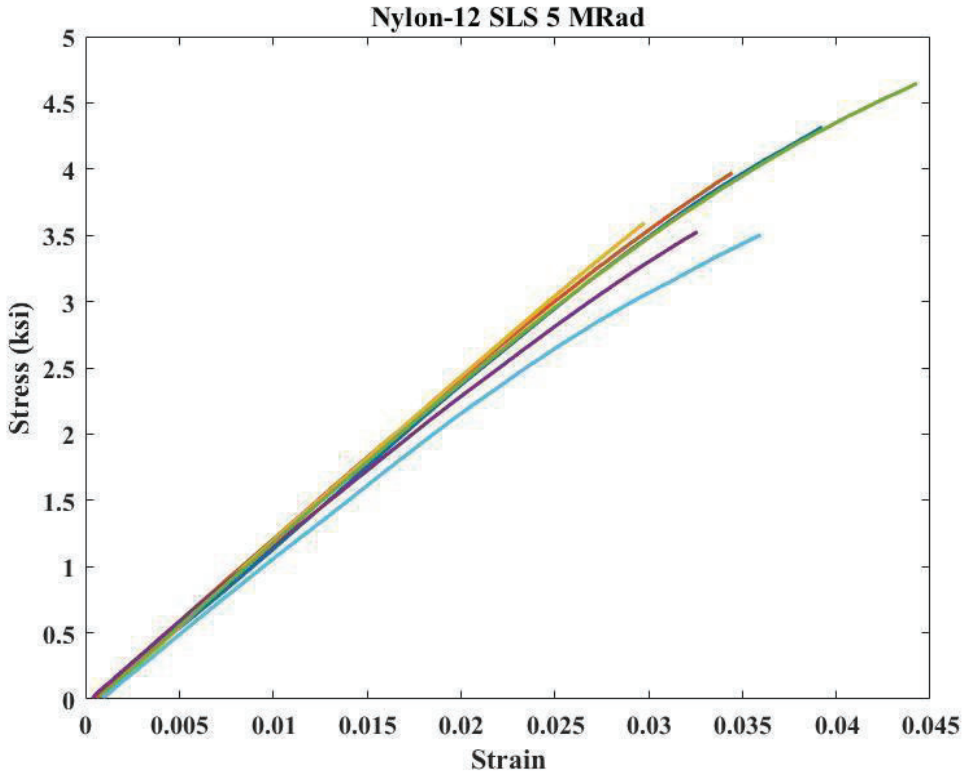

Nylon-12 IM 10 MRad
Stress (ksi)
Strain
0
1
2
3
4
5
6
7
8
0
0.1
0.2
0.3
0.4
0.5
0.6
0.7
0.8

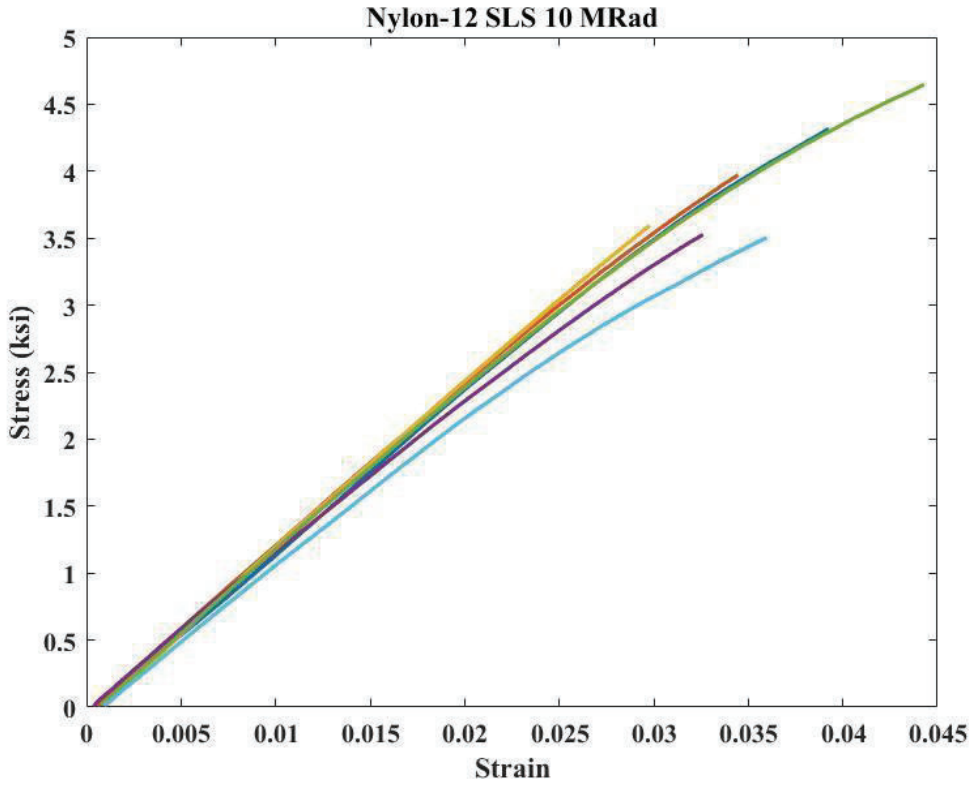

Nylon-12 IM 15 MRad
Stress (ksi)
Strain
0
1
2
3
4
5
6
7
0
0.02
0.04
0.06
0.08
0.1
0.12

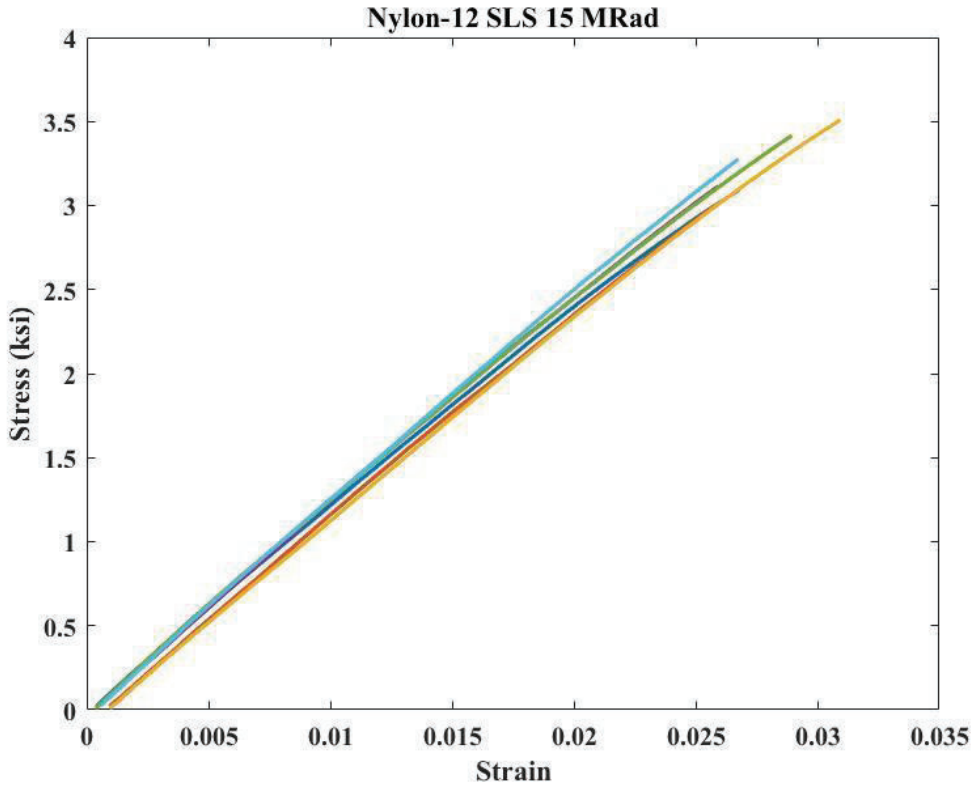

Nylon-12 IM 20 MRad
Stress (ksi)
Strain
0
1
2
3
4
5
6
7
0
0.02
0.04
0.06
0.08
0.1
0.12
0.14

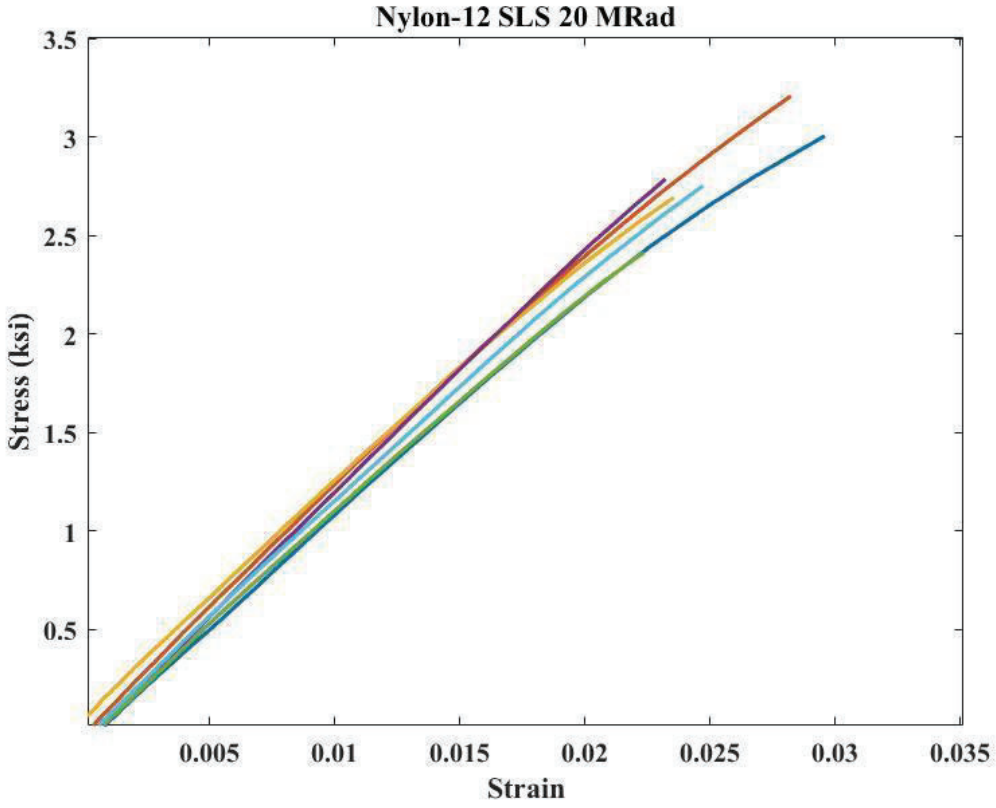
Nylon-12 SLS


Nylon-12 SLS 1 MRad
Stress (ksi)
Strain
0
1
2
3
4
5
6
0
0.01
0.02
0.03
0.04
0.05
0.06
0.07
0.08

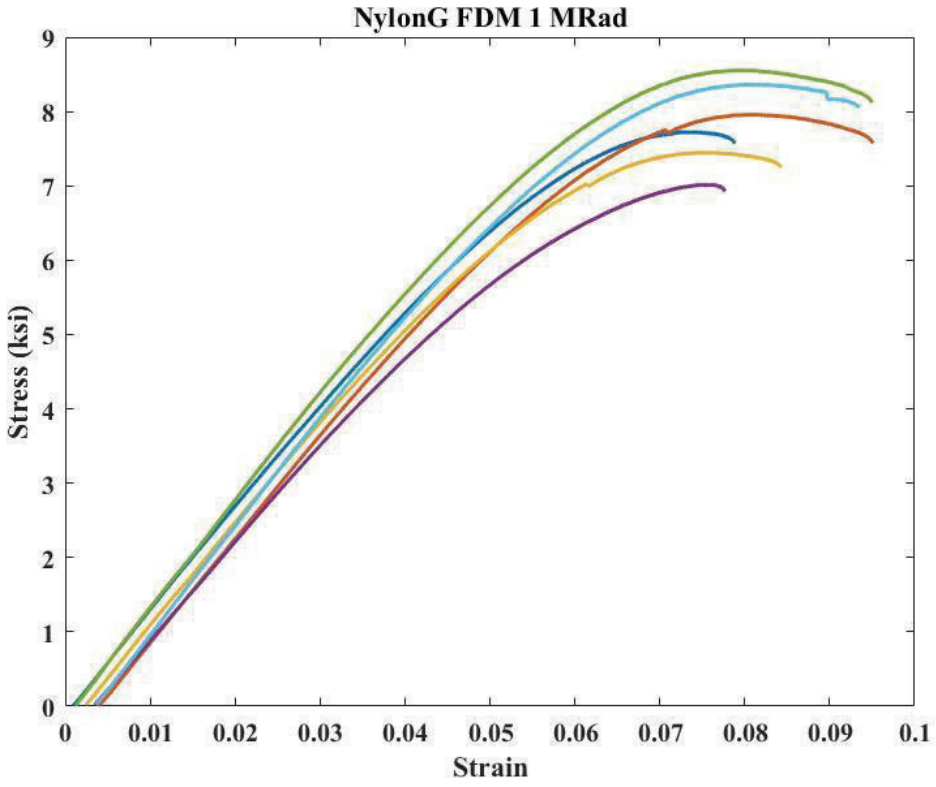

Nylon-12 SLS 5 MRad
Stress (ksi)
Strain
0
0.5
1
1.5
2
2.5
3
3.5
4
4.5
5
0
0.005
0.01
0.015
0.02
0.025
0.03
0.035
0.04
0.045

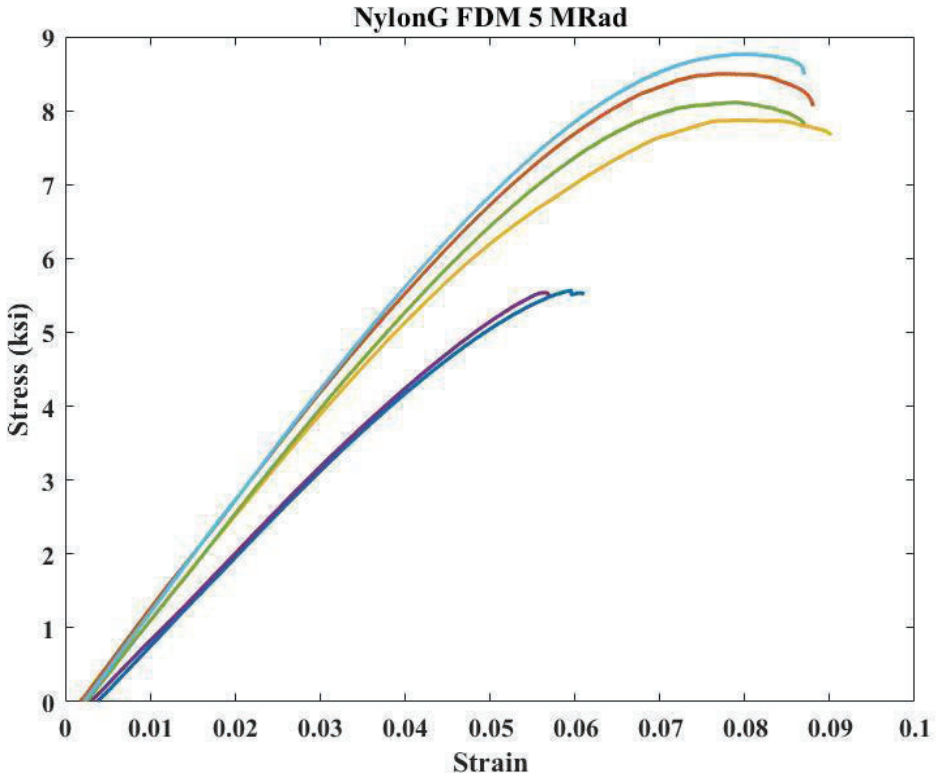

Nylon-12 SLS 10 MRad
Stress (ksi)
Strain
0
0.5
1
1.5
2
2.5
3
3.5
4
4.5
5
0.005
0.01
0.015
0.02
0.025
0.03
0.035
0.04
0.045

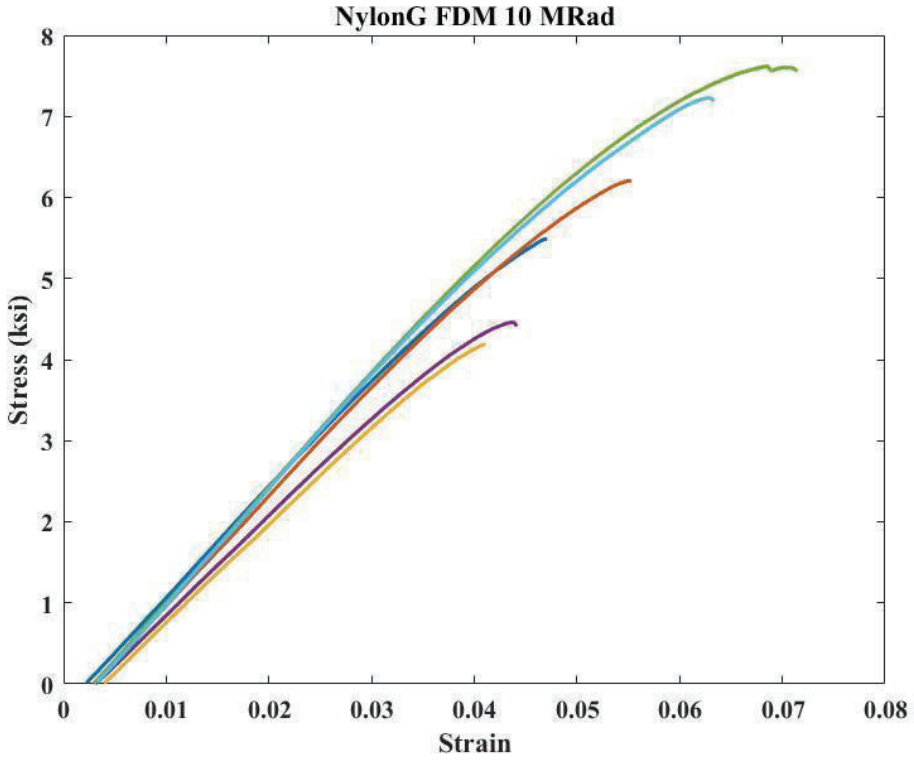

Nylon-12 SLS 15 MRad
Stress (ksi)
Strain
0
0.5
1
1.5
2
2.5
3
3.5
4
0.005
0.01
0.015
0.02
0.025
0.03
0.035

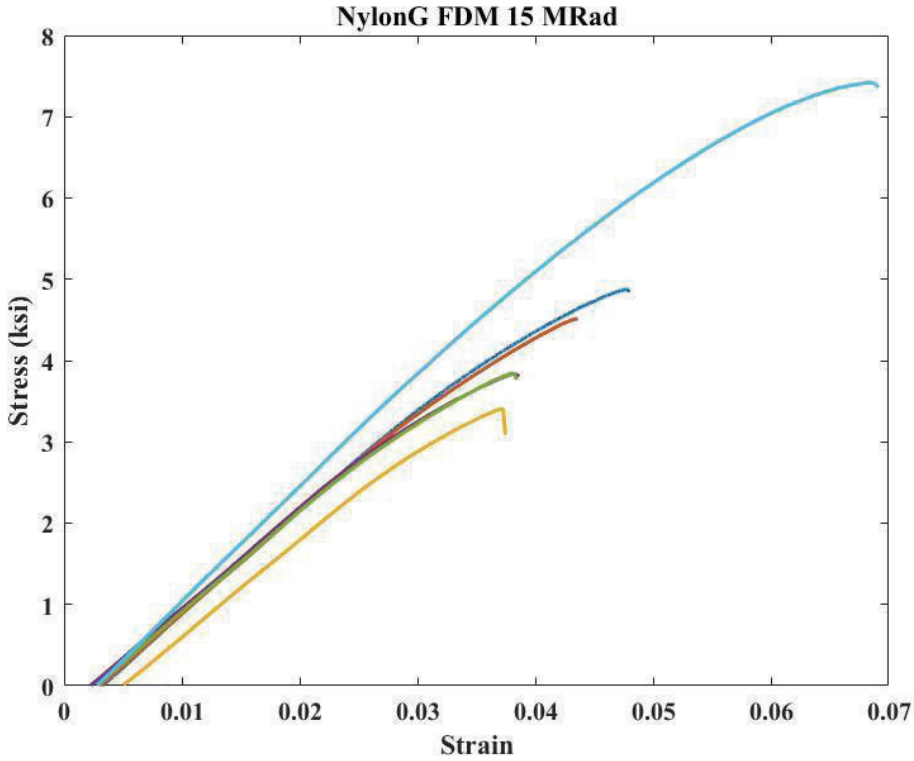

Nylon-12 SLS 20 MRad
Stress (ksi)
Strain
3.5
3
2.5
2
1.5
1
0.5
0.005
0.01
0.015
0.02
0.025
0.03
0.035

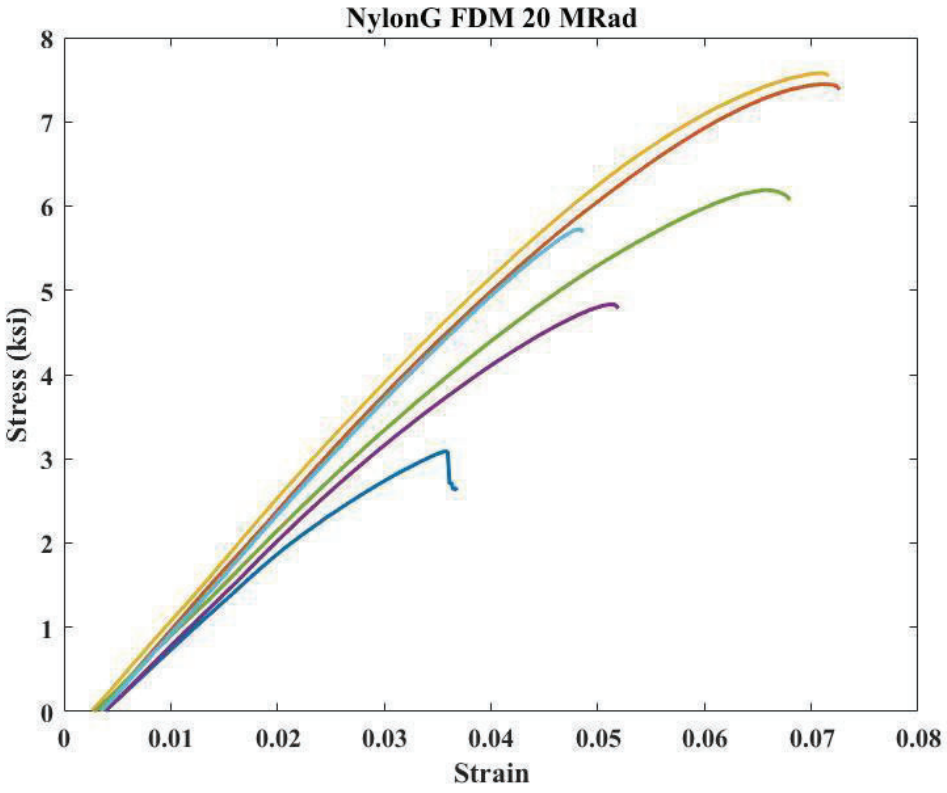
NylonG FDM


NylonG FDM 1 MRad
Stress (ksi)
Strain
0
1
2
3
4
5
6
7
8
9
0
0.01
0.02
0.03
0.04
0.05
0.06
0.07
0.08
0.09
0.1

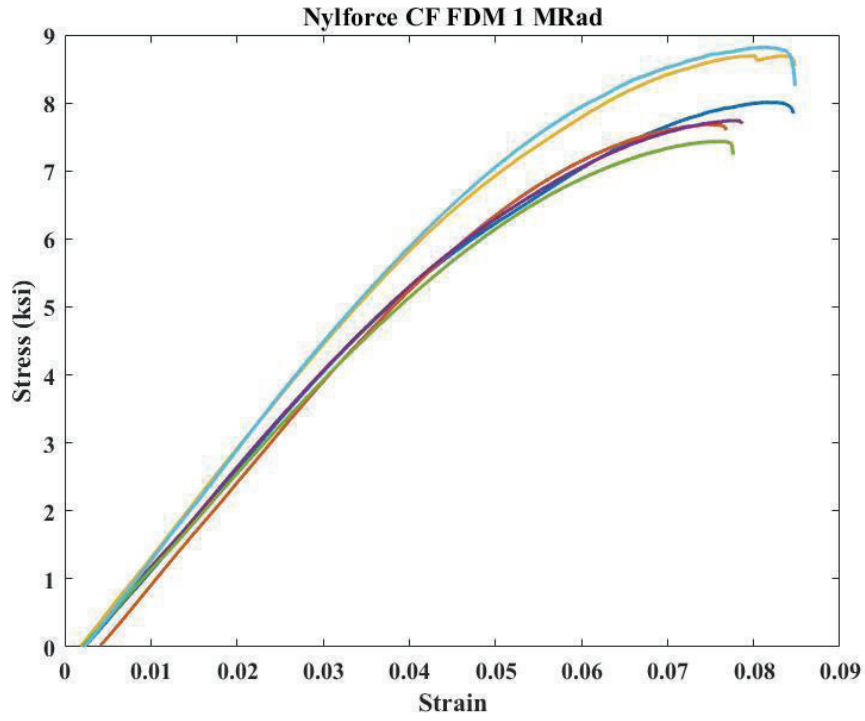

NylonG FDM 5 MRad
Stress (ksi)
Strain
0
1
2
3
4
5
6
7
8
9
0
0.01
0.02
0.03
0.04
0.05
0.06
0.07
0.08
0.09
0.1

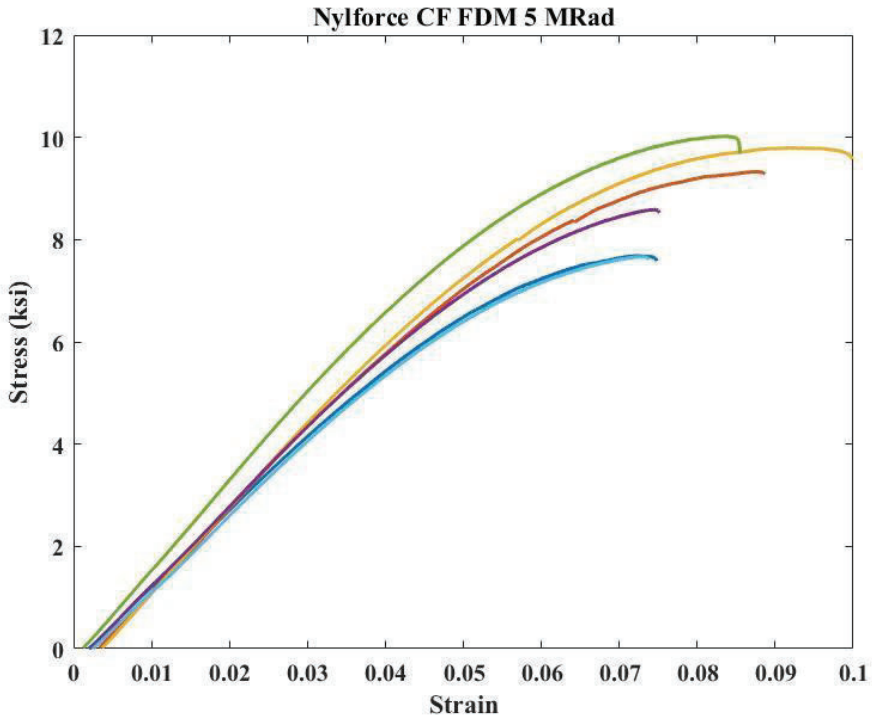

NylonG FDM 10 MRad
Stress (ksi)
Strain
0
1
2
3
4
5
6
7
8
0
0.01
0.02
0.03
0.04
0.05
0.06
0.07
0.08

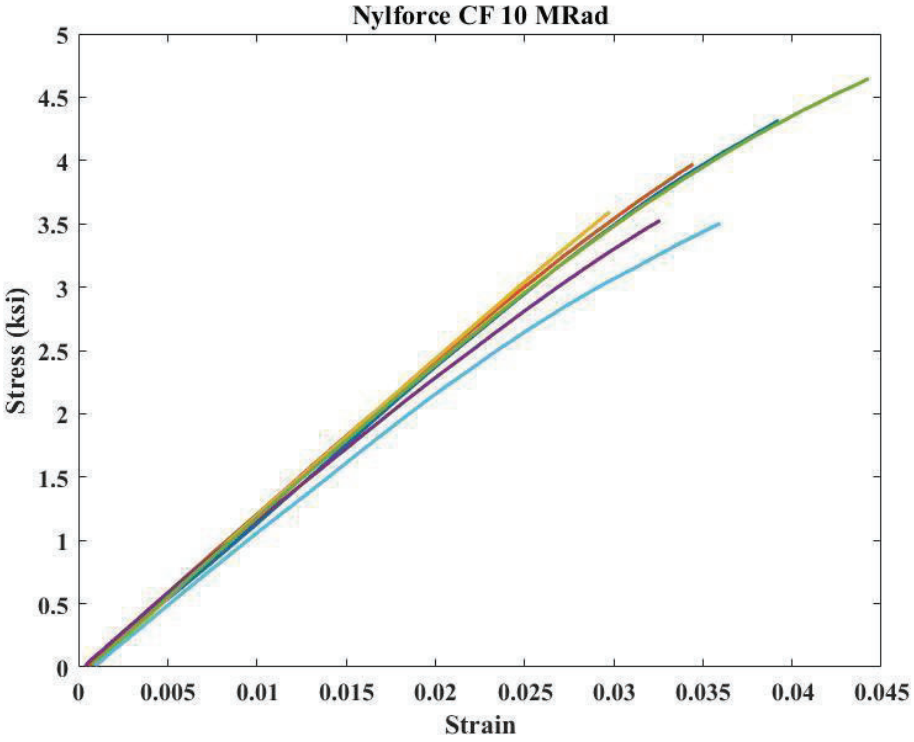

NylonG FDM 15 MRad
Stress (ksi)
Strain
0
1
2
3
4
5
6
7
8
0
0.01
0.02
0.03
0.04
0.05
0.06
0.07

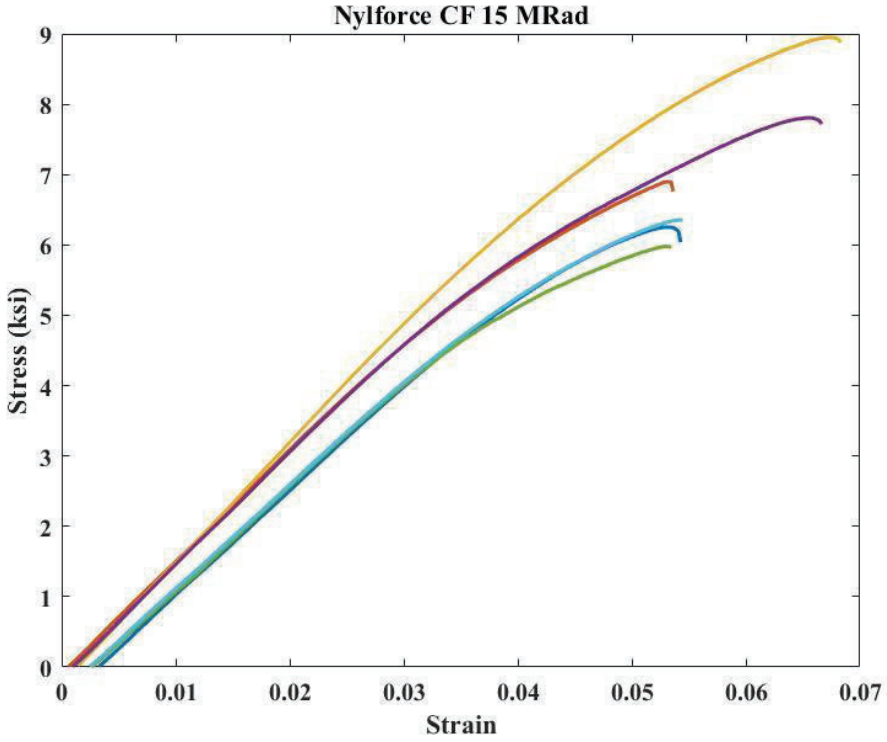

NylonG FDM 20 MRad
Stress (ksi)
Strain
0
1
2
3
4
5
6
7
8
0
0.01
0.02
0.03
0.04
0.05
0.06
0.07
0.08

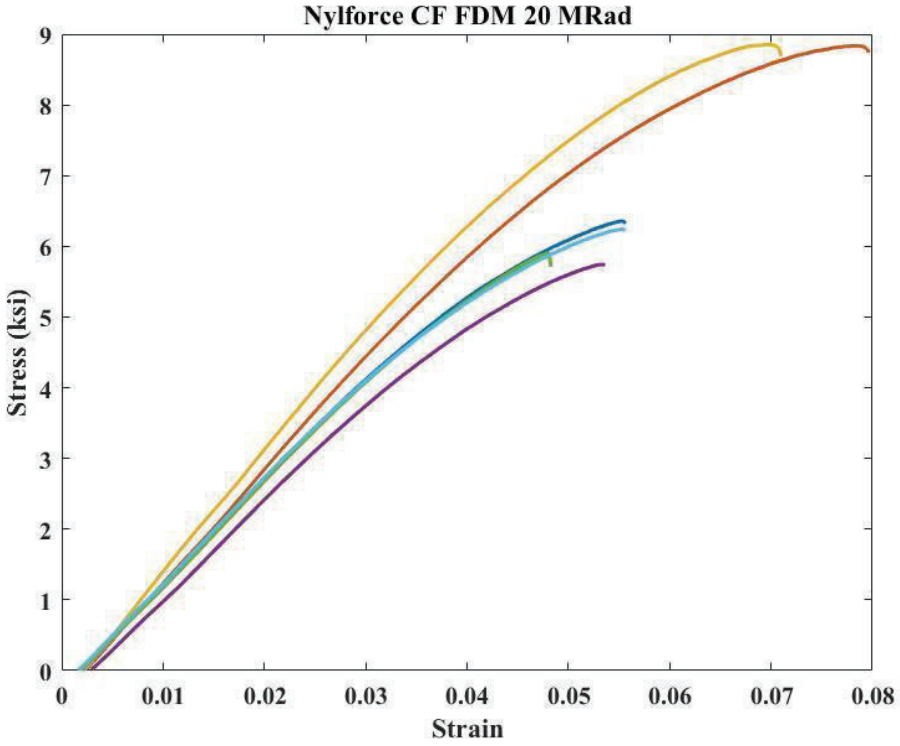
Nylforce CF


Nylforce CF FDM 1 MRad
Stress (ksi)
Strain
0
1
2
3
4
5
6
7
8
9
0
0.01
0.02
0.03
0.04
0.05
0.06
0.07
0.08
0.09

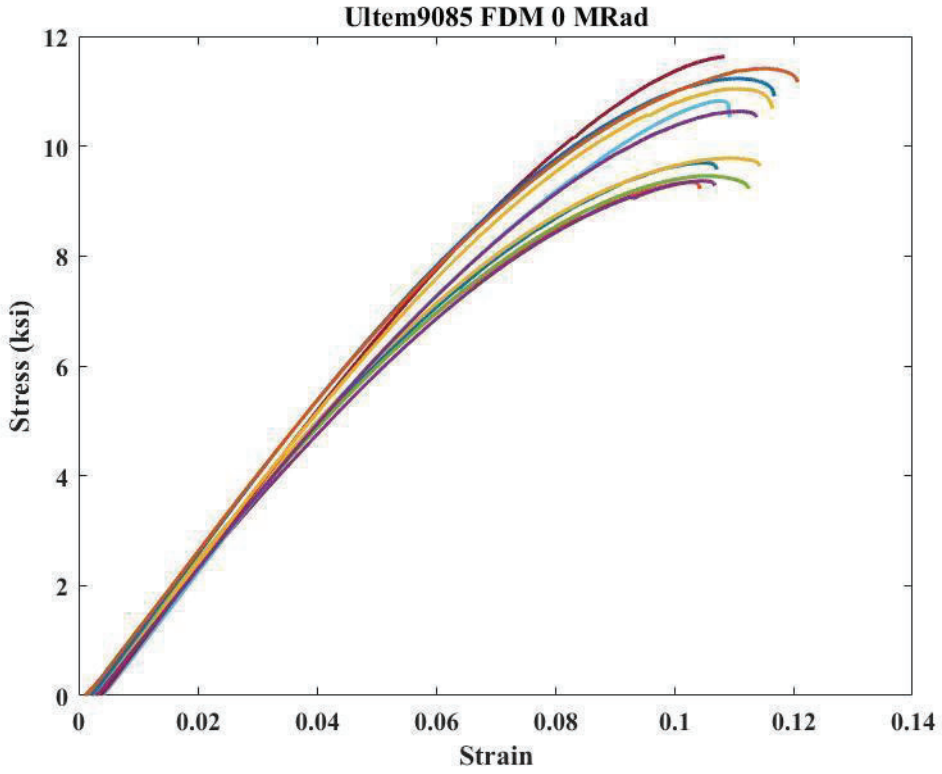

Nylforce CF FDM 5 MRad
Stress (ksi)
Strain
0
2
4
6
8
10
12
0
0.01
0.02
0.03
0.04
0.05
0.06
0.07
0.08
0.09
0.1

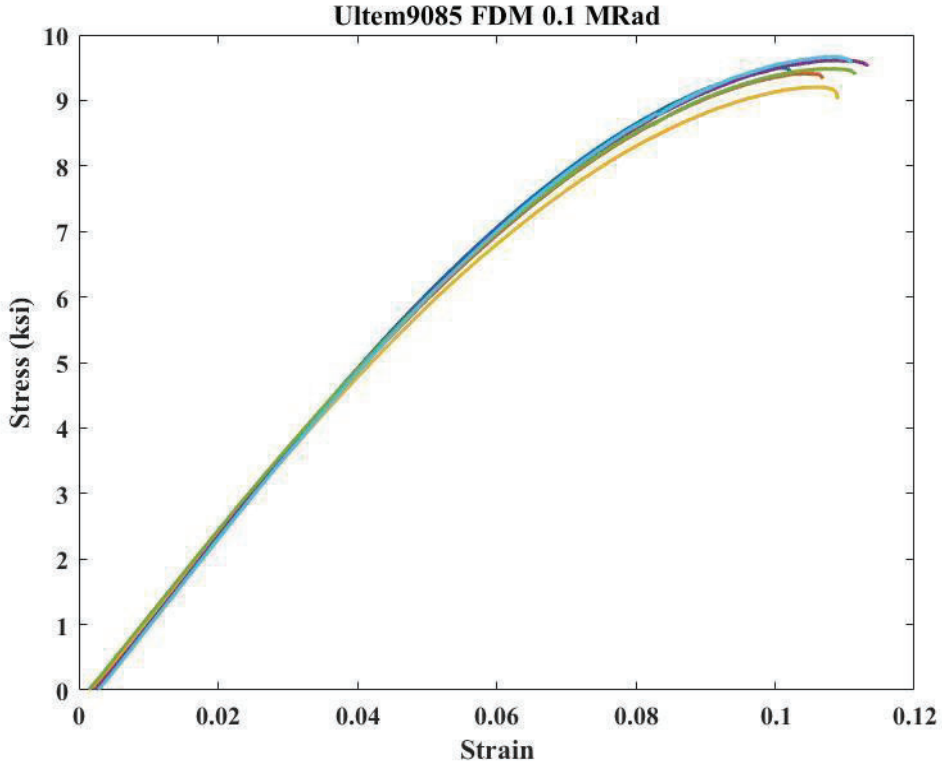

Nylforce CF 10 MRad
Stress (ksi)
Strain
0
0.5
1
1.5
2
2.5
3
3.5
4
4.5
5
0
0.005
0.01
0.015
0.02
0.025
0.03
0.035
0.04
0.045

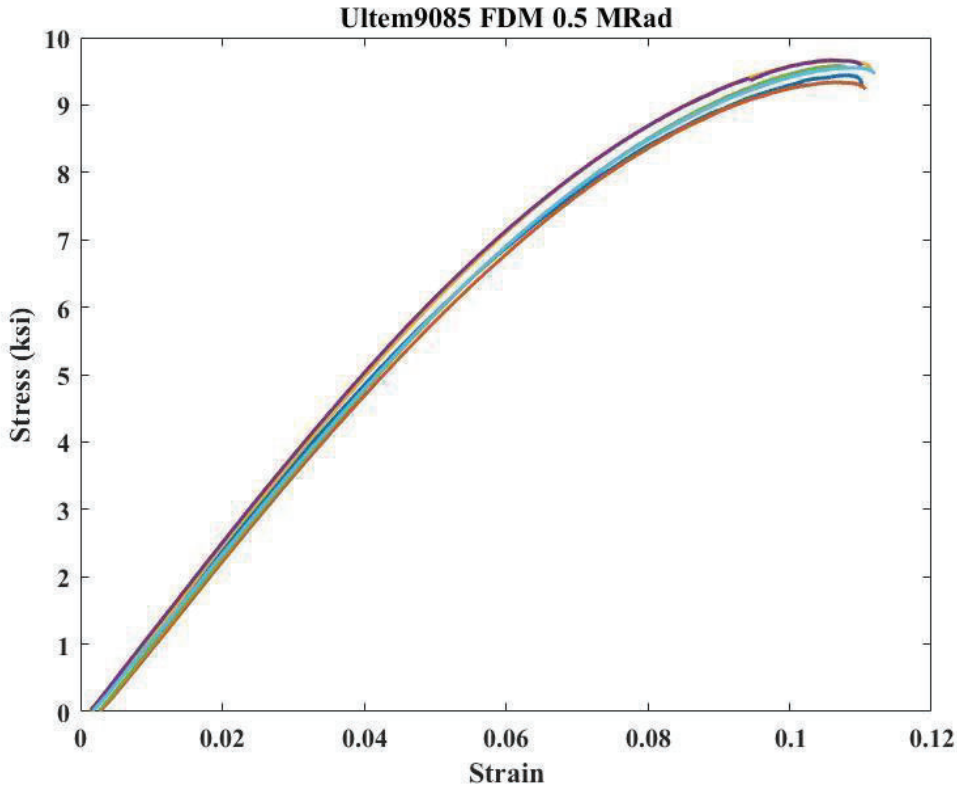

Nylforce CF 15 MRad
Stress (ksi)
Strain
0
1
2
3
4
5
6
7
8
9
0
0.01
0.02
0.03
0.04
0.05
0.06
0.07

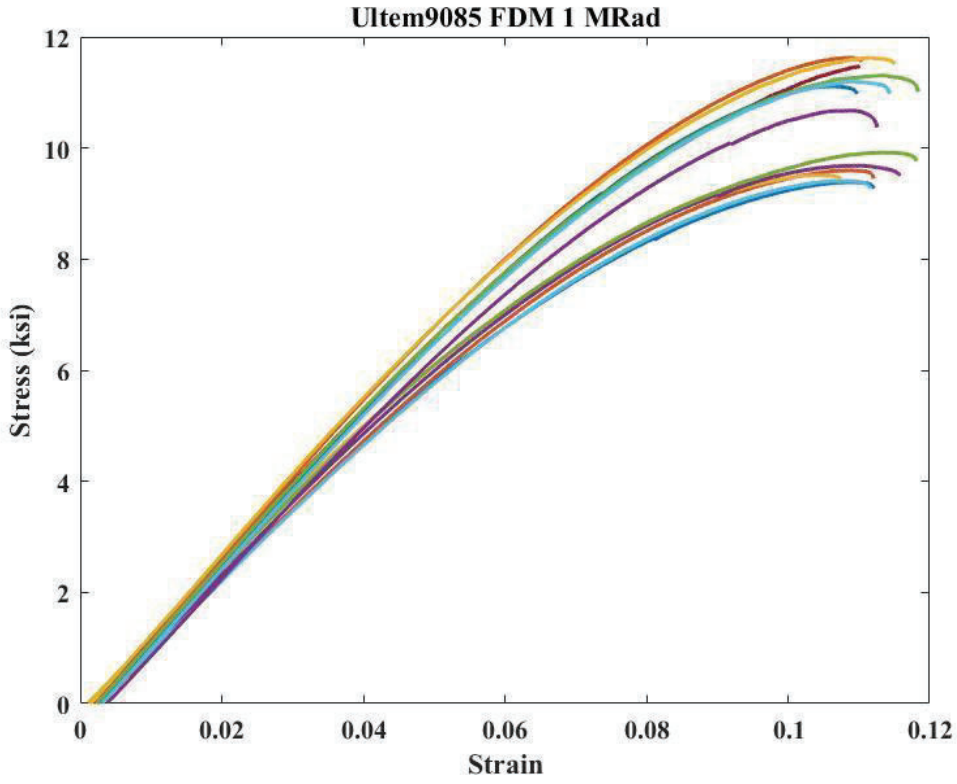

Nylforce CF FDM 20 MRad
Stress (ksi)
Strain
0
1
2
3
4
5
6
7
8
9
0
0.01
0.02
0.03
0.04
0.05
0.06
0.07
0.08

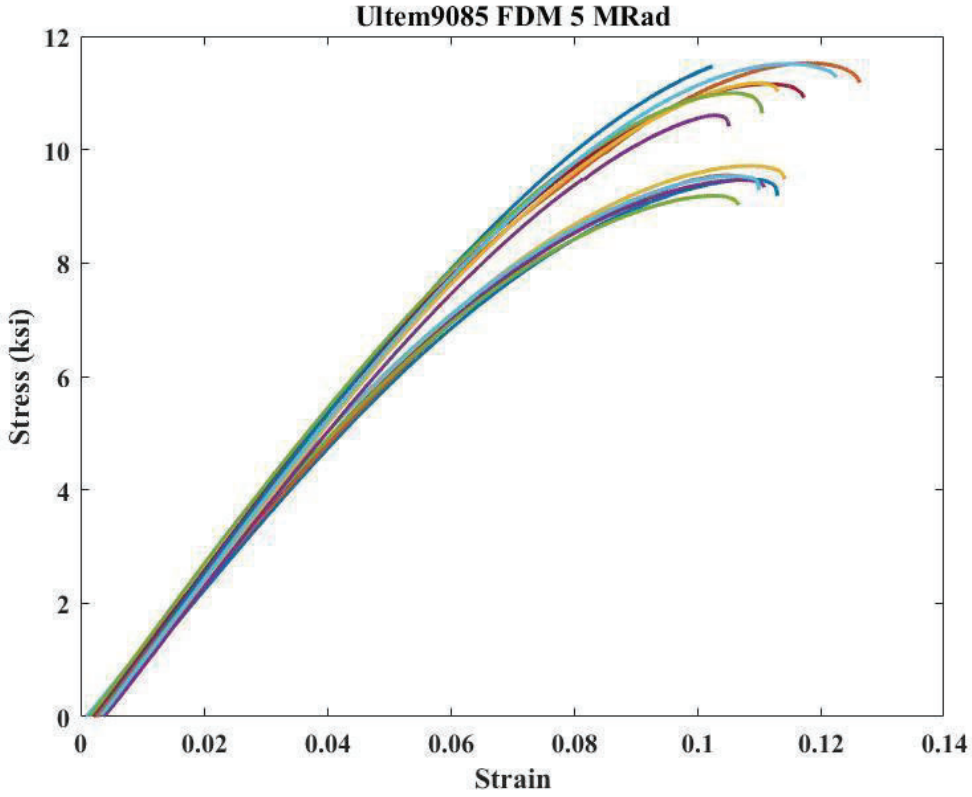
Ultem 9085

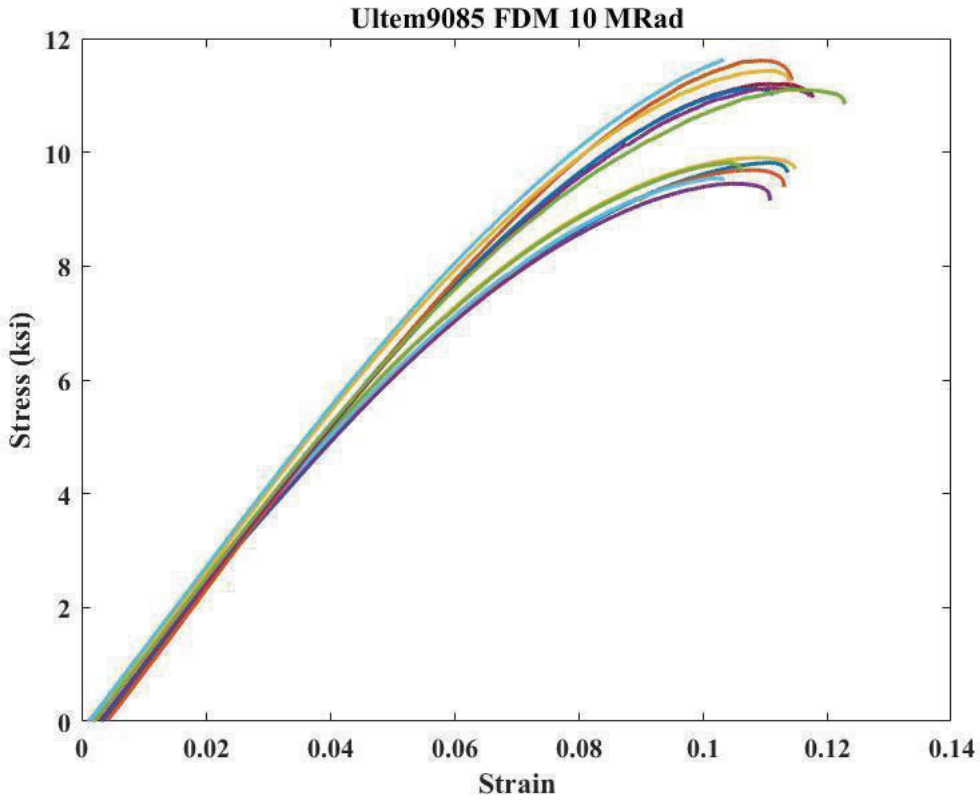

Ultem9085 FDM 0 MRad
Stress (ksi)
Strain
0
2
4
6
8
10
12
0
0.02
0.04
0.06
0.08
0.1
0.12
0.14

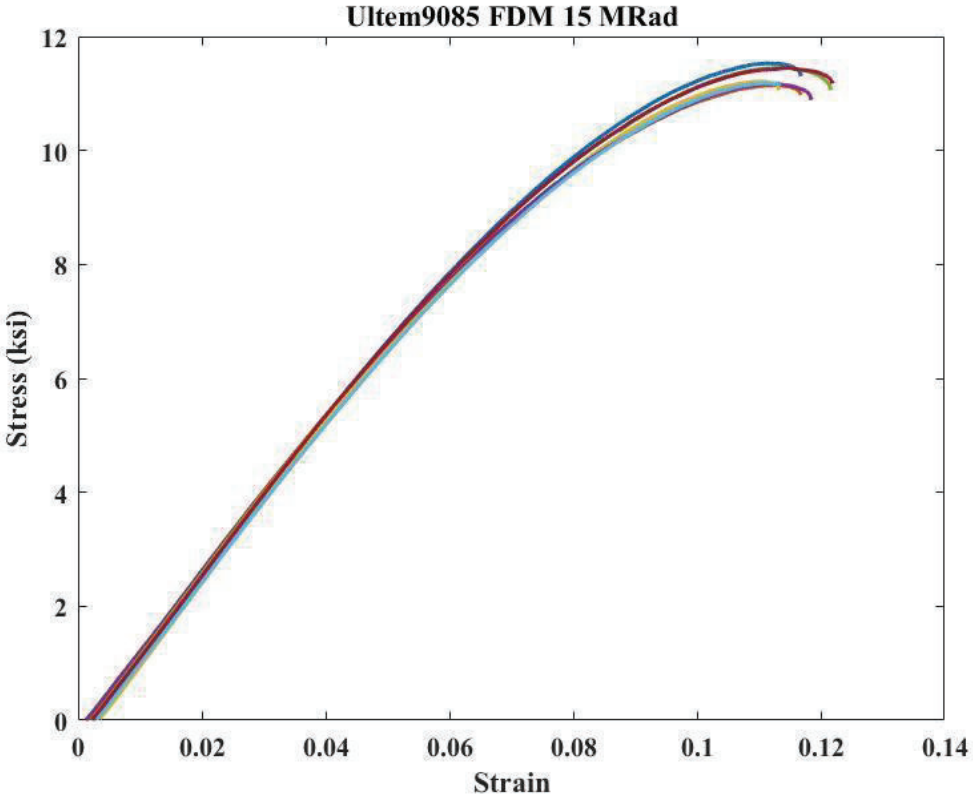

Ultem9085 FDM 0.1 MRad
Stress (ksi)
Strain
0
1
2
3
4
5
6
7
8
9
10
0
0.02
0.04
0.06
0.08
0.1
0.12

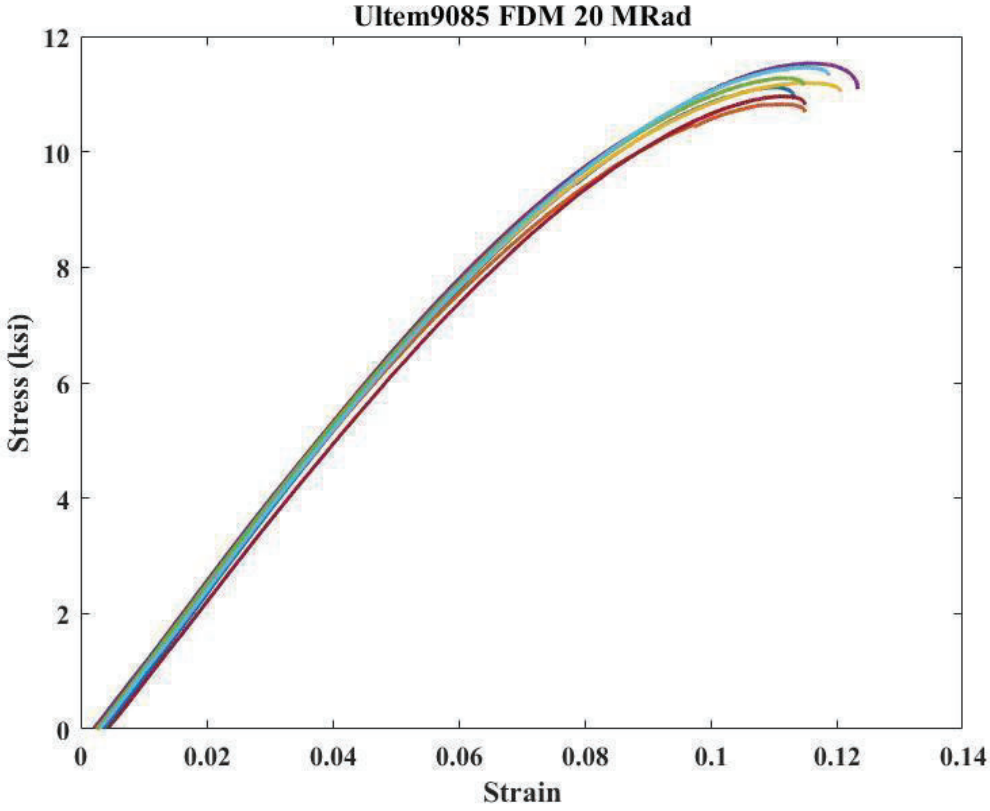

Ultem9085 FDM 0.5 MRad
Stress (ksi)
Strain
0
1
2
3
4
5
6
7
8
9
10
0
0.02
0.04
0.06
0.08
0.1
0.12


Ultem9085 FDM 1 MRad
Stress (ksi)
Strain
0
2
4
6
8
10
12
0
0.02
0.04
0.06
0.08
0.1
0.12


Ultem9085 FDM 5 MRad
Stress (ksi)
Strain
0
2
4
6
8
10
12
0
0.02
0.04
0.06
0.08
0.1
0.12
0.14


Ultem9085 FDM 10 MRad
Stress (ksi)
Strain
0
2
4
6
8
10
12
0
0.02
0.04
0.06
0.08
0.1
0.12
0.14


Ultem9085 FDM 15 MRad
Stress (ksi)
Strain
0
2
4
6
8
10
12
0
0.02
0.04
0.06
0.08
0.1
0.12
0.14


Ultem9085 FDM 20 MRad
Stress (ksi)
Strain
0
2
4
6
8
10
12
0
0.02
0.04
0.06
0.08
0.1
0.12
0.14